

Copyright  
by  
Patrick John Mickler  
2004

**The Dissertation Committee for Patrick John Mickler Certifies  
that this is the approved version of the following dissertation:**

**Controls on the stable isotopic composition of speleothems,  
Barbados, West Indies**

**Committee:**

---

Jay Banner, Supervisor

---

Libby Stern, Supervisor

---

Frederick Taylor

---

Bridget Scanlon

---

Liang Yang

**Controls on the stable isotopic composition of speleothems,  
Barbados, West Indies**

**by**

**Patrick John Mickler, M.S., B.A.**

**Dissertation**

Presented to the Faculty of the Graduate School of  
The University of Texas at Austin  
in Partial Fulfillment  
of the Requirements  
for the Degree of

**Doctor of Philosophy**

**The University of Texas at Austin  
May 2004**

## **Acknowledgements**

This work was supported by grants from the Geology Foundation of the University of Texas at Austin, the US Department of Energy (DE-FG03-97ER14812), the National Science Foundation (EAR95-26714), and the Geological Society of America (7220-02). We appreciate the assistance provided by the management of Harrison's Cave, the Barbados National Trust, and Bwalya Mwansa of the Barbados Water Authority, the management of Apes Hill Quarry.

I would also like to thank everyone who has helped with this project, including members of our research group; Ian Jones, Marylynn Musgrove, Deanna Combs, Amber Guilfoyle, Molly Pursell, Sarah Pierson and Lance Christian.

Finally, I would like to thank my friends and family for all the support they have given me through this process.



# **Controls on the stable isotopic composition of speleothems, Barbados, West Indies**

Publication No. \_\_\_\_\_

Patrick John Mickler, Ph. D.

The University of Texas at Austin, 2004

Supervisors: Jay Banner and Libby Stern

Applications of speleothem calcite geochemistry in climate change studies require the evaluation of the accuracy and sensitivity of speleothem proxies to most correctly infer paleoclimatic information. The present study of Harrison's Cave, Barbados, uses the analysis of the modern climatology and groundwater system to evaluate controls on the C and O isotopic composition of modern speleothem calcite. This new approach directly compares the  $\delta^{18}\text{O}$  and  $\delta^{13}\text{C}$  values of modern speleothem calcite formations with the values for their corresponding drip waters in order to assess the degree to which isotopic equilibrium is achieved during calcite precipitation.

Carbon isotope values for the majority of modern speleothem calcite samples from Harrison's Cave fall within the range of equilibrium values predicted from the combined use of 1) calcite-water fractionation factors from the literature, 2) measured temperatures, and 3) measured  $\delta^{13}\text{C}$  values of the dissolved

inorganic carbon of drip waters. Enrichments and depletions in  $^{13}\text{C}$ , relative to equilibrium C isotopic compositions, are also observed. The  $^{13}\text{C}$  depletions are likely caused by kinetically driven departures in the fractionation between  $\text{HCO}_3^-$  (aq) and  $\text{CaCO}_3$  from equilibrium conditions, caused by rapid calcite growth.  $^{13}\text{C}$  enrichments can be accounted for by Rayleigh distillation of the  $\text{HCO}_3^-$  (aq) reservoir during degassing of  $^{13}\text{C}$ -depleted  $\text{CO}_2$ .

In contrast to the C isotopic results, most modern speleothem calcites from Harrison's Cave are not in O isotopic equilibrium with their corresponding drip water and are enriched in  $^{18}\text{O}$  relative to equilibrium values.  $\delta^{18}\text{O}$  variations of modern calcite are likely controlled by kinetically driven changes in the fractionation between  $\text{HCO}_3^-$  (aq) and  $\text{CaCO}_3$  from inferred equilibrium conditions to non-equilibrium conditions, consistent with rapid speleothem calcite growth. In contrast to  $\delta^{13}\text{C}$ , the effects of Rayleigh distillation on the  $\delta^{18}\text{O}$  values of modern calcite are buffered by  $\text{CO}_2$  hydration and hydroxylation reactions that influence the O isotopic composition of the  $\text{HCO}_3^-$  (aq) reservoir. The effects of Rayleigh distillation manifest themselves in samples taken along a growth layer by producing a progressive enrichment away from the growth axis with a constant  $\delta^{13}\text{C}$  vs.  $\delta^{18}\text{O}$  slope. This observation has significance to ancient speleothem studies. A review of the literature has found that 62% of 141 studies show positive  $\delta^{13}\text{C}$  vs.  $\delta^{18}\text{O}$  correlation consistent with our non equilibrium models.

## Table of Contents

List of Tables.....	ix
List of Figures .....	x
CHAPTER 1: INTRODUCTION .....	1
CHAPTER SUMMARIES.....	3
CHAPTER 2: STABLE ISOTOPE VARIATIONS IN MODERN TROPICAL SPELEOTHEMS: EVALUATING EQUILIBRIUM VS. KINETIC ISOTOPE EFFECTS .....	7
ABSTRACT .....	7
INTRODUCTION.....	8
ISOTOPE METEOROLOGY AND HYDROLOGY OF BARBADOS .....	11
STUDY SITES AND SAMPLE DESCRIPTIONS .....	12
ANALYTICAL METHODS.....	18
RESULTS.....	25
DISCUSSION .....	31
CONCLUSIONS .....	44
CHAPTER 3: LARGE KINETIC ISOTOPE EFFECTS IN MODERN SPELEOTHEMS.....	46
ABSTRACT .....	46
INTRODUCTION.....	48
HENDY’S TESTS FOR EQUILIBRIUM PRECIPITATION.....	49
MODERN SPELEOTHEMS .....	51
METHODS.....	54
RESULTS.....	61
DISCUSSION .....	66
CONCLUSIONS .....	76

CHAPTER 4: APPLICATION OF HIGH-RESOLUTION X-RAY COMPUTED TOMOGRAPHY IN DETERMINING THE SUITABILITY OF SPELEOTHEMS FOR USE IN PALEOCLIMATIC, PALEOHYDROLOGIC RECONSTRUCTIONS .....	98
ABSTRACT .....	98
INTRODUCTION.....	99
MATERIALS AND METHODS .....	101
CHAPTER 5: BARBADOS SPELEOTHEM STABLE ISOTOPE RECORD.	109
INTRODUCTION.....	109
APPENDICES.....	128
APPENDIX 1. GLASS PLATE CALCITE FROM HARRISON’S CAVE SAMPLED ALONG THE GROWTH AXIS.....	128
APPENDIX 2. GLASS PLATE CALCITE FROM HARRISON’S CAVE SHOWING SPATIAL VARIABILITY .....	134
APPENDIX 3. U-TH SYSTEMATICS .....	137
APPENDIX 4. ANCIENT SPELEOTHEM GEOCHEMISTRY FROM HARRISON’S CAVE AND APES HILL QUARRY.....	138
APPENDIX 5. BC-61 ELEMENTAL GEOCHEMISTRY .....	146
BIBLIOGRAPHY .....	150
VITA .....	161

## List of Tables

TABLE 2.1: Site conditions, glass plate calcite thickness and number of samples .....	15
TABLE 2.2: EQUILIBRIUM OXYGEN ISOTOPE FRACTIONATION ( $1000 \ln \alpha$ ) AT 26.6° .....	21
Table 2.3: Equilibrium carbon isotope fractionation ( $1000 \ln \alpha$ ) at 26.6°C .....	21
Table 3.1. Calcite and water stable isotopic compositions .....	78
Table 3.2. Harrison's Cave water chemistry .....	79
Table 3.3 Compilation of published $\delta^{18}\text{O}$ and $\delta^{13}\text{C}$ speleothem records .....	81
Table 3.4 Summary of speleothem records with $\delta^{18}\text{O}$ and $\delta^{13}\text{C}$ value correlations .....	97

## List of Figures

Figure 2.1A: Map of Harison's Cave .....	13
Figure 2.1B: Map of Barbados with location of Harison's Cave.....	13
Figure 2.1C: Average monthly $\delta^{18}\text{O}$ values of average monthly rainfall .....	13
Figure 2.2: Carbon isotopic compositions from Harison's Cave .....	24
Figure 2.3: Oxygen isotopic compositions from Harison's Cave .....	28
Figure 2.4A: Monthly rainfall totals .....	29
Figure 2.4B: Average monthly temperature.....	29
Figure 2.4C: $\delta^{13}\text{C}$ vs. time.....	29
Figure 2.4D: $\delta^{18}\text{O}$ vs. time .....	29
Figure 2.5: Mechanisms to account for enrichments and depletions .....	33
Figure 2.6: Rayleigh distillation model.....	36
Figure 3.1. Rayleigh distillation model showing the O and C isotope effects of progressive loss of $\text{HCO}_3^-$ during $\text{CO}_2$ degassing and calcite precipitation..	50
Figure 3.2. Glass plates experiment at stalagmite sites in the Upper Passage .....	53
Figure 3.3. Spatial variations in the stable isotopic composition of calcite on glass plate BC-98-3. ....	57
Figure 3.4. $\delta^{13}\text{C}$ vs. $\delta^{18}\text{O}$ plot of glass plate calcite samples sampled along the growth layer.....	63
Figure 3.5. $\delta^{13}\text{C}$ vs. $\delta^{18}\text{O}$ plot of glass plate calcite sampled near the locus of precipitation to determine the temporal variation in stable isotopic composition. ....	65
Figure 3.6. Model showing the effects of progressive $\text{CO}_2$ degassing and calcite precipitation with variable O buffering of the $\text{HCO}_3^-$ reservoir.....	68

Figure 3.7. $\delta^{13}\text{C}$ vs. $\delta^{18}\text{O}$ plots for several speleothem studies from the literature	69
Figure 4.1A: Photograph of unsliced, unpolished stalagmite sample AH-M	102
Figure 4.1B: Three-dimensional volume rendering of sample AH-M	102
Figure 4.2: HRXCT slice through AH-M showing density variations	106
Figure 4.3: Volume renderings of ANY-01	107
Figure 5.1: Map of Barbados, West Indies showing the location of Harrison's Cave and Apes Hill Quarry	119
Figure 5.2: Speleothem BC-53 collected from Harrison's Cave	120
	121
Figure 5.4: Speleothem AH-L bottom collected at Apes Hill Quarry	122
Figure 5.5: Speleothem AH-M collected at Apes Hill quarry	123
Figure 5.6: Speleothem AH-S collected at Apes Hill quarry	124
Figure 5.7: Temporal $\delta^{18}\text{O}$ trend of the Barbados speleothems	125
Figure 5.8: Temporal $\delta^{13}\text{C}$ trend of the Barbados speleothems	126
Figure 5.9: $\delta^{13}\text{C}$ vs. $\delta^{18}\text{O}$ plot of ancient speleothem calcite from Barbados, West Indies	127

## CHAPTER 1: INTRODUCTION

The isotopic and elemental composition of speleothems, secondary cements found in caves, have been used to elucidate past climate changes. Speleothems are well suited for climatic study for several reasons: 1) The stable and radiogenic isotopic composition as well as trace elemental composition of calcite speleothems may preserve evidence of climatic change (Hendy, 1971; Gascoyne, 1992; Lauritzen, 1995; Banner et al., 1996; Baker et al., 1998b; Desmarchelier et al., 2000; Finch et al., 2001; Bar-Matthews et al., 2003a). 2) speleothems can be continuously deposited in low latitude, low altitude terrestrial environments where other high resolution records may be absent. 3) Speleothems can be precisely dated using U-series techniques, which allow climatic information inferred from speleothem chemistry to be put in a high resolution chronostatigraphy (Edwards et al., 1987; Musgrove, 2000; Musgrove et al., 2001). These factors allow speleothems to be used produce long, continuous, high-resolution records of terrestrial climate change.

The  $\delta^{18}\text{O}$  and  $\delta^{13}\text{C}$  values of ancient speleothems have been studied extensively. This is because, when precipitated in O and C isotopic equilibrium with their corresponding drip water, the stable isotopic composition of speleothems can provide paleoenvironmental information (Hendy, 1971). It has been proposed that changes in  $\delta^{18}\text{O}$  values of ancient speleothems are controlled by changes in temperature and/or the O isotopic composition of cave drip water, and by inference the  $\delta^{18}\text{O}$  of rainwater, which usually reflects temperature of



condensation (Dansgaard, 1964; Gascoyne, 1992). It has also been proposed that changes in the  $\delta^{13}\text{C}$  values of speleothem calcite are controlled by changes in vegetation type above the cave system (Hendy, 1971; Dorale et al., 1998) changes in the C isotopic composition of atmospheric  $\text{CO}_2$  (Baskaran and Krishnamurthy, 1993) and the relative proportions of soil derived vs. limestone derived C (Hendy, 1971). Despite their value, speleothem calcite samples must be precipitated in O and C isotopic equilibrium with their corresponding drip water, or exhibit regular and predictable deviations from equilibrium values, in order to be quantitatively useful.

When studying ancient speleothems, it is difficult to measure the O and C isotopic composition of the water from which the speleothems precipitated. Without these data, it is difficult to accurately ascertain the degree to which equilibrium calcite precipitation is achieved. Tests for equilibrium precipitation that measure the  $\delta^{18}\text{O}$  and  $\delta^{13}\text{C}$  values of speleothem calcite along discrete growth-layers have been proposed (Hendy, 1971; Gascoyne, 1992). Even these tests do not provide information on the direction or magnitude of non-equilibrium isotope offsets nor do they identify the mechanisms responsible for those offsets.

This study determines the extent to which modern speleothem calcite from Harrison's Cave, Barbados, is precipitating in isotopic equilibrium with its corresponding drip water. This is determined through the use of new empirical tests using modern speleothem calcite and cave drip waters. Evidence is presented for the presence of both equilibrium and non-equilibrium isotope effects in the Barbados speleothems. The direction and magnitude of the offsets from

equilibrium have been quantified and this has led to the tentative identification of the non-equilibrium isotope effects operating in Harrison's Cave.

## **CHAPTER SUMMARIES**

### **Chapter 2**

This chapter addresses the  $\delta^{18}\text{O}$  and  $\delta^{13}\text{C}$  values of modern speleothems collected on glass plates from Harrison's Cave. Frosted glass plates, 10 X 10 cm, were placed under cave drips that were actively precipitating calcite speleothems. The speleothems calcite was then precipitated on the glass plates. Because I know precisely when the plates were placed and collected there is no doubt that the calcite is actively growing and I know its precise age. During plate placement and collection, the water from which the speleothem precipitated was collected. The  $\delta^{18}\text{O}$  value of the water and the  $\delta^{13}\text{C}$  value of the dissolved inorganic carbon in the water were analyzed and directly compared to the isotopic composition of the cave calcite. In this way, the extent to which isotopic equilibrium was achieved is evaluated. The results show  $^{13}\text{C}$  enrichments and depletions from equilibrium values whereas there are only  $^{18}\text{O}$  enrichments in the glass plate calcite. I describe two mechanisms that are likely responsible for the observations. This is a new method in speleothem research which may significantly improve our understanding on the controls on the stable isotopic composition of speleothems.

### **Chapter 3**

This chapter addresses the spatial distribution of  $\delta^{18}\text{O}$  and  $\delta^{13}\text{C}$  values of glass plate calcite collected in the Upper Passage of Harrison's Cave, Barbados. Sampling the spatial distribution of O and C isotopes on the glass plates is analogous to sampling a speleothem along a growth layer. This is equivalent to the tests for equilibrium calcite precipitation proposed by (Hendy, 1971). My results show that there is a progressive enrichment in  $\delta^{18}\text{O}$  and  $\delta^{13}\text{C}$  values away from the growth axis. This enrichment produces a strong positive correlation between  $\delta^{18}\text{O}$  and  $\delta^{13}\text{C}$  values of speleothem calcite that can be expressed in  $\delta^{13}\text{C}$  vs.  $\delta^{18}\text{O}$  space as a line with a correlation coefficient. My model explains the synchronous enrichment in  $\delta^{18}\text{O}$  and  $\delta^{13}\text{C}$  values of modern speleothem calcite by progressive loss of DIC during calcite precipitation, modulated by O isotope exchange with  $\text{H}_2\text{O}$ . A literature review discovered that the preponderance of stable isotopic studies on speleothems calcite identified positive covariation between  $\delta^{18}\text{O}$  and  $\delta^{13}\text{C}$  values. Some undetermined percent of those studies are likely controlled by the non-equilibrium isotope effects outlined in this chapter.

### **Chapter 4**

This chapter addresses a new technique for imaging the internal stratigraphy of speleothems using high-resolution X-Ray computed tomography (HRXCT), an instrument similar to a medical CAT scanner. As outlined in Ch. 2 and 3, it is important to sample speleothem calcite, most commonly from stalagmites, along the speleothem growth axis to minimize non-equilibrium isotope effects. The position of the growth axis is difficult to determine when

examining unslabbed-unpolished speleothems. The use of HRXCT allows the position of the growth axis to be determined prior to slabbing. Also, this new method can help ascertain the suitability of a speleothem for use in paleoclimatic studies. Speleothems that are determined to be unsuitable for use in paleoclimatic studies, due to post depositional alteration or extensive porosity along the growth axis, can be excluded from study before destructive and time consuming sample preparation. In addition, HRXCT can quickly identify the size and location of all voids in a speleothem and may be able to determine if those voids are air or water filled. Large fluid inclusions in speleothems have been used to reconstruct the O and H isotopic composition of cave drip water. Although this was not done in this study, this method will be valuable to other paleoclimate researchers.

## **Chapter 5**

This chapter addresses the application of the non-equilibrium isotopic effects outlined in Ch. 2 and 3 in the analysis of the ancient speleothem record from Barbados. These non-equilibrium isotope effects were considered when evaluating  $\delta^{18}\text{O}$  and  $\delta^{13}\text{C}$  record from five speleothems, with overlapping chronologies, from Harrison's Cave and Apes Hill quarry that covered the time interval from 11573 to 0 yr. Four of five speleothems used in this study show strong positive correlation between  $\delta^{18}\text{O}$  and  $\delta^{13}\text{C}$  values consistent with the non-equilibrium isotope effects outlined in Ch. 3. These speleothems contain large  $\delta^{18}\text{O}$  and  $\delta^{13}\text{C}$  variations that can not be explained by environmental change assuming isotopic equilibrium during calcite precipitation. In addition, the large rapid shifts in the  $\delta^{18}\text{O}$  and  $\delta^{13}\text{C}$  records do not correlate with known

paleoclimatic fluctuations presented by other researchers from the area. The rates of change, if solely due to environmental change and equilibrium isotope effects are too rapid to be physically realistic.

## **CHAPTER 2: STABLE ISOTOPE VARIATIONS IN MODERN TROPICAL SPELEOTHEMS: EVALUATING EQUILIBRIUM VS. KINETIC ISOTOPE EFFECTS**

### **ABSTRACT**

Applications of speleothem calcite geochemistry in climate change studies require the evaluation of the accuracy and sensitivity of speleothem proxies to correctly infer paleoclimatic information. The present study of Harrison's Cave, Barbados, uses the analysis of the modern climatology and groundwater system to evaluate controls on the C and O isotopic composition of modern speleothems. This new approach directly compares the  $\delta^{18}\text{O}$  and  $\delta^{13}\text{C}$  values of modern speleothems with the values for their corresponding drip waters in order to assess the degree to which isotopic equilibrium is achieved during calcite precipitation. If modern speleothems can be demonstrated to precipitate in isotopic equilibrium, then ancient speleothems, suitable for paleoclimatic studies, from the same cave environment may also have been precipitated in isotopic equilibrium. If modern speleothems are precipitated out of isotopic equilibrium, then the magnitude and direction of the C and O isotopic offsets may allow specific kinetic and/or equilibrium isotopic fractionation mechanisms to be identified.

Carbon isotope values for the majority of modern speleothem samples from Harrison's Cave fall within the range of equilibrium values predicted from the combined use of 1) calcite-water fractionation factors from the literature, 2) measured temperatures, and 3) measured  $\delta^{13}\text{C}$  values of the dissolved inorganic carbon of drip waters. Calcite samples range from ~0.8‰ higher to ~1.1‰ lower

than predicted values. The  $^{13}\text{C}$  depletions are likely caused by kinetically driven departures in the fractionation between  $\text{HCO}_3^-$  (aq) and  $\text{CaCO}_3$  from equilibrium conditions, caused by rapid calcite growth.  $^{13}\text{C}$  enrichments can be accounted for by Rayleigh distillation of the  $\text{HCO}_3^-$  (aq) reservoir during degassing of  $^{13}\text{C}$ -depleted  $\text{CO}_2$ .

Modern speleothems from Harrison's Cave are not in O isotopic equilibrium with their corresponding drip waters and are 0.2‰ to 2.3‰ enriched in  $^{18}\text{O}$  relative to equilibrium values.  $\delta^{18}\text{O}$  variations in modern calcite are likely controlled by kinetically-driven changes in the fractionation between  $\text{HCO}_3^-$  (aq) and  $\text{CaCO}_3$  from equilibrium conditions to non-equilibrium conditions, consistent with rapid calcite growth. In contrast to  $\delta^{13}\text{C}$ ,  $\delta^{18}\text{O}$  values of modern calcite may not be affected by Rayleigh distillation during degassing because of  $\text{CO}_2$  hydration and hydroxylation reactions that will buffer the O isotopic composition of the  $\text{HCO}_3^-$  (aq) reservoir. If the effects of Rayleigh distillation manifest themselves in the O isotopic system they will result in  $^{18}\text{O}$  enrichment in the  $\text{HCO}_3^-$  (aq) reservoir and ultimately the precipitated  $\text{CaCO}_3$ .

## INTRODUCTION

As studies of climate change have become a rapidly growing part of the Earth sciences, applications of speleothem (cave calcite deposit) geochemistry to these studies have also grown. This increased interest has come from: 1) the numerous geochemical tracers of climatic and hydrologic processes that are incorporated into speleothem calcite, 2) advances in geochronologic methods for Quaternary carbonate deposits, which allow the geochemical tracers to be put into

a high-resolution time series (Musgrove et al., 2001), and 3) the widespread geographic occurrence of speleothems, including low-altitude, low-latitude terrestrial environments where other high-resolution climate records may be scarce. These tracers have been used to infer changes in paleoprecipitation, paleotemperature, and paleovegetation (Dorale et al., 1992; Winograd et al., 1992; Baker et al., 1998b; Genty et al., 1998). Tropical climate change studies are of particular interest because this is where the vast majority of tropospheric moisture originates, driving the global hydrologic cycle (Masson et al., 2000).

Most paleoclimate reconstructions apply proxy data to infer changes in some environmental parameter. Evaluating the utility, accuracy and sensitivity of a given proxy is critical for valid paleoclimate reconstruction. Rigorous testing of the geochemical proxies preserved in corals and marine foraminifera through calibration of experimental or modern natural systems (Spero and Williams, 1988; Beck et al., 1992; Spero, 1992) has evaluated the applicability of these proxies. Despite the growing use of speleothems in paleoenvironmental reconstructions, studies that evaluate the extent to which isotopic equilibrium is reached during speleothem formation, or that attempt to calibrate speleothem isotope variations, are lacking. Speleothem proxies are inherently more complex than marine proxies, given the much wider variations in cave water geochemistry relative to seawater and the significant kinetic isotope effects caused by rapid CO<sub>2</sub> degassing, rapid calcite precipitation and cave water evaporation. Nonetheless, terrestrial climate is ultimately of great concern for future climate predictions.



The use of carbon and oxygen isotope records requires an evaluation of whether the isotopic composition of speleothem calcite directly reflects the isotopic composition of water and dissolved inorganic carbon upon entry into the cave. The oxygen isotope composition of the calcite can be used to infer the isotope composition of rainfall, which is climatically controlled (Dansgaard, 1964), and/or temperature at the time of speleothem formation. The carbon isotopic composition of speleothems can be used to infer the isotopic composition of atmospheric CO<sub>2</sub> (Baskaran and Krishnamurthy, 1993), the type of vegetation growing above the cave (Dorale et al., 1992) and the relative contributions of soils vs. aquifer limestone to the dissolved inorganic carbon that forms the speleothem (Hendy, 1971; Genty et al., 1998).

In this study, I evaluate equilibrium vs. kinetic isotope effects and determine the extent to which speleothems record variations in environmental parameters through the study of modern speleothems precipitated in Harrison's Cave, Barbados. The modern speleothems I examine include samples from the tips of actively growing stalagmites, flowstones grown since development of the cave in 1978, and speleothem calcite grown on glass plates placed under active drips in the cave. I collected the calcite, precipitated under current climatic conditions, and the water from which the calcite precipitated. The C and O isotopic composition of modern speleothem-drip water pairs were used to determine the extent to which isotopic equilibrium is achieved during calcite precipitation. This information can be applied to speleothem isotopic records

collected from the same cave environment that are used for paleoclimatic reconstructions.

## **ISOTOPE METEOROLOGY AND HYDROLOGY OF BARBADOS**

Barbados' Pleistocene limestone aquifer is well suited for studying the links between modern climate, the isotopic composition of cave drip water and the calcite that precipitates from this water. Within this aquifer system, Harrison's Cave contains multiple speleothems that form in a variety of cave microenvironments. The island's isolated setting, removed from large sized landmasses, and its low topographic relief reduce the O isotopic variability of rainfall on the island. Isotopic effects that operate on larger landmasses, such as topographic and continentality effects and mixing of distant water vapor sources with significantly different isotopic compositions, have minor control on the O isotopic composition of rainfall on Barbados. In addition, the tropical location of Barbados lowers its seasonal temperature range, approximately 4-5°C, limiting the effects of temperature on the O isotopic composition of rainfall. These factors combine to produce a location with ample actively growing speleothems for study and a simplified O isotopic rainfall and groundwater system already well characterized (Jones et al., 1998; Jones et al., 2000; IAEA/WMO, 2001).

Oxygen isotopic compositions and amounts of rainfall have been measured in Barbados for the past 30 years (IAEA/WMO, 2001) and for cave drip water data from 1997 to 2000 (this study). The seasonal distribution and oxygen isotopic compositions of rainfall on Barbados vary as a function of tropical weather patterns (Jones et al., 2000). During the dry season, from January to

April, rainfall results from local heating and rising of air, with rainfall focused over the island's central elevated portions. Most rain falls from June to December, and is associated with the seasonal movement of the low pressure intertropical convergence zone and with passing tropical weather systems. Monthly averaged isotopic compositions of Barbados rainwater range in  $\delta^{18}\text{O}$  from  $-4\text{‰}$  to  $+2\text{‰}$ , with lower  $\delta^{18}\text{O}$  values occurring during the wet season. Groundwaters, by contrast, have a narrower range of  $\delta^{18}\text{O}$  values, with most values between  $-3.5\text{‰}$  to  $-3.0\text{‰}$ , reflecting the effects of evapotranspiration, which limits recharge to the Pleistocene limestone aquifer to the two to three wettest months of the year (Jones et al., 2000; Jones and Banner, 2003). The isotopic composition of rainfall during these months controls the isotopic composition of groundwater and cave drip waters, including those in Harrison's Cave, resulting in groundwater with a narrow O isotopic composition (Jones et al. 2000).

## **STUDY SITES AND SAMPLE DESCRIPTIONS**

Three locations were studied in Harrison's Cave for modern speleothems and drip water collection: The Upper Passage, Crystal Droppings and Spur 1 (Fig. 2.1). These sites represent the range of microenvironments found in the cave and samples collected record the sensitivity of speleothems to modern climatic and hydrologic variations. Low relative humidity at the site of calcite precipitation may cause high  $\delta^{18}\text{O}$  values in the calcite due to evaporative  $^{18}\text{O}$  enrichment in the cave drip water and rapid  $\text{CO}_2$  degassing may cause  $^{13}\text{C}$  enrichments in the speleothem precipitated from that water

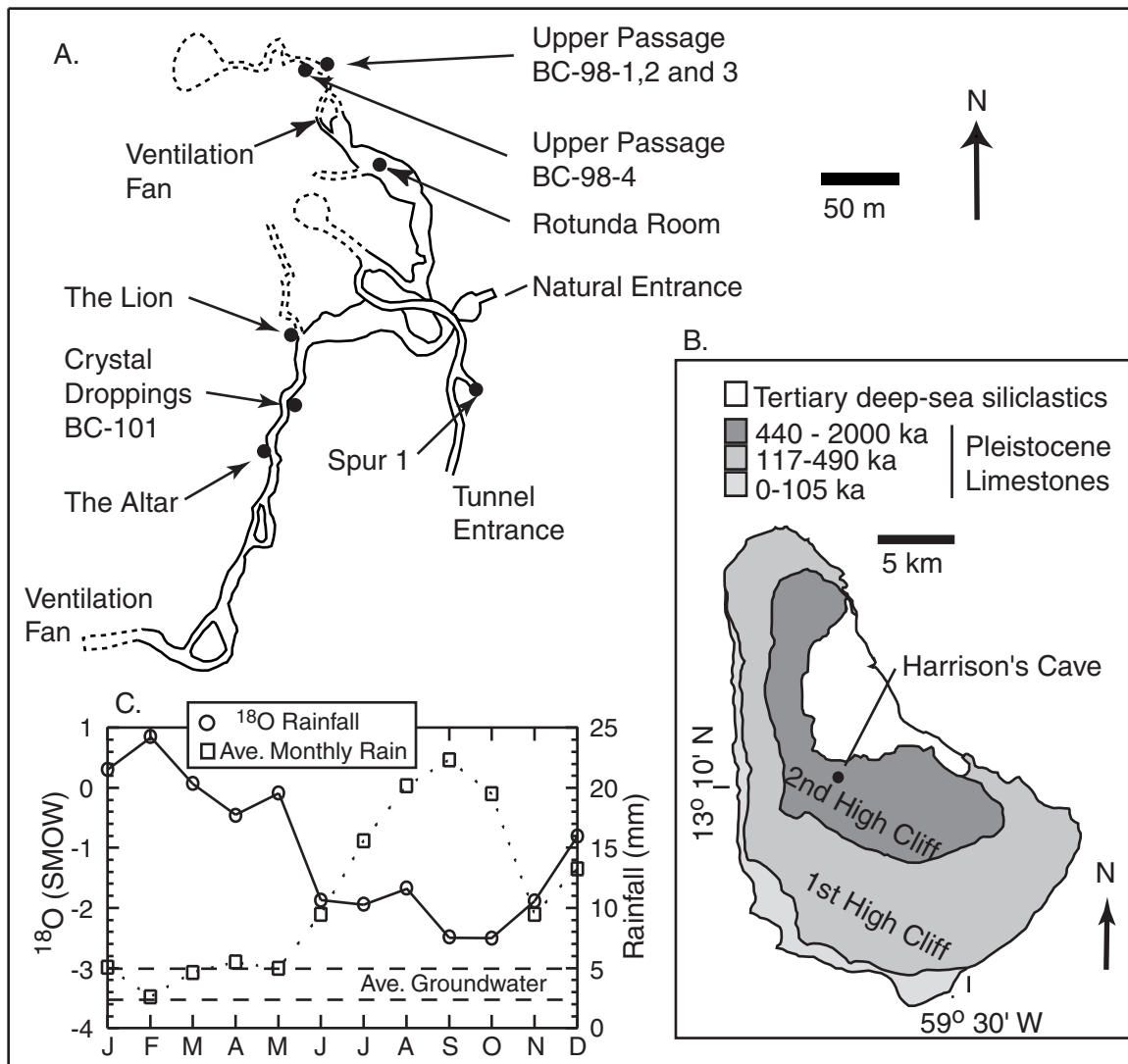


Figure 2.1A. Map of Harrison's Cave showing the location of modern speleothem sample sites, humidity measurement sites (Wefer, 1994) and B. the cave's location on Barbados, West Indies (Hobbs, 1994). Dashed passages have not been surveyed. Harrison's Cave is located above the Second High Cliff. Limestone above the second high cliff ranges in age from 440 ka to 2.0 Ma and limestone above the Second High Cliff and below the elevation of Harrison's Cave range in age from 440 to 640 ka (Banner et al., 1994). C. Average monthly  $\delta^{18}\text{O}$  values of average monthly rainfall collected on Barbados between 1961 and 1997 (IAEA/WMO, 2001) and of average monthly rainfall amounts from 1994 to 2000 (IAEA/WMO, 2001). Range of Harrison's Cave groundwater  $\delta^{18}\text{O}$  values, between 3.0 and 3.5‰, indicated by dashed lines.

(Gonzalez and Lohmann, 1988). Therefore, I would expect speleothems precipitated under high humidity conditions from relatively slow steady drips would have the highest potential for precipitation in O and C isotopic equilibrium with their corresponding drip water. Conditions at my study sites are outlined in Table 2.1.

I would expect that conditions in the Upper Passage sites are the most conducive to the precipitation of speleothems in isotopic equilibrium with their corresponding drip water for several reasons. Meteorological data indicate that the Upper Passage has had humidity levels close to 100% during its history. High humidity values in the Upper Passage are maintained by the presence of airflow bottlenecks on each end of the passage (Fig. 2.1), which act to limit air exchange. Development of the cave in 1978-1979 included excavation of a 5 m diameter tunnel entrance, and the excavation of two ventilation shafts. Even after development, humidity in the deeper parts of the cave are above 98.2% during the day while ventilation fans operate and with the rolling steel door on the tunnel entrance open, and above 99% at night with the fans off and the door closed (Wefer, 1994). The Upper Passage sample locations are approximately 21 m below the land surface. Speleothems at this site form under high humidity conditions, from relatively slow steady drips. These conditions limit evaporative  $^{18}\text{O}$  enrichment in the drip water and may limit kinetic isotope effects caused by large variations in drip rates and the accompanying changes in drip water chemistry.

TABLE 2.1: Site conditions, glass plate calcite thickness and number of samples

Site	Drip rate (ml/min)	Drip water pH	Drip water temp. (°C)	Relative humidity (%)	Depth below surface (m)	Calcite thickness at sample location (mm)		
						Plate placed 7-11-1998 Plate Set 1	Plate placed 2-1-1999 Plate collected 7-1-00 Plate Set 2	Set1, Set2 <sup>c</sup>
Spur 1	0 to 18.8	7.6	27.5	97.8 to 99.6	12	0.4	NA	15,NA
Crystal Droppings	86 to 96	7.4 to 7.5	25.0 to 28.5	97.8 to 99.6	40	NA	NA	NA,NA
<u>Upper Passage Sites</u>								
BC-98-1	0.1 to 0.3	7.8 to 8.1	26.0 to 29.6	>98.2 <sup>a</sup>	21	0.4	0.6	11,32 <sup>b</sup>
BC-98-2	0.1 to 0.2	8.1	25.6 to 30.0	>98.2 <sup>a</sup>	21	0.4	0.7	11, 27 <sup>b</sup>
BC-98-3	0.1 to 0.3	7.7 to 8.1	26.8 to 29.9	>98.2 <sup>a</sup>	21	0.3	0.8	13,47 <sup>b</sup>
BC-98-4	<0.008	NA	NA	>98.2 <sup>a</sup>	21	<0.1	NA	NA,NA

Relative Humidity, depth below surface was measured by Wefer (1994)

- Relative Humidity at the Upper Passage sites were assumed to be at least equivalent to the relative humidity measured at the Rotunda Room. The presence of air flow bottlenecks that isolate the Upper Passage sites suggest that relative humidity may be slightly higher.
- Not all samples were analyzed.
- Set 1 and Set 2 refer to the number of calcite samples collected by sampling in 0.02 mm layers. Set 1 plates were placed in the cave on 7-11-98 and set 2 plates were placed in the cave on 2-1-99.

Modern speleothems were collected from four sites from the Upper Passage, BC-98-1 through BC-98-4. BC-98-1, BC-98-2 and BC-98-3 were collected from the tops of active stalagmites that are approximately 1 m in height. The drips feeding these speleothems are slow, less than 0.3 ml/min. These speleothems occupy an area of a square meter. Ten meters away, BC-98-4 is several cm in height, precipitating from a very slow drip.

Among the sample sites studied, I would expect that conditions in Spur 1 are least conducive to the precipitation of speleothems in isotopic equilibrium with their corresponding drip water for several reasons. 1) The proximity of the room to the tunnel entrance (approximately 75 m) results in variable humidity ranging from 97.8% to 99.6% (Wefer, 1994), which might allow evaporative increases in the  $\delta^{18}\text{O}$  values of cave drip water. More importantly, the proximity to the tunnel entrance may also allow greater ventilation, which could result in lower  $\text{CO}_2$  concentrations in the cave atmosphere, which in turn will promote greater  $\text{CO}_2$  degassing from cave drip waters.  $\text{CO}_2$  degassing is a more significant factor than evaporation of cave drip water in driving  $\text{CaCO}_3$  precipitation in these high humidity environments. 2) Drips that are currently precipitating speleothems in this room respond to seasonal variations in rainfall rate. Drip rates ranged from approximately 0 ml/min, during the dry season, to at least 18.8 ml/min, resulting in variable calcite precipitation rates. 3) Spur 1 is much closer to the land surface (approximately 12 m) than the other sites in the cave, likely resulting in less water-rock interaction prior to speleothem precipitation. The combination of these variables would more likely result in speleothems with isotopic

compositions that are distinct from other sites in the cave and will most likely result in disequilibrium isotope effects during calcite precipitation.

The third sampling site in the cave is Crystal Droppings. This site is located in a man-made tunnel approximately 250 meters from the artificial cave entrance at a depth of approximately 40 m. Tunnel construction was completed in 1979-1980 (Hobbs, 1994). Flowstone calcite is being precipitated from a continuously flowing sheet of water on the walls of the tunnel where I measured a relative humidity of 99.6% in July 2000. Wefer (1994) measured humidity at two sites within 40 meters of Crystal Droppings. At these sites, the Alter and the Lion, the relative humidity varies between 97.8% and 99.1%. Based on the close proximity of these sites to Crystal Droppings, I conclude that the three sites share the same relative humidity conditions such that Wefer's measurements are applicable to Crystal Droppings (Fig. 2.1).

Two types of modern speleothem samples were used in this study. Modern speleothems include cores from the tips of actively growing stalagmites and flowstones, and calcite grown on glass plates placed under active drips. Cores were taken from several actively growing speleothems in the Upper Passage and Crystal Droppings in 1998. The cores are approximately 1 cm in diameter and 5 cm in length and consist of dense, translucent calcite. Calcite was sampled from the top 20  $\mu\text{m}$  of the cores from the Upper Passage. Based on a long-term growth rate of 0.2 mm/yr (Appendix, Table 5), the calcite was likely deposited within the year prior to coring. The Crystal Dropping core contained 2



cm of flowstone calcite deposited on the host limestone since tunnel excavation. Two samples, one from the base and one from the top, were taken from this core.

Glass plates, prepared by frosting with a sandblaster followed by cleaning, were placed under active drips in the Upper Passage and Spur 1. The plates were left under the drips for six months and 18 months and then collected. The glass plate calcite is composed of intergrown, flat-faced rhombohedral calcite crystals typically 100's of microns in diameter. Glass plate calcite yielded a record of oxygen and carbon isotope variations for the period July 1998 to July 2000.

## **ANALYTICAL METHODS**

### **C and O isotopic composition of calcite**

The majority of modern calcite samples were analyzed for C and O stable isotopes at the University of Texas at Austin. Approximately 200-350  $\mu\text{g}$  was analyzed using a Micromass Multiprep system on a Prism II dual inlet triple collector mass spectrometer. Analytical precision was 0.18‰ for  $\delta^{18}\text{O}$  and 0.12‰ for  $\delta^{13}\text{C}$  ( $2\sigma$  of 40 standard runs). Several samples were analyzed at The University of Minnesota, where 100 to 200  $\mu\text{g}$  of  $\text{CaCO}_3$  were reacted with 100%  $\text{H}_3\text{PO}_4$ , cryogenically purified and analyzed on a Finnigan MAT delta E triple-collector mass spectrometer, method modified after McCrea (1950). Precision ( $2\sigma$ ) was reported by the University of Minnesota as 0.2‰ for  $\delta^{18}\text{O}$  and 0.13‰ for  $\delta^{13}\text{C}$ . For smaller samples, 20 to 40  $\mu\text{g}$  of  $\text{CaCO}_3$ , were reacted using a Kiel II carbonate preparation device and analyzed on a Finnigan MAT 252 triple-collector mass spectrometer. Precision ( $2\sigma$ ) was reported by the University of Minnesota as 0.08‰ for  $\delta^{18}\text{O}$  and 0.06‰ for  $\delta^{13}\text{C}$ . The results of isotopic

analysis are presented in conventional delta ( $\delta$ ) notation, defined as  $\delta = (R_{\text{sample}} - R_{\text{standard}})/R_{\text{standard}} \times 1000$ , where R is the ratio of  $^{18}\text{O}/^{16}\text{O}$  or  $^{13}\text{C}/^{12}\text{C}$ . The O and C isotopic values for carbonate samples and the C isotopic values of DIC are expressed relative to the standard VPDB.

### **O and C isotopic composition of waters**

Three groups have collected oxygen isotope compositions of rainwater and groundwater used in this study: 1) Rainwater  $\delta^{18}\text{O}$  values have been collected on Barbados over the past 30 years (IAEA/WMO, 2001). 2) Cave drip water and rainwater data has been collected over the past seven years (Jones et al., 1998; Jones et al., 2000). 3) Cave drip waters from Harrison's Cave were collected in July 1998, February 1999 and July 2000, synchronous with deployment and collection of the glass plate experiment. In the Upper Passage water was collected by leaving a 1L wide mouth plastic bottle beneath each drip for approximately 24 hours because drips were too slow to collect an adequate sample size manually. In Spur 1 and Crystal Droppings water was collected by holding sample bottles, ranging from 12 ml to 60 ml, directly under the cave drips. Cave water samples analyzed in the present study were analyzed for  $^{18}\text{O}$  using a Micromass multi-prep system and analyzed on a Prism II dual inlet mass spectrometer at the University of Texas at Austin. The O isotopic values of water samples are expressed relative to the VSMOW standard. Analytical precision ( $2\sigma$ ) was 0.1‰.

### **DIC sample collection**

Dissolved inorganic carbon (DIC) samples were collected in the cave by filling 20 ml, amber, VOA vials with unfiltered cave drip water with no head space and stored, dark and refrigerated, until analysis. The C isotopic composition DIC was determined by injecting 5 ml of the cave drip water into an evacuated sample vial containing 1 ml 100% H<sub>3</sub>PO<sub>4</sub>. The resulting mixture of CO<sub>2</sub>, water vapor and non-condensable gasses was cryogenically purified in a vacuum line. An analytical precision (2σ of 0.1‰) was estimated by analyzing a solution of Na<sub>2</sub>CO<sub>3</sub> (aq) with a known C isotopic composition and DIC concentrations similar to cave drip waters.

### **Equations for determining O and C isotopic equilibrium**

The extent to which O and C isotopic equilibrium is reached during calcite precipitation was determined using fractionation factors from the literature (Table 2.2 and 2.3). During equilibrium precipitation of calcite the relationship between the oxygen isotopic composition of calcite and its corresponding host fluid and the temperature of formation is (O'Neil et al., 1969 as modified in Friedman and O'Neil, 1977):

$$1000\ln\alpha_{\text{calcite-water}} = 2.78(10^6/T^2) - 2.89 \quad (1)$$

where:

$$\alpha_{\text{calcite-water}} = (\delta_{\text{calcite}} + 1000)/(\delta_{\text{water}} + 1000) \quad (2)$$

Likewise the relationship between the C isotopic composition of HCO<sub>3</sub><sup>-</sup>, the dominant species in the DIC, calcite and, to a small extent, the temperature during equilibrium calcite precipitation is (Deines, 1974):

**TABLE 2.2: EQUILIBRIUM OXYGEN ISOTOPE FRACTIONATION ( $1000 \ln \alpha$ ) AT 26.6°C**

<u>Species Pair</u>	<u>Fractionation factor (‰)</u>	<u>Reference</u>
CaCO <sub>3</sub> – H <sub>2</sub> O	27.73	(Kim and O'Neil, 1997)
CO <sub>2</sub> (g) – CaCO <sub>3</sub>	12.55	(Bottinga, 1968)
CO <sub>2</sub> (g) – H <sub>2</sub> O	39.83	(Bottinga, 1968)
HCO <sub>3</sub> <sup>-</sup> (aq) – H <sub>2</sub> O (25°C)	34.0 <sup>a</sup>	(Usdowski and Hoefs, 1993)
CO <sub>2</sub> (g) – CO <sub>2</sub> (aq)	0.8‰ <sup>b</sup>	(Vogel et al., 1970)

a. this value is poorly constrained and is based on a reevaluation of an experiment first conducted by McCrea (McCrea, 1950).

b. this value is based on the equilibrium fractionation at 0°C. The magnitude of this fractionation will be less than this value at 26.6°C.

**Table 2.3: Equilibrium carbon isotope fractionation ( $1000 \ln \alpha$ ) at 26.6°C**

<u>Species Pairs</u>	<u>Fractionation Factor (‰)</u>	<u>Reference</u>
CaCO <sub>3</sub> – HCO <sub>3</sub> <sup>-</sup> (aq)	1.96	(Deines, 1974)
CO <sub>2</sub> (g) – CO <sub>2</sub> (aq)	1.05	(Vogel et al., 1970)
HCO <sub>3</sub> <sup>-</sup> (aq) - CO <sub>2</sub> (aq)	8.79	(Mook et al., 1974)
HCO <sub>3</sub> <sup>-</sup> (aq) - CO <sub>2</sub> (g)	7.77	(Mook et al., 1974)

$$1000\ln\alpha_{\text{calcite-HCO}_3^-} = 0.095(10^6 \cdot T^{-2}) + 0.90 \quad (3)$$

where:

$$\alpha_{\text{calcite-HCO}_3^-} = (\delta_{\text{calcite}} + 1000) / (\delta_{\text{HCO}_3^-} + 1000) \quad (4)$$

Note: T in equations (1) and (3) is in Kelvin

### **High-resolution sampling of modern calcite**

Glass plate calcite from the Upper Passage (BC-98-1, BC-98-2 and BC-98-3) and Spur 1 were sampled at high-resolution. Glass plate calcite deposited between July 1998 and February 1999 and between February 1999 and July 2000 was collected from the Upper Passage sites. Unfortunately, the plate in Spur 1 placed in February of 1999 was broken prior to collection so only the July 1998 to February 1999 time interval is available.

Approximately one square cm areas, near the locus of precipitation, on the plates were sampled in 20- $\mu\text{m}$  layers by moving the glass plate under a fixed dental drill and collecting the resulting powder for C and O isotopic analysis. The relative height of the glass plate and dental drill was monitored with the use of a digital micrometer with 1-micron resolution. The maximum thickness of glass plate calcite varied between the sites (Table 2.1). The thickness of the calcite decreased away from the locus of precipitation to less than 0.1mm near the glass plate's edge producing a calcite dome consistent with natural stalagmite formation. The area of maximum calcite thickness on the glass plates was the target of microsampling. Since the maximum calcite thickness varied between the glass plates, the time interval represented by each sample varied, estimated by assuming a constant calcite growth rate.

The lowest calcite thicknesses were seen in glass plate BC-98-4 where <0.1 mm of calcite was collected between July 1998 and February 1999. Not enough calcite grew at this site to allow the high-resolution sampling, so bulk sampling of the entire thickness of the calcite was performed.

There are three sources of error in determining the chronology of individual high resolution glass plate calcite samples: 1) A constant calcite growth rate was assumed. It is likely that initial calcite growth rates were slower while calcite crystals were nucleating on the glass plate surface and increased until the surface of the glass plate was completely covered by calcite. 2) In Spur 1 the drip was dry when the plate was collected, indicating non deposition. This was not the case in the Upper Passage. 3) Changes in growth rate, caused by changing drip water chemistry, could not be determined between sampling trips.

#### **Plate retrieval methodology**

During plate retrieval, the plates were rinsed in de-ionized water, applied using a squirt bottle, to remove residual cave drip water from the plate surface and prevent further calcite precipitation. The plate was then tilted so the de-ionized water would run off and a clean Kim-wipe was used to blot excess water from the plate edge. The plates were then stored in a clean, padded, Tupperware container for travel back to the University of Texas. Once back at the University of Texas, the plates were rinsed again in de-ionized water and allowed to dry in a hepa-filtered laminar flow hood in preparation for sample storage.

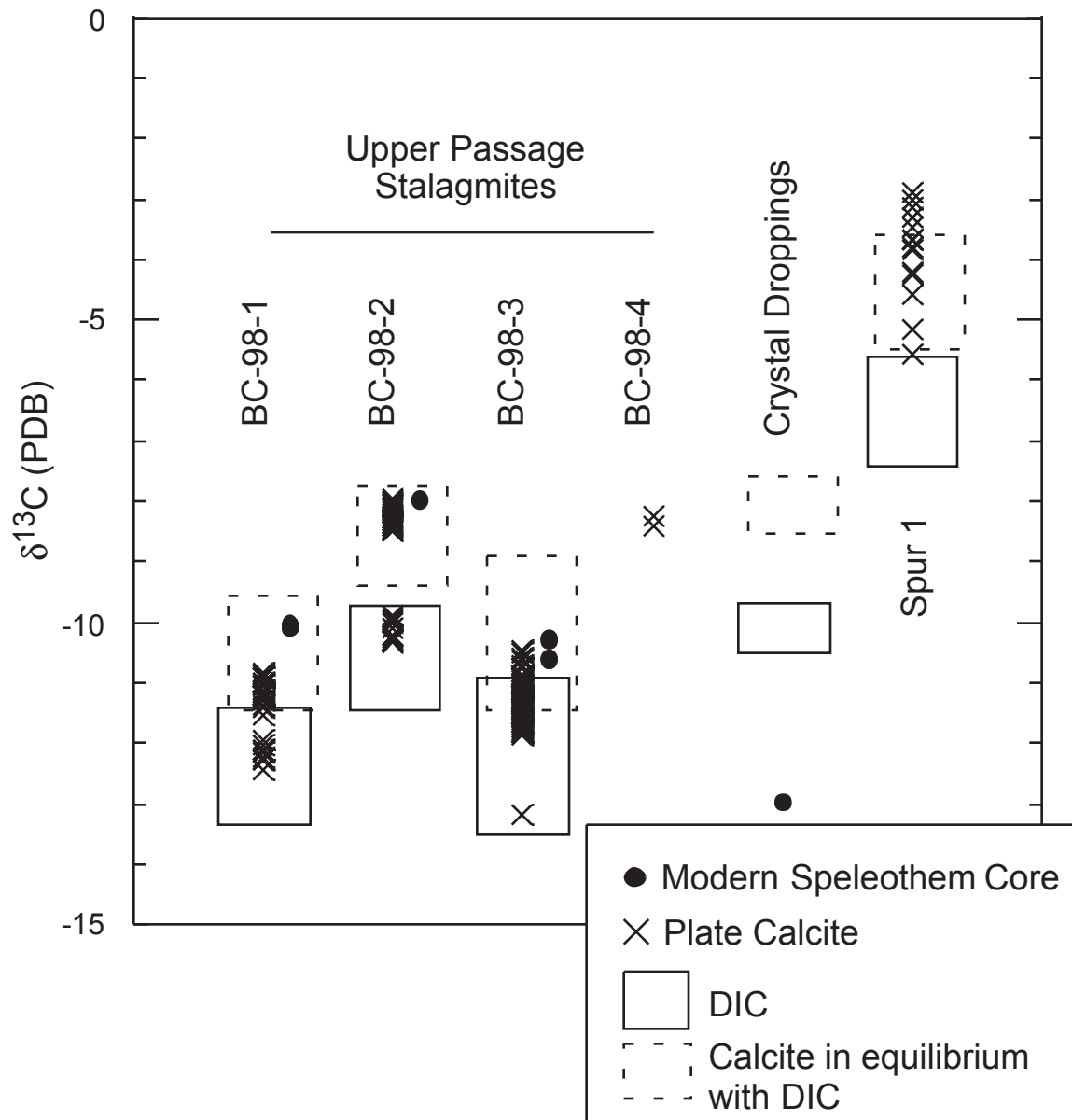


Figure 2.2. Carbon isotopic composition of modern calcite and dissolved inorganic carbon (DIC) in cave drip water in Harrison's Cave, Barbados, West Indies. Solid boxes represent the range of C isotopic compositions of DIC collected at the site. The dashed boxes represent the theoretical range of C isotopic compositions of calcite precipitated in isotopic equilibrium with the corresponding drip water. All the sites except Crystal Droppings have precipitated calcite with a C isotopic composition consistent with equilibrium precipitation. DIC values were not obtained from the BC-98-4 site due to the

## RESULTS

### Carbon isotopic results for modern speleothems

Modern speleothems collected at Harrison's Cave show a large C isotopic variability with  $\delta^{13}\text{C}$  values ranging from -13.2‰ to -2.9‰ PDB (Fig. 2.2). Large C isotopic variability is also seen in the composition of cave drip waters where the  $\delta^{13}\text{C}$  value of drip waters varies from -13.5‰ to -5.7‰ PDB. I assessed carbon isotopic equilibrium of modern speleothems by comparing fractionation factors (Table 2.3) with the C isotopic composition of the modern calcite and the dissolved inorganic carbon (DIC) in the drip water at 26.6°C, the average annual air temperature of Barbados. At the pH range of 7.3 to 8.1 of the cave drip waters, the majority of DIC occurs as  $\text{HCO}_3^-$  (aq) (Plummer and Busenberg, 1982) and at equilibrium the  $\delta^{13}\text{C}$  value of the  $\text{CaCO}_3$  formed from a drip water will be 1.96‰ higher than the  $\text{HCO}_3^-$  (aq) measured as DIC of the drip water.

The carbon isotope composition of modern speleothem calcite in Harrison's Cave ranges from values that are consistent with precipitation at isotopic equilibrium, to values slightly enriched (0.8‰) or depleted (-1.1‰) in  $^{13}\text{C}$  (Fig. 2.2), with Crystal Droppings being an exception. Only one of five sites tested (Spur 1) has calcite enriched in  $^{13}\text{C}$  relative to equilibrium. At four of five sites tested, (BC-98-1, BC-98-2, BC-98-3 and Spur 1) calcite samples show  $^{13}\text{C}$  depletions relative to equilibrium. The departures from equilibrium towards both higher and lower  $^{13}\text{C}$  values suggests that more than one mechanism may be responsible for the deviations from equilibrium.



Crystal Droppings is the only location tested with modern speleothems that are far from C isotopic equilibrium, with  $\delta^{13}\text{C}$  values 4.9‰ lower than calcite predicted to be in isotopic equilibrium with the average drip water collected at the site. The Crystal Droppings site is distinct because, unlike the other sampling sites, the calcite is not precipitated from a discrete drip but rather from a film of water that may have resulted from the coalescing of many sources. In addition, the water at Crystal Droppings was sampled at a spot where it first entered the cave but before it had a chance to travel over the flowstone where the calcite sample was taken. This is in contrast with the other sampling sites where the water enters the cave environment, flows a short distance down a corresponding stalactite, and is collected at the site of stalagmite precipitation. It is possible that the water that was collected at Crystal Droppings can not be directly compared to its corresponding calcite because of the drip water's flow path.

### **Sensitivity of C isotopes to seasonal changes**

Glass plate calcite, sampled at high-resolution at Spur 1 and the Upper Passage sites show that these two sites respond differently to seasonal variability. The  $\delta^{13}\text{C}$  values of the calcite from the Spur 1 plate show seasonal variability,  $\delta^{13}\text{C}$  increasing from -5.6‰ to -2.9‰ before decreasing to -3.7‰ (Fig. 2.4C). The glass plate calcite in the Upper Passage shows seasonal change similar to that of Spur 1, however, the range of the variation is much less. Site BC-98-3 shows the largest variation of approximately 1.2‰ within a single plate placed between February 1999 and July 2000. In addition, the timing of the maximum  $\delta^{13}\text{C}$  values varies between the Upper Passage glass plate calcite and the Spur 1 glass

plate calcite. In Spur 1, where drip rates are variable and respond to changes seasonal rainfall, the timing of the maximum  $\delta^{13}\text{C}$  values closely matches that of maximum rainfall, and highest drip rates. In the Upper Passage, where drip rates do not vary seasonally, the timing of the maximum  $\delta^{13}\text{C}$  values lags behind the maximum monthly rainfall by approximately 4 to 7 months (Fig. 2.4C).

### **Oxygen isotopic results for modern speleothems**

Modern speleothem cores and glass plate calcite collected at Harrison's Cave show lower O isotopic variability, relative to the C isotopic system, with  $\delta^{18}\text{O}$  values ranging from -5.3‰ to -3.0‰ PDB (Fig. 2.3). The corresponding drip waters also show lower O isotopic variability, with  $\delta^{18}\text{O}$  values from -3.6‰ to -3.0‰ SMOW. None of the modern speleothems collected in Harrison's Cave precipitated in O isotopic equilibrium with its corresponding drip water. The extent to which modern speleothems attained oxygen isotope equilibrium was assessed using the full range of O isotopic composition of drip waters collected in Harrison's Cave, fractionation factors (Table 2.2) and the mean annual temperature of Barbados, 26.6°C. Only one site, BC-98-4, from the Upper Passage, precipitated calcite close to oxygen isotopic equilibrium with its corresponding drip water, within 0.2‰. The drip associated with BC-98-4 was much slower than the other drips studied, and the thickness of calcite collected on the plate was the lowest (Table 2.1).

### **Sensitivity of O isotopes to seasonal change**

High resolution sampling of glass plate calcite grown in Spur 1 and the Upper Passage shows intra-annual O isotopic variability. Variations in the Spur 1

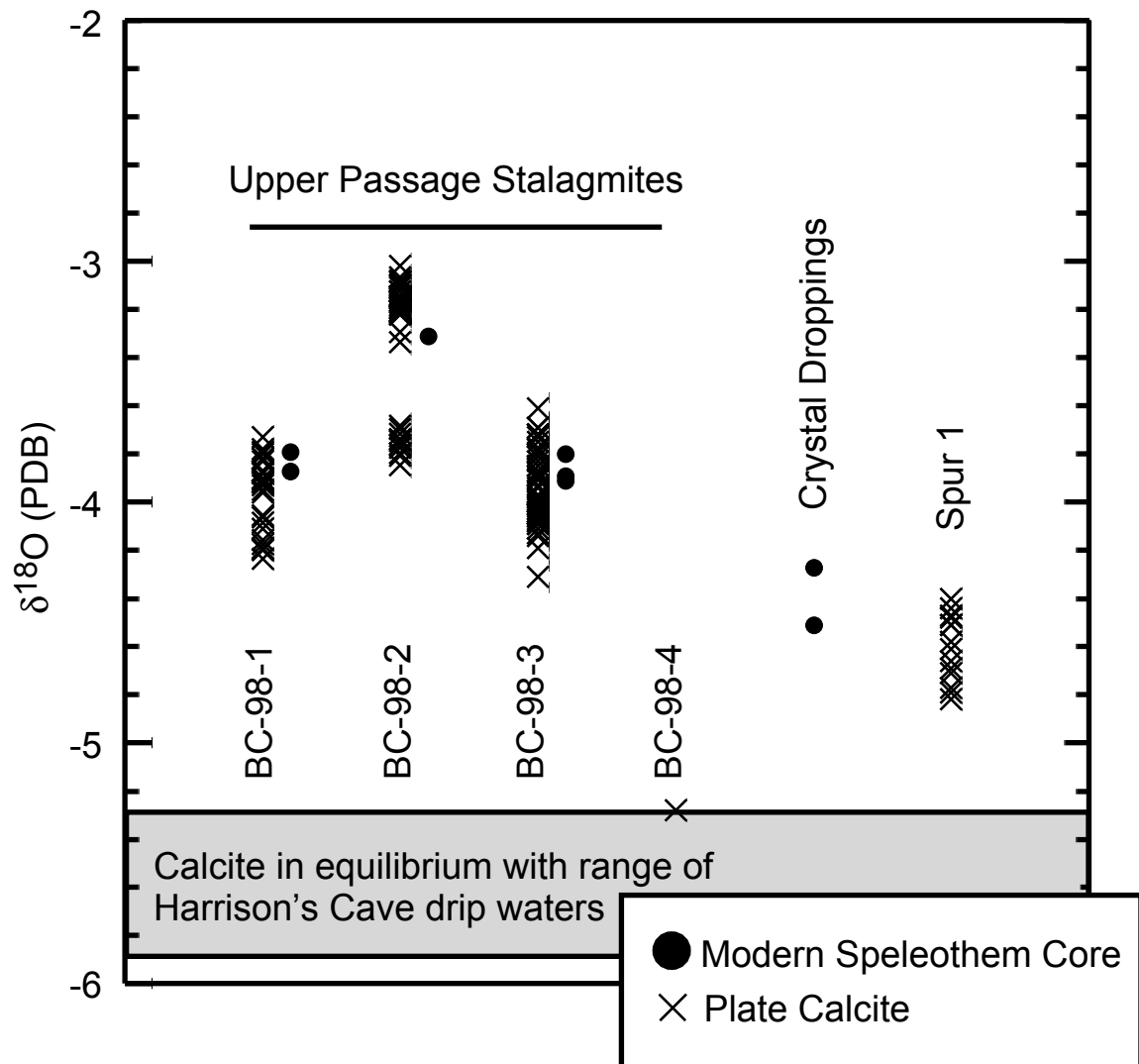


Fig. 2.3. Oxygen isotopic composition of modern calcite from Harrison's Cave, Barbados, West Indies. The theoretical O isotopic composition of calcite in isotopic equilibrium with the range of cave drip waters is indicated by the gray bar. Only BC-98-4 has precipitated calcite close to O isotopic equilibrium with cave water. All other sites are as much as 2.3‰ higher than equilibrium.

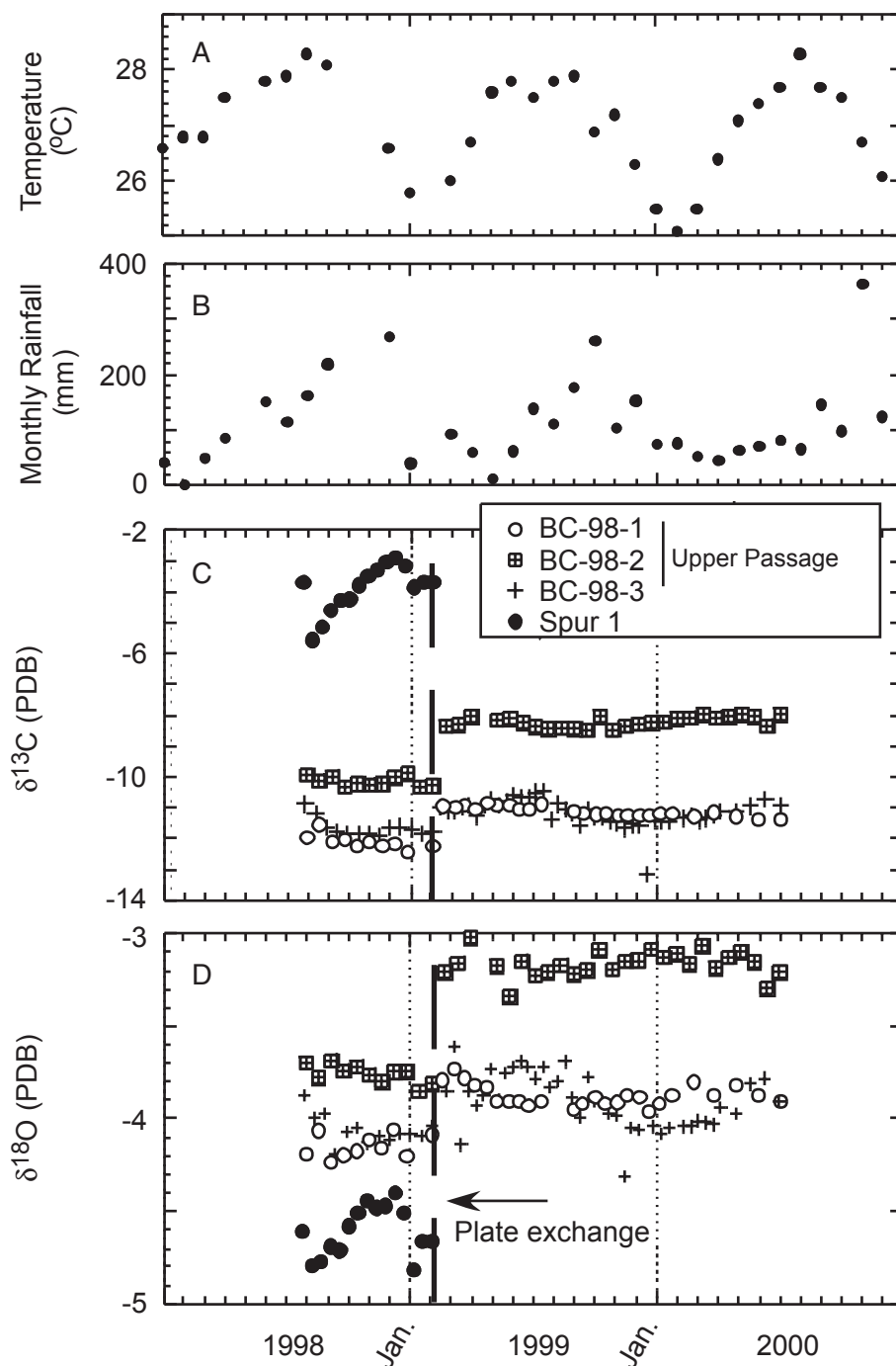


Figure 2.4A. Monthly rainfall totals and B. average monthly temperature collected from the Grantely Adams weather station, Barbados, and distributed by the National Climatic Data Center. C.  $\delta^{13}\text{C}$  vs. time and D)  $\delta^{18}\text{O}$  values vs. time for the calcite grown on glass plates and sampled at high-resolution.

glass plate calcite  $\delta^{18}\text{O}$  values correspond to intra-annual climate variability. The oxygen isotopic composition of the calcite increases from  $-4.8\text{‰}$  to  $-4.4\text{‰}$ , then decreases towards lower values of  $-4.7\text{‰}$  (Fig. 2.4D). The shift towards lower  $\delta^{18}\text{O}$  values is closer to isotopic equilibrium with the drip water, although equilibrium is not achieved. Similar to the  $\delta^{13}\text{C}$  values of the glass plate calcite from Spur 1, the timing of maximum  $\delta^{18}\text{O}$  values corresponds to maximum monthly rainfall amounts and higher drip rates.

The  $\delta^{18}\text{O}$  values of the Upper Passage glass plate calcite show a correspondence to intra-annual variability very similar to the  $\delta^{13}\text{C}$  values. The similarities include: 1) BC-98-3 has the largest variability of the three Upper Passage sites, approximately  $0.5\text{‰}$  between February 1999 and July 2000. 2) The timing of the maximum  $\delta^{18}\text{O}$  values of the Upper Passage sites lag behind the maximum  $\delta^{18}\text{O}$  values seen in Spur 1 by 4 to 7 months. 3) The magnitude of the  $\delta^{18}\text{O}$  shift is much greater in the Spur 1 site than the Upper Passage sites (Fig. 2.4D).

### **O and C isotopic shift during plate exchange**

In February of 1999, the glass plates were exchanged in the Upper Passage sites. The gap in time between glass plate collection and new glass plate deployment was only 24 hours, so the oldest calcite collected on the first glass plate should have the same  $\delta^{18}\text{O}$  and  $\delta^{13}\text{C}$  composition as the youngest calcite sample from the second glass plate. The samples are essentially coeval, yet there is an isotopic enrichment seen in both  $^{18}\text{O}$  and  $^{13}\text{C}$  in the Upper Passage glass

plates BC-98-1, BC-98-2 and BC-98-3 (Fig. 2.4). The largest enrichment, a  $\delta^{13}\text{C}$  increase of  $\sim 2.0\text{‰}$  and a  $\delta^{18}\text{O}$  increase of  $\sim 0.6\text{‰}$ , is recorded at the BC-98-2 site.

## DISCUSSION

Modern speleothems in Barbados have a range of  $\delta^{18}\text{O}$  and  $\delta^{13}\text{C}$  values that are consistent with precipitation under isotopic equilibrium to non-equilibrium conditions. The following lines of evidence indicate the operation of kinetic isotope effects. 1) The  $\delta^{18}\text{O}$  and  $\delta^{13}\text{C}$  composition of modern speleothems depart from equilibrium values calculated from the fractionation factors from the literature, the average temperature of Barbados, and  $\delta^{18}\text{O}$  and  $\delta^{13}\text{C}$  values of the waters feeding the modern calcite samples. 2) There is a  $\delta^{18}\text{O}$  and  $\delta^{13}\text{C}$  shift during glass plate exchanges at the Upper Passage sites. It is highly unlikely that there was a fundamental change in the isotopic system during the 24 hours between the placements of the glass plates. It is more likely that there was a change in the extent to which the kinetic isotope effects alter the isotopic composition of the calcite. Slight changes the sampling location relative to the locus of calcite precipitation is likely responsible for the isotopic shifts, rather than changes in climatic conditions within or outside the cave. There is a progressive  $^{13}\text{C}$  and  $^{18}\text{O}$  enrichment in the calcite away from the center of the plate. These spatial isotope variations in plate calcite are detailed in Chapter 3. 3) The  $\delta^{18}\text{O}$  and  $\delta^{13}\text{C}$  compositions of modern calcite co-vary. This is a proposed criterion for kinetic isotope effects in the formation of ancient speleothems (Hendy, 1971). Here I discuss the potential mechanistic controls on the extent of kinetic and equilibrium isotope effects.

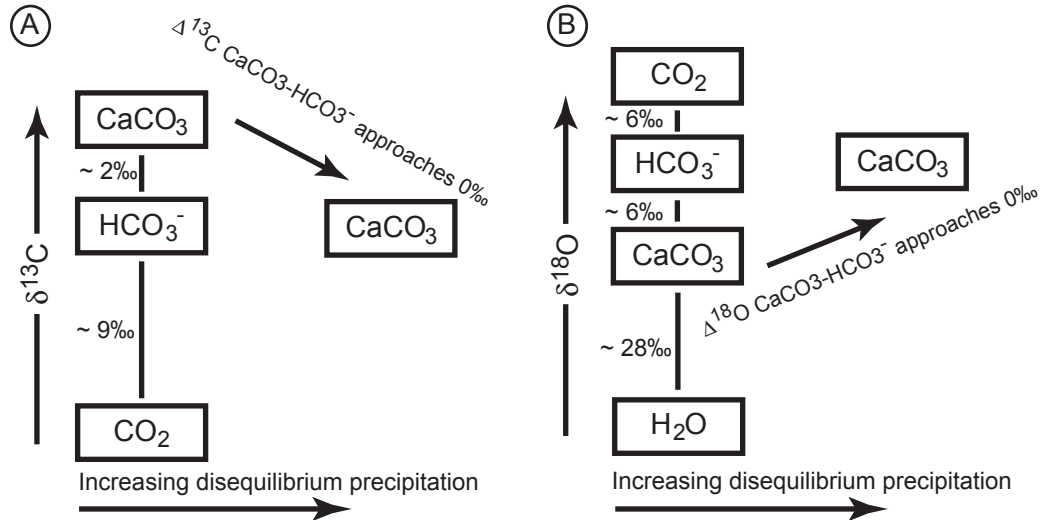
### **Controls on the $\delta^{13}\text{C}$ composition of modern speleothems**

The carbon isotope composition of modern speleothems in Harrison's Cave exhibit three ranges of values: 1)  $\delta^{13}\text{C}$  values consistent with equilibrium precipitation. 2) C isotope compositions that are lower than predicted equilibrium values but generally not lower than the  $\delta^{13}\text{C}$  value of the corresponding drip water's DIC. 3) C isotope compositions that are higher than predicted equilibrium values. Previous theoretical and laboratory studies may help explain the slight  $^{13}\text{C}$  enrichments and depletions seen in the modern calcite collected in Harrison's Cave.

#### **Control on $\delta^{13}\text{C}$ values lower than equilibrium values**

The  $\delta^{13}\text{C}$  values of modern calcite that depart from predicted equilibrium values towards lower values approach, and in some cases are equivalent to, the C isotopic compositions of DIC in its corresponding drip water (BC-98-1, BC-98-2 and BC-98-3). This process likely results from the incorporation of  $\text{HCO}_3^-$  (aq) into calcite during rapid mineral precipitation, such that isotopic fractionation is minimized (Michaelis et al., 1985). This mechanism is graphically portrayed as mechanism 1A (Fig. 2.5). Researchers studying kinetic isotopic behavior in rapidly precipitating calcite formation have observed similar results. Clark and Lauriol (1992) studied the  $\delta^{13}\text{C}$  and  $\delta^{18}\text{O}$  composition of calcite precipitated from rapidly frozen water in both laboratory and field based studies. They suggest that the  $^{13}\text{C}$  partitioning between calcite and DIC decreases from equilibrium conditions ( $\Delta^{13}\text{C}_{\text{CaCO}_3 - \text{HCO}_3^-} = 1.96\text{‰}$ ) to lower non-equilibrium values ( $\Delta^{13}\text{C}$

MECHANISM 1: Kinetically driven change in  $\text{CaCO}_3\text{-HCO}_3^-$



MECHANISM 2: Rayleigh distillation driven by  $\text{CO}_2$  degassing

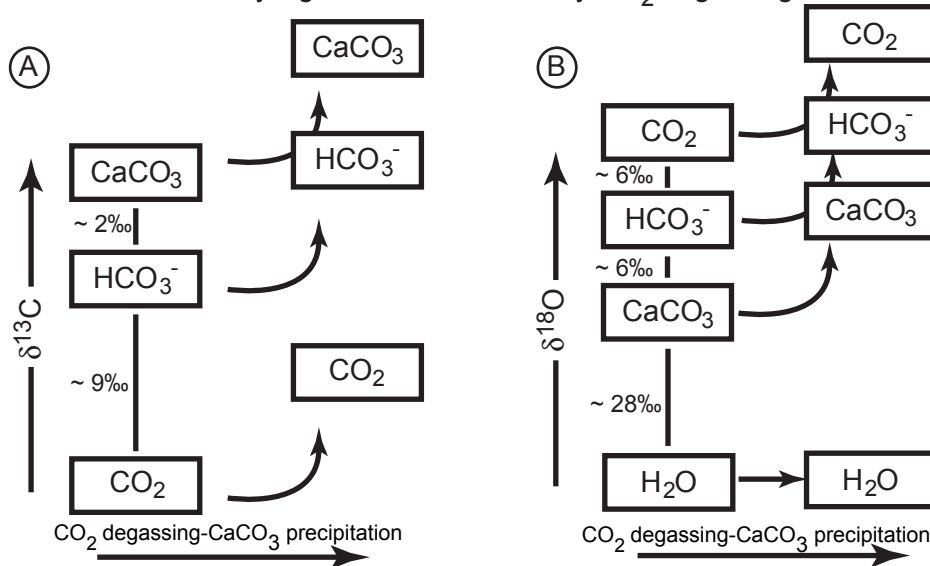


Figure 2.5. Graphical representation of the mechanisms discussed in text to account for  $\delta^{13}\text{C}$  enrichments and depletions and  $\delta^{18}\text{O}$  enrichments, relative to predicted equilibrium values, observed in modern speleothem calcite collected on Barbados. Equilibrium fractionation values outlined in Table 2 and 3 are represented here by ‰ values between phases. In instances where no fractionation factor is listed in the tables (in the case of the O isotope system the fractionation between  $\text{CaCO}_3$  and  $\text{HCO}_3^-$ , the fractionation factor is calculated by the difference of the other fractionation factors.



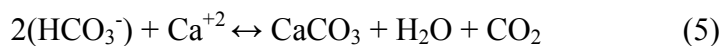
$\text{CaCO}_3 - \text{HCO}_3^-$  approaches 0‰) during kinetic isotope fractionation produced by rapid calcite precipitation.

### **Control on $\delta^{13}\text{C}$ values higher than equilibrium values**

Samples of glass plate calcite at Spur 1 show  $\delta^{13}\text{C}$  values that are higher than predicted by equilibrium precipitation (Fig. 2.2). There are two possible explanations for this behavior. 1) The calcite is precipitating in C isotopic equilibrium with its corresponding drip water but the full range of the  $\delta^{13}\text{C}$  values of drip water DIC has not been determined by intermittent sampling. 2) The calcite reflects disequilibrium precipitation likely resulting from  $^{13}\text{C}$  enrichment of the  $\text{HCO}_3^-$  (aq) reservoir caused by  $\text{CO}_2$  degassing.

Degassing is driven by the gradient between the  $P_{\text{CO}_2}$  of the cave drip water and the  $P_{\text{CO}_2}$  of the cave environment. The  $P_{\text{CO}_2}$  of the cave drip water is controlled by the  $P_{\text{CO}_2}$  of the soil zone, which can be ~2 orders of magnitude greater than atmospheric values. Large  $P_{\text{CO}_2}$  gradients engender fast degassing that may drive the dissolved inorganic carbon species away from isotopic equilibrium with respect to calcite.

The calcite dissolution/precipitation reaction can be expressed by the following equation:



$\text{CO}_2$  degasses from the solution into the cave environment's lower  $P_{\text{CO}_2}$  atmosphere, driving the dissolution/precipitation reaction to the right and causing speleothem  $\text{CaCO}_3$  precipitation. The equilibrium  $\delta^{13}\text{C}$  value of  $\text{CO}_2$  (g) at 26.6°C is 7.8‰ lower than the  $\text{HCO}_3^-$  (aq) (Table 2.3), and the  $\text{CaCO}_3$  is 2.0‰ higher

than the  $\text{HCO}_3^-$  (aq). As degassing of  $^{13}\text{C}$  depleted  $\text{CO}_2$  progresses, the reservoir of  $\text{HCO}_3^-$  (aq) will become isotopically heavier. The loss of isotopically heavy C via  $\text{CaCO}_3$  precipitation is not enough to offset the loss of the more  $^{13}\text{C}$ -depleted carbon via  $\text{CO}_2$  degassing. The  $\delta^{13}\text{C}$  value of the  $\text{HCO}_3^-$  (aq) reservoir will follow Rayleigh type distillation  $^{13}\text{C}$  enrichment as  $\text{CO}_2$  degassing continues (Michaelis et al., 1985; Dulinski and Rozanski, 1990). I use the term Rayleigh distillation to refer to the process by which the O and C isotopic composition of the reactant is modified by the formation of products having a different isotopic composition. These products do not react with the remaining reactant reservoir after formation. This mechanism is portrayed in mechanism 2A (Fig. 2.5).

The effects of Rayleigh distillation on the  $\delta^{13}\text{C}$  value of the  $\text{HCO}_3^-$  (aq) reservoir can be modeled by:

$$(\delta+1000)/(\delta_0+1000)=f^{(\alpha_{p-r}-1)} \quad (6)$$

where  $\delta$  is the C isotopic composition of  $\text{HCO}_3^-$  (aq),  $\delta_0$  is the initial C isotopic composition of  $\text{HCO}_3^-$  (aq),  $f$  is the fraction of  $\text{HCO}_3^-$  (aq) remaining and  $\alpha_{p-r}$  is the equilibrium fractionation factor between  $\text{HCO}_3^-$  (aq) and the bulk product. Because the C in  $\text{HCO}_3^-$  (aq) is evenly divided between  $\text{CaCO}_3$  and  $\text{CO}_2$  (g) during calcite precipitation, two fractionation factors must be considered. I define a fractionation factor between  $\text{HCO}_3^-$  (aq) and a bulk product such that  $\alpha_{(\text{bulk product} - \text{HCO}_3^-)}$  is  $1/2(\alpha_{\text{CO}_2-\text{HCO}_3^-}) + 1/2(\alpha_{\text{CaCO}_3-\text{HCO}_3^-})$ . This can be used to model the evolution of the  $\text{HCO}_3^-$  (aq) reservoir (Fig. 2.6).

Other authors have stated that because generally less than 10% of the DIC is lost to degassing, there is a negligible change to the isotopic composition of the

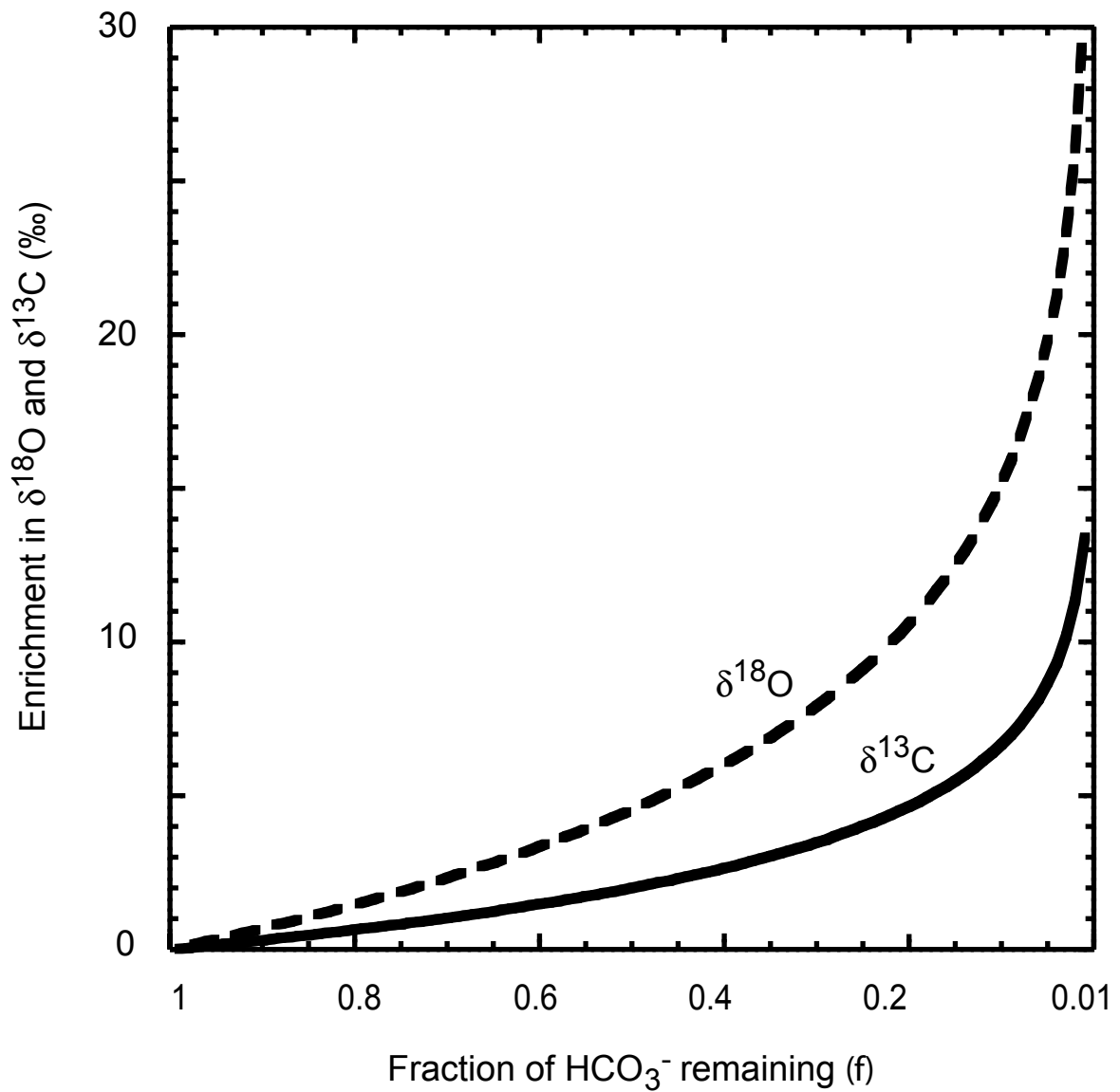


Figure 2.6. Rayleigh distillation model of the  $\delta^{13}\text{C}$  and  $\delta^{18}\text{O}$  values of  $\text{HCO}_3^-$  (aq) during  $\text{CO}_2$  degassing and  $\text{CaCO}_3$  precipitation. The  $\delta^{18}\text{O}$  curve does not consider  $\text{CO}_2$  hydration and hydroxylation reactions, which would buffer the  $\delta^{18}\text{O}$  composition of the  $\text{HCO}_3^-$  (aq) reservoir through isotopic exchange with the very large O reservoir held in  $\text{H}_2\text{O}$ . Thus, this is an end member condition and the  $^{18}\text{O}$  enrichments predicted by the model are not likely to be observed in natural systems. If Rayleigh distillation has any effect of the  $\delta^{13}\text{C}$  and  $\delta^{18}\text{O}$  values of calcite, it will manifest itself as a  $^{13}\text{C}$  and  $^{18}\text{O}$  enrichment.

$\text{HCO}_3^-$  (aq) reservoir due to the loss of isotopically light  $\text{CO}_2$  (Hendy, 1971; Clark and Lauriol, 1992). The observations in this study, where calcite was sampled close to the site of drip impact (analogous to sampling speleothems along their growth axis), support this conclusion. If any  $^{13}\text{C}$  enrichment was due to  $\text{CO}_2$  degassing, the effect was small (Fig. 2.2). Spur 1 shows maximum  $^{13}\text{C}$  enrichments of 0.8‰, which could result from the reaction of 24% of the  $\text{HCO}_3^-$  reservoir (Fig. 2.6). This is in contrast with other studies that predict large  $^{13}\text{C}$  enrichments, ~10‰, with relatively small change in the  $\text{HCO}_3^-$  (aq) reservoir (Dulinski and Rozanski, 1990).

In summary, my results suggest that two kinetic isotope processes could cause departures from predicted equilibrium values in the  $\delta^{13}\text{C}$  value of modern calcite. First, rapid calcite precipitation rates lower the  $\delta^{13}\text{C}$  value of calcite by lowering the C isotope fractionation between calcite and DIC from equilibrium values,  $\Delta^{13}\text{C}_{\text{CaCO}_3 - \text{HCO}_3^-} = 1.96$ , to non-equilibrium values,  $\Delta^{13}\text{C}_{\text{CaCO}_3 - \text{HCO}_3^-}$  approaching 0, (Clark and Lauriol, 1992). Second, rapid  $\text{CO}_2$  degassing could cause an increase the  $\delta^{13}\text{C}$  value of the modern speleothems through Rayleigh distillation of the  $\text{HCO}_3^-$  (aq) reservoir.

### **Controls on the $\delta^{18}\text{O}$ composition of modern speleothems**

There are distinct differences between the behavior of the O isotopic system and C isotopic system in modern speleothems in Harrison's Cave. The O isotopic compositions of modern speleothems are all higher than that predicted by the oxygen isotope equilibrium fractionation factor and no  $^{18}\text{O}$  depletions are observed. In addition, there are two important differences in the general

fractionation behavior between the C and O isotopic systems. 1) The O isotopic composition of  $\text{HCO}_3^-$  (aq) is buffered by the O reservoir within  $\text{H}_2\text{O}$  and the moderately fast rate of  $\text{CO}_2$  hydration/hydroxylation and dissociation (Mills and Urey, 1940). 2) The O isotopic composition of the  $\text{HCO}_3^-$  (aq) reservoir may not be as precisely predicted as the C isotopic composition of  $\text{HCO}_3^-$  (aq). Despite these differences, the behavior of the C isotopic system is helpful in interpreting the behavior of the O isotopic compositions of the modern calcite because the mechanisms driving calcite precipitation must affect both isotopic systems.

### **Control on $\delta^{18}\text{O}$ values higher than equilibrium values**

Kinetic isotope effects may be controlling the  $\delta^{18}\text{O}$  values of modern calcite in the same way that  $\delta^{13}\text{C}$  values are affected by the path outlined in mechanism 1A (Fig. 2.5). As calcite precipitation rates increase, the system departs from O isotopic equilibrium and the  $\Delta^{18}\text{O}_{\text{CaCO}_3 - \text{HCO}_3^-}$  value changes from a poorly constrained equilibrium value of  $\sim -6\text{‰}$  (Usdowski and Hoefs, 1993) to a disequilibrium value ( $\Delta^{18}\text{O}_{\text{CaCO}_3 - \text{HCO}_3^-}$  approaching 0). The  $\delta^{18}\text{O}$  value of the resulting calcite will approach the  $\delta^{18}\text{O}$  value of the  $\text{HCO}_3^-$  (aq) reservoir and the modern calcite will show an  $^{18}\text{O}$  enrichment (Clark and Lauriol, 1992). This mechanism is akin to that causing the small  $^{13}\text{C}$  depletions observed in the same specimens (Fig. 2.5, mechanism 1B).

If the  $\Delta^{18}\text{O}_{\text{CaCO}_3 - \text{HCO}_3^-}$  value approaches 0 then the modern calcite in Harrison's Cave would show an  $^{18}\text{O}$  enrichment of up to 6‰ relative to equilibrium values. The observed  $^{18}\text{O}$  enrichments are 0.2‰ to 2.3‰ (Fig. 2.3). This suggests that either; 1)  $\Delta^{18}\text{O}_{\text{CaCO}_3 - \text{HCO}_3^-}$  never reaches 0 during calcite

precipitation and, thus, the kinetic isotope effects of direct  $\text{HCO}_3^-$  (aq) assimilation into calcite are modulated from the maximum possible effect, or 2) the O isotopic fractionation factor between  $\text{HCO}_3^-$  -  $\text{H}_2\text{O}$  is less than the 6‰ reported by Usdowski and Hoefs, (1993). Clark and Lauriol (1992) report kinetically controlled  $^{18}\text{O}$  enrichments in cryogenic calcites that average  $5.5 \pm 0.5\text{‰}$ . This is consistent with the  $\Delta^{18}\text{O}_{\text{CaCO}_3\text{-HCO}_3^-}$  value approaching 0 and the  $\text{HCO}_3^-$  -  $\text{H}_2\text{O}$  O isotopic fractionation factors reported by Usdowski and Hoefs, (1993).

### **Uncertainties in bicarbonate oxygen isotope fractionation factors**

The C isotopic fractionation factors between the inorganic carbon species of interest in speleothem formation are well known, however the O isotopic fractionation factors for DIC species are not precisely known because of difficulty in the analytical determination of their isotopic compositions. The C isotopic composition of  $\text{HCO}_3^-$  (aq) is analytically determined by quantitative conversion of the DIC (dominantly  $\text{HCO}_3^-$ ) to  $\text{CO}_2$  (g), measurement of the  $\delta^{13}\text{C}$  value of this  $\text{CO}_2$ , followed by a pH dependent correction for other minor DIC species. Because no other inorganic reservoir of dissolved carbon exists, there is no possibility of isotopic exchange reactions altering the C isotopic composition of this  $\text{CO}_2$ . This method, however, cannot be used to determine the O isotopic composition of the  $\text{HCO}_3^-$  (aq) because as  $\text{HCO}_3^-$  (aq) is converted to  $\text{CO}_2$ , it will continue to undergo oxygen isotope exchange reactions with  $\text{H}_2\text{O}$  via  $\text{CO}_2$  hydration and hydroxylation (Eq. 7 and 8) in the reaction vessel. The O isotopic composition of the collected  $\text{CO}_2$  will likely lie somewhere between the  $\delta^{18}\text{O}$

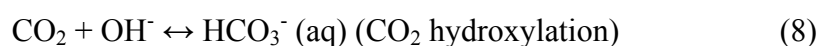
value of the  $\text{HCO}_3^-$  (aq) and the  $\delta^{18}\text{O}$  value of  $\text{CO}_2$  in isotopic equilibrium with the  $\text{H}_2\text{O}$ . Because the O isotopic fractionation factors between  $\text{HCO}_3^-$  (aq) -  $\text{CaCO}_3$  and  $\text{HCO}_3^-$  (aq) -  $\text{CO}_2$  (g) cannot be precisely determined, the effect of  $\text{CO}_2$  degassing and  $\text{CaCO}_3$  precipitation on the O isotopic composition of  $\text{HCO}_3^-$  (aq) is impossible to determine by direct measurement and, thus, theoretical models must be used (Uzdowski and Hoefs, 1993).

### **Potential effect of Rayleigh distillation on $\delta^{18}\text{O}$ compositions**

The effect of  $\text{CO}_2$  degassing on the  $\delta^{18}\text{O}$  value of calcite may be assessed using the same pathway outlined in mechanism 2A for the carbon isotopic system (see mechanism 2B, Fig. 2.5). The O isotopic composition of  $\text{HCO}_3^-$  (aq) is buffered by two isotopic exchange reactions with  $\text{H}_2\text{O}$ ,  $\text{CO}_2$  hydration and  $\text{CO}_2$  hydroxylation and their corresponding reverse reactions:



and



In comparison to the rates of the  $\text{CO}_2$  hydration and hydroxylation reactions, the protonation of  $\text{CO}_3^{2-}$  and de-protonation of  $\text{HCO}_3^-$  (aq) are nearly instantaneous (Mills and Urey, 1940), and so are not considered further. If  $\text{CO}_2$  degassing and calcite precipitation proceed faster than the  $\text{CO}_2$  hydration and hydroxylation reactions, then the  $\text{HCO}_3^-$  (aq) may deviate from O isotopic equilibrium with the water. In this case, the  $\delta^{18}\text{O}$  value of the  $\text{CaCO}_3$  may reflect the instantaneous  $\delta^{18}\text{O}$  value of the  $\text{HCO}_3^-$  (aq) rather than that of the  $\text{H}_2\text{O}$ . The effect of  $\text{CO}_2$  degassing will range from no effect when O isotope exchange

reactions keep up with calcite precipitation reactions and the  $\text{HCO}_3^-$  (aq) remains in O isotopic equilibrium with  $\text{H}_2\text{O}$ , to a system governed by a Rayleigh distillation process, where the  $\delta^{18}\text{O}$  value of  $\text{CaCO}_3$  reflects the evolution of the  $\delta^{18}\text{O}$  value of the bicarbonate reservoir.

I attempt to model the oxygen isotope effects of  $\text{CO}_2$  degassing using a Rayleigh distillation approach with the following assumptions: 1) there is no oxygen isotope exchange between the DIC and the water, 2) the  $\Delta^{18}\text{O}_{\text{CO}_2-\text{HCO}_3^-}$  is  $\sim 6\text{‰}$ , and 3) the fractionation factor between bulk products and  $\text{HCO}_3^-$  (reactant) is  $2/6(\alpha_{\text{CO}_2-\text{HCO}_3^-}) + 3/6(\alpha_{\text{CaCO}_3-\text{HCO}_3^-}) + 1/6(\alpha_{\text{H}_2\text{O}-\text{HCO}_3^-})$  (in other words, in proportion to the amount of oxygen in each product). The result of this model is given in Fig. 2.6 and suggests that  $\text{CO}_2$  degassing could cause an  $^{18}\text{O}$  enrichment in the resulting calcite with respect to equilibrium with water. This result, however, is only an end member calculation because it neglects  $\text{CO}_2$  hydration and hydroxylation reactions which will buffer the isotopic composition of the  $\text{HCO}_3^-$  (aq) reservoir and reduce the magnitude of the isotope effects of  $\text{CO}_2$  degassing. Nonetheless, this calculation should provide the correct sign to the isotope effect of  $\text{CO}_2$  degassing on speleothem calcite.

It may be impossible to determine the relative contributions to calcite  $\delta^{18}\text{O}$  values from  $\text{CO}_2$  degassing (Mechanism 2B, Fig. 2.6) vs. changes in the  $\Delta^{18}\text{O}_{\text{CaCO}_3-\text{HCO}_3^-}$  due to rapid precipitation of calcite (Mechanism 1B, Fig. 2.6). However, both of these mechanisms of kinetic isotope fractionation should cause speleothem calcite to be enriched in  $^{18}\text{O}$  with respect to isotopic equilibrium with drip water, and both mechanisms may be active given their apparent effects on the



carbon isotope deviations from isotopic equilibrium in the same speleothem calcite samples.

### **High-resolution variations in plate calcite**

The glass plate calcite appears to record temporal variations in  $\delta^{13}\text{C}$  and  $\delta^{18}\text{O}$  values which directly or indirectly reflect seasonal changes in air temperature or rainfall on Barbados. The  $\delta^{13}\text{C}$  and  $\delta^{18}\text{O}$  values of glass plate calcite from Spur 1 correspond to changes in rainfall. This is significant because the identification of seasonally controlled changes in speleothem chemistry has the potential to aid in chronologic control and provide insights into inter-annual climatic variability in speleothem studies (Shopov et al., 1994; Roberts et al., 1998). In Harrison's Cave, several variables may influence the isotopic composition of the calcite. I evaluate here the potential control of seasonal changes in temperature and rainfall on the  $\delta^{18}\text{O}$  and  $\delta^{13}\text{C}$  composition of glass plate calcite in Harrison's Cave.

Over the time interval during which the Spur 1 glass plate collected calcite, the mean monthly air temperature dropped from approximately 28.5°C to 25.5°C (Fig. 2.4A). The isotopic shifts seen in  $\delta^{13}\text{C}$ , approximately 5‰, are much larger than those seen in  $\delta^{18}\text{O}$ , approximately 0.4‰. Although changes in temperature will affect the fractionation factors of the C species, the effect will be much smaller (<0.01‰/°C) than that seen in O isotopes (0.2‰/°C). Temperature alone cannot be responsible for the magnitude of the C-isotopic shift observed. Thus, changes in monthly mean temperature are likely not the cause of the observed isotopic shifts.

The glass plates were placed before and collected after the wet season. Because the drip rate at the Spur 1 site is sensitive to changes in precipitation it is likely that the drip rate at the site mirrors the monthly precipitation curve. The temporal variations in Spur 1 glass plate calcite O and C isotopic compositions are synchronous, although they differ in magnitude with peak isotope ratios coinciding with time of peak precipitation. Kinetic and equilibrium isotope effects previously discussed may explain the synchronous changes in calcite  $\delta^{18}\text{O}$  and  $\delta^{13}\text{C}$  values. If increasing drip rates in Spur 1 caused an increase in calcite precipitation rates and/or an increase in the percentage of  $\text{HCO}_3^-$  (aq) incorporated into glass plate calcite, the isotopic composition of the calcite may be affected in the following ways: 1) As calcite precipitation rates increase, the  $\delta^{13}\text{C}$  values of the calcite will become isotopically heavier as the  $\text{HCO}_3^-$  (aq) reservoir is enriched in  $^{13}\text{C}$  by increased Rayleigh distillation. 2) At the same time,  $\delta^{18}\text{O}$  values of calcite will become isotopically heavier as increased precipitation rates lower the fractionation between  $\text{HCO}_3^-$  (aq) and  $\text{CaCO}_3$ . Rayleigh distillation may or may not affect the O-isotopic system because of reasons outlined in the section entitled *Potential effect of Rayleigh distillation on  $\delta^{18}\text{O}$  compositions*. Thus, the observed changes in the  $\delta^{18}\text{O}$  and  $\delta^{13}\text{C}$  values of the glass plate calcite may be caused by both kinetic and equilibrium isotope effects.

Calcite grown on the glass plates from the Upper Passage shows similar temporal isotopic variations seen in the Spur 1 glass plate calcite, but the isotopic shifts are smaller and lag behind the shifts seen in Spur 1 glass plate calcite. Because the two sites show the same general trend in both isotopic systems, it is

likely that the same mechanisms are responsible for the isotopic shifts seen in the Upper Passage and Spur 1. Differences in the magnitude and timing of the shifts are likely due to differences in hydrologic conditions at the drip sites. The drips feeding water to the Upper Passage drip sites are generally slower and do not show the variability in drip rates observed in Spur 1 (Table 2.1). The more consistent hydrologic conditions found in the Upper Passage drip sites result in lower O and C isotopic variability. There is likely more mixing of slow and fast flow path water feeding the Upper Passage drip sites resulting in a smoothing of the climate signal and an averaging  $\delta^{18}\text{O}$  and  $\delta^{13}\text{C}$  values.

## CONCLUSIONS

The precipitation of speleothem calcite in O and C isotopic equilibrium with its corresponding drip water can not be assumed. This fact was known early in speleothem research, resulting in tests to identify equilibrium precipitation (Hendy, 1971). This study represents a contribution to speleothem-based climate studies by not only outlining new definitive tests for O and C isotopic equilibrium in modern speleothems, but also by determining the magnitude and direction of offsets from equilibrium. These offsets were used to propose mechanisms responsible for the non-equilibrium isotope effects observed. Mechanism 1 results in changes in the fractionation between  $\text{HCO}_3^-$  (aq) and  $\text{CaCO}_3$  from equilibrium towards lower values resulting in  $^{13}\text{C}$  depletions and  $^{18}\text{O}$  enrichments in speleothem calcite. Mechanism 2 results in both  $^{13}\text{C}$  and  $^{18}\text{O}$  enrichments in speleothem calcite caused by Rayleigh distillation in the  $\text{HCO}_3^-$  (aq) reservoir and the calcite precipitated from it.

This study has implications for paleoclimate studies that use ancient speleothems, deposited in the past when the water from which the speleothem precipitated could not be directly measured. Firstly, this study demonstrates that even in areas that one may expect speleothems to be precipitated in O and C isotopic equilibrium, significant non-equilibrium isotope effects may be operating. If C and O isotopic equilibrium in modern speleothems from a cave environment can be demonstrated, then the stable isotopic composition of ancient speleothems, from that same environment, may be interpreted with greater confidence. In addition, the study of glass plate calcite is non-destructive, such that a great number of speleothem sites can be studied with no negative effect on the cave, such as breakage or drilling. Prior to speleothem collection, the glass plate methods outlined in this paper will allow the assessment of the extent to which calcite achieves O and C isotopic equilibrium in the modern system. This will allow the identification of speleothems best suited for paleoclimatic studies. Aside from the larger issues of data quality, this methodology is a significant contribution to cave conservation.

### **CHAPTER 3: LARGE KINETIC ISOTOPE EFFECTS IN MODERN SPELEOTHEMS**

#### **ABSTRACT**

Temporal variations in the O and C isotopic composition of calcium carbonate speleothems, which are secondary cements formed in caves, have been used to infer past environmental change. Variations in climatic parameters, recorded in speleothem geochemical proxies, are reconstructed by extracting calcite samples along the growth axes of speleothems.

In this study, modern speleothem calcite was grown on glass plates, placed on the top of actively growing stalagmites, at three locations in Harrison's Cave, Barbados. Collecting modern speleothems allows the comparison of the stable isotopic composition of calcite with its corresponding drip water to assess the degree to which isotopic equilibrium precipitation is attained. Each site deposited calcite with a unique  $\delta^{18}\text{O}$  and  $\delta^{13}\text{C}$  composition. On each plate, speleothem calcite sampled progressively farther from the growth axis exhibits a linear increase in both  $\delta^{13}\text{C}$  and  $\delta^{18}\text{O}$  values. This increase is away from O and C isotopic equilibrium with the calcite's corresponding drip water. This trend is likely a result of  $^{18}\text{O}$  and  $^{13}\text{C}$  Rayleigh-distillation enrichment in the  $\text{HCO}_3^-$  reservoir due to progressive  $\text{CO}_2$  degassing and  $\text{CaCO}_3$  precipitation. The extent of isotopic enrichment at each plate site may be a function of the amount of calcite precipitated on the drip's corresponding stalactite that feeds each plate. The slope of the  $\delta^{13}\text{C}$  vs.  $\delta^{18}\text{O}$  trend is likely controlled by the ability of  $\text{CO}_2$

hydration/hydroxylation reactions to buffer the O isotopic composition of the  $\text{HCO}_3^-$  reservoir. Modern speleothem calcite and four of five ancient Barbados speleothems, sampled temporally along the growth axis, show similar consistent  $\delta^{13}\text{C}$  vs.  $\delta^{18}\text{O}$  trends. This suggests that the  $\delta^{13}\text{C}$  and  $\delta^{18}\text{O}$  composition of speleothem calcite is in part controlled by non-equilibrium isotope effects and these effects influence temporal  $\delta^{13}\text{C}$  and  $\delta^{18}\text{O}$  isotopic records produced from ancient speleothems collected on Barbados.

The majority of stable isotopic studies on speleothems, compiled from the literature, show a positive covariation between  $\delta^{13}\text{C}$  and  $\delta^{18}\text{O}$  values sampled along the growth axis (62% of 141 studies). It is likely that the stable isotopic composition of some speleothems used in these studies is controlled by the non equilibrium processes outlined in this paper. Direct application of equilibrium fractionation factors may be unwarranted when interpreting speleothem stable isotopic variability.

## INTRODUCTION

The geochemistry of speleothems, which are secondary mineral cements formed in caves, may be used to infer past environmental change. Speleothems, in particular stalagmites, have the potential to be a powerful tool in climatic studies because: 1) The isotopic and chemical composition of speleothems records temporal changes in groundwater chemistry that may be controlled by local environmental conditions (Banner et al., 1996; Bar-Matthews et al., 2000). 2) Speleothems can be continuously deposited over thousands of years and can be placed into a precise chronostratigraphy using U series dating techniques (Edwards et al., 1987; Musgrove et al., 2001), and 3) Speleothems can form in low altitude, low latitude, terrestrial environments where other high-resolution climatic records may be absent. These factors can combine to produce a long continuous high-resolution record of terrestrial climate change.

The O and C isotopic composition of calcite speleothems, particularly stalagmites, are of particular interest to climate researchers.  $\delta^{18}\text{O}$  variations in speleothems have been used to infer the following; temporal changes in cave temperature, which is approximately equivalent to the mean annual temperature outside the cave environment (Hendy and Wilson, 1968; Hendy, 1969; Tan et al., 2003) and average  $\delta^{18}\text{O}$  value of precipitation (Hellstrom et al., 1998), which may reflect ice volume or atmospheric temperature effects (Harmon et al., 1978b).  $\delta^{13}\text{C}$  variations in speleothems have been used to infer: 1) relative proportions of  $\text{C}_3$  vs.  $\text{C}_4$  plants controlling the  $\delta^{13}\text{C}$  value of organic carbon ( $\text{C}_{\text{org}}$ ) (Holmgren et al., 1995). 2) Changes in ecosystem productivity controlling soil  $\text{P}_{\text{CO}_2}$  (Frappier

et al., 2002). 3) Changes in the  $\delta^{13}\text{C}$  value of atmospheric  $\text{CO}_2$  (Baskaran and Krishnamurthy, 1993). 4) changes in water/rock interactions (Musgrove, 2000). More detailed explanations outlining the interpretations of stable isotope ratios of speleothems in climatic studies can be found in the literature (Hendy, 1971; Gascoyne, 1992; Lauritzen, 1995; Desmarchelier et al., 2000). When interpreting the stable isotopic composition of speleothem stable a common assumption is that calcite is precipitated in C and O isotopic equilibrium with its corresponding drip.

#### **HENDY'S TESTS FOR EQUILIBRIUM PRECIPITATION**

In order for temperature dependant equilibrium fractionation factors to be used in interpreting speleothem stable isotope records, the speleothems must be precipitated in isotopic equilibrium. The requirement for speleothems to be precipitated in C and O isotope equilibrium with their corresponding drip water was recognized early in speleothem studies. Hendy and Wilson (1971) suggested the following tests for isotopic equilibrium precipitation of speleothems: 1)  $\delta^{18}\text{O}$  and  $\delta^{13}\text{C}$  values of samples along a single growth layer of a speleothem should lack a progressive increase away from the growth axis of the speleothem. Cartoon depiction of growth axis and growth layer sampling scheme is given in Fig. 3.1, inset A. 2)  $\delta^{18}\text{O}$  and  $\delta^{13}\text{C}$  values of samples taken along a single growth layer should not be positively correlated. Criteria 1 and 2 may be dismissed by calling on the difficulty of sampling a discrete layer as it thins away from the growth axis. 3) Samples taken along the growth axis should lack a positive correlation in  $\delta^{18}\text{O}$  and  $\delta^{13}\text{C}$  values. This last criterion has been disputed by other



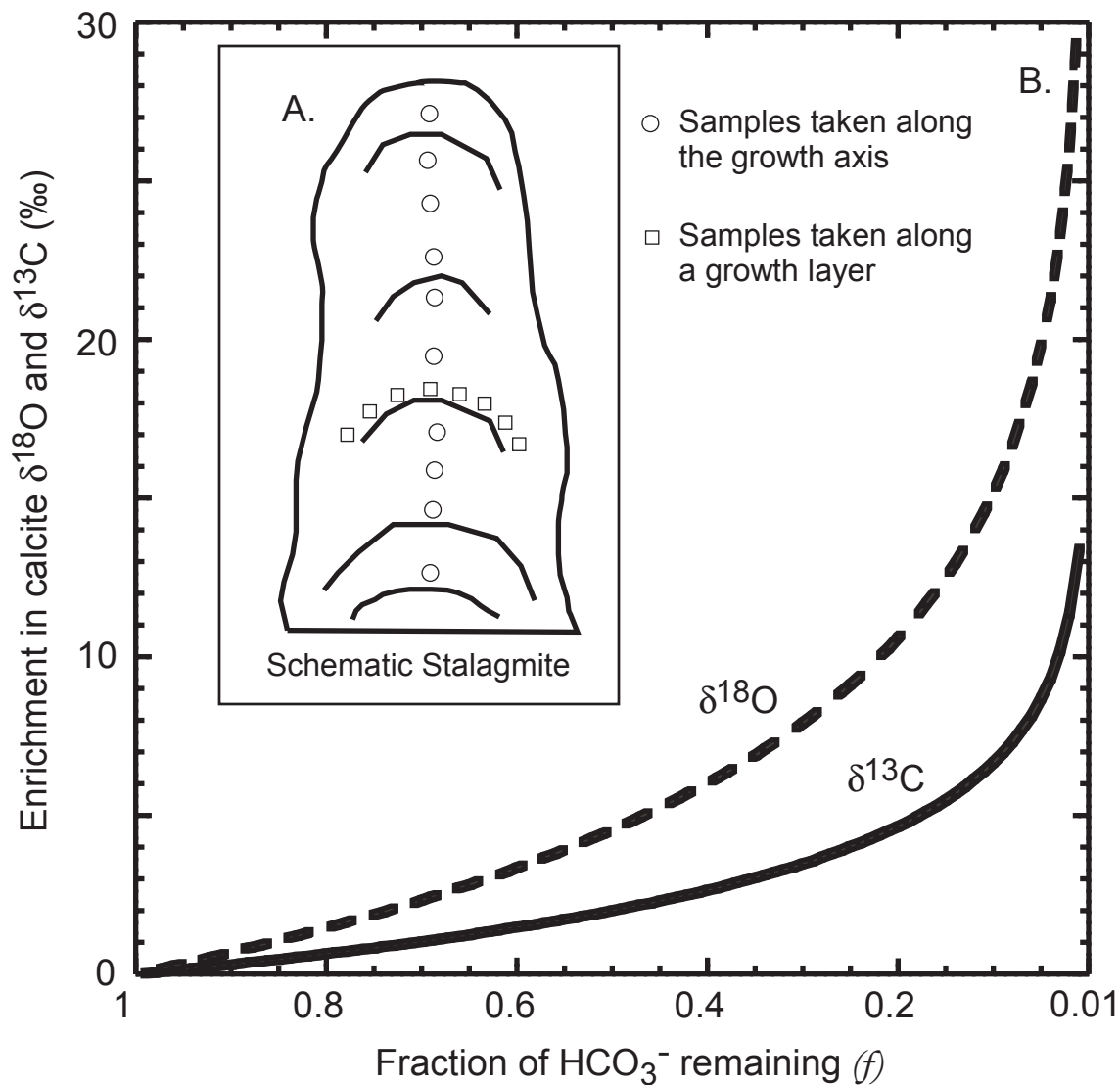


Figure 3.1. A. Schematic diagram of a stalagmite showing the geometry of samples taken along a growth axis, open circles, and samples taken along a growth layer, open squares. B. Rayleigh distillation model of the  $\delta^{13}\text{C}$  and  $\delta^{18}\text{O}$  values of  $\text{CaCO}_3$  during progressive  $\text{CO}_2$  degassing and  $\text{CaCO}_3$  precipitation. The  $\delta^{18}\text{O}$  curve neglects  $\text{CO}_2$  hydration and hydroxylation reactions, which would buffer the  $\delta^{18}\text{O}$  composition of the  $\text{HCO}_3^-$  (aq) reservoir through isotopic exchange with the very large O reservoir held in  $\text{H}_2\text{O}$ . Thus, this is an end member condition and the  $\delta^{18}\text{O}$  enrichments predicted by the model are not likely to be observed in natural systems (Fig. 6, curve b). This model can be used to predict the  $\delta^{13}\text{C}$  evolution during calcite precipitation if equilibrium fractionation between the carbon species is maintained.

authors who attribute the positive correlation in  $\delta^{18}\text{O}$  and  $\delta^{13}\text{C}$  values of calcite along the growth axis to represent environmental change affecting both vegetation ( $\delta^{13}\text{C}$ ) and the  $\delta^{18}\text{O}$  of precipitation. Failure of speleothems to pass these three tests is thought to result from rapid  $\text{CO}_2$  degassing and calcite precipitation.

Positive  $\delta^{18}\text{O}$  and  $\delta^{13}\text{C}$  covariation in speleothem calcite can be caused by two alternative mechanisms. First, the operation of kinetic isotope effects caused by progressive  $\text{CO}_2$  degassing and calcite precipitation (Hendy, 1971), and second, changes in environmental conditions that simultaneously produce increases (or decreases) in the  $\delta^{18}\text{O}$  and  $\delta^{13}\text{C}$  value of speleothem calcite. This study documents the extent to which kinetic isotope effects produce a positive stable isotopic covariation with a consistent  $\delta^{13}\text{C}$  vs.  $\delta^{18}\text{O}$  slope in modern speleothems from Harrison's Cave, Barbados. In addition, this study shows that the majority of stable isotope speleothem records, compiled from the literature, also show positive correlation between  $\delta^{18}\text{O}$  and  $\delta^{13}\text{C}$  values. This suggests that kinetic isotope effects may commonly influence speleothem stable isotope records.

## **MODERN SPELEOTHEMS**

In this study I compare the isotopic compositions of speleothem calcite and the water from which the speleothems precipitate in order to assess conditions where isotopic equilibrium and non-equilibrium occur. I refer to modern speleothems as the tips of actively growing stalagmites and calcite grown on frosted glass plates placed on those stalagmites (Fig. 3.2). The analysis of the spatial variations in  $\delta^{18}\text{O}$  and  $\delta^{13}\text{C}$  values of calcite grown on these plates is

analogous to Hendy's tests (Hendy, 1971) on calcite along single growth layers in ancient speleothems (tests 1 and 2) with three important distinctions: 1) There is no ambiguity regarding the age of the glass plate calcite layer because the timing of the placement and collection of the plate is precisely known. Stalagmite growth layers thin away from the growth axis so the ability to sample the same time interval along a growth layer is dependent on the resolution of the sampling method. This introduces errors that increase as growth layers thin. 2) Glass plate calcite can be sampled in any direction relative to the growth axis. Natural speleothems, which are commonly sliced in half, allow sampling along only one plane. 3) The C and O isotopic composition of the corresponding drip water, and the temperature of formation, can be measured and compared to the corresponding glass plate calcite, providing a direct test for C and O isotopic equilibrium precipitation.

## **SAMPLE SITE AND DESCRIPTION**

Modern speleothem calcite was sampled from the tips of three actively forming stalagmites from Harrison's Cave. The three stalagmites are located in the Upper Passage and occupy an area of approximately one m<sup>2</sup> (Fig. 3.2). A map of Harrison's Cave showing the sample locations have been published elsewhere (Wefer, 1994; Banner et al., 1996; Mickler et al., 2003). I would expect that conditions in the Upper Passage sites are the most conducive to the precipitation of speleothems in isotopic equilibrium with their corresponding drip water. Speleothems at this site form under high humidity conditions (>98.2% RH), from



Figure 3.2 Glass plates experiment at stalagmite sites BC-98-1, 2 and 3 in the Upper Passage, Harrison's Cave, Barbados, West Indies.

relatively slow steady drips. These conditions limit evaporative  $^{18}\text{O}$  enrichment in the drip water and may limit kinetic isotope effects caused by large variations in drip rates and the accompanying changes in drip water chemistry.

All three stalagmites are approximately 1 m in height and of comparable diameter. The drips feeding the stalagmites originate from the tips of corresponding stalactites of different shapes and sizes. BC-98-1 is fed by a bent soda-straw stalactite approximately 25 cm long that thickens towards the roof of the cave. BC-98-2 is fed from a carrot-shaped stalactite that formed by the connection of two soda straws. The carrot is approximately 40 cm in length and 7 cm in diameter near its top. BC-98-3 is fed from a 7 cm long bent soda straw, a much smaller speleothem than those at the other sites. The drips feeding these speleothems flow at less than 0.3 ml/min.

## **METHODS**

### **COLLECTION OF MODERN CALCITE**

Modern calcite was collected by placing 10 x 10 cm frosted glass plates on actively growing stalagmites. These stalagmites were first covered with a plastic bag to protect them from the experiment (Fig. 3.2). A modeling clay base was constructed on the bag and the plates were placed on the clay base so they were nearly horizontal and the discrete drip feeding the speleothem fell in the middle of the plate. Glass plates were prepared by frosting them with a sandblaster and then cleaned in an ultrasonic bath in micro solution followed by de-ionized water. Glass plates were placed on 2/1/1999 and collected on 7/1/2000.

This glass plate method of evaluating speleothem isotopic equilibrium is a contribution to cave conservation because collecting speleothem calcite on glass plates does not adversely affect the cave environment. After the experiment is concluded the cave will be left exactly as it was found. In addition, a great many sites may be studied, potentially increasing our understanding of the controls on the chemistry of speleothems.

## **PLATE SAMPLING**

The temporal variability in the  $\delta^{18}\text{O}$  and  $\delta^{13}\text{C}$  composition of plate calcite was assessed by sampling calcite, using a dentil drill, from a  $1\text{ cm}^2$  area near the locus of precipitation on the glass plate (Fig. 3.3A). The calcite within this  $1\text{ cm}^2$  area was sampled in 0.02 mm layers over its entire thickness. This is analogous to sampling a speleothem along the growth axis.

The spatial variability in the O and C isotopic composition of the calcite was assessed by sampling calcite in a grid with a spacing of  $2\text{ cm}^2$  (Fig. 3.3). At each grid point, a small area,  $\sim 2\text{ mm}$  in diameter, was sampled using a dental drill, encompassing the entire thickness of the calcite. This is analogous to sampling a speleothem along an individual growth layer.

## **C AND O ISOTOPIC COMPOSITION OF CALCITE**

Calcite samples were analyzed for C and O stable isotopes at the University of Texas at Austin. Approximately 200-350  $\mu\text{g}$  of calcite was analyzed in individual reaction vessels at  $90^\circ\text{C}$  using a Micromass Multiprep system. The resulting gas was released into a Prism II dual inlet triple collector

mass spectrometer and analyzed using standard procedures. Analytical precision was 0.18‰ for  $\delta^{18}\text{O}$  and 0.12‰ for  $\delta^{13}\text{C}$  ( $2\sigma$  of 40 standard runs). The results of isotopic analysis are presented in conventional delta ( $\delta$ ) notation, defined as  $\delta = (R_{\text{sample}} - R_{\text{standard}})/R_{\text{standard}} \times 1000$ , where R is the ratio  $^{18}\text{O}/^{16}\text{O}$  or  $^{13}\text{C}/^{12}\text{C}$ . The O and C isotopic values for carbonate samples and the C isotopic values of DIC are expressed relative to the standard VPDB.

## **C AND O ISOTOPIC COMPOSITION OF WATERS**

Cave water samples were analyzed for  $\delta^{18}\text{O}$  by equilibrating  $\text{CO}_2$  with 300  $\mu\text{l}$  of water at 40° C using a Micromass multi-prep system and analyzed on a Prism II dual inlet mass spectrometer at the University of Texas at Austin. The O isotopic values of water samples are expressed relative to the VSMOW standard. Analytical precision ( $2\sigma$ ) was 0.1‰.

The C isotopic composition of dissolved inorganic carbon dissolved inorganic carbon was determined at The University of Texas by injecting 5 ml of the cave drip water into an evacuated sample vial with  $\text{H}_3\text{PO}_4$ . The resulting mixture of  $\text{CO}_2$ , water vapor and non-condensable gasses was released into a vacuum line and the  $\text{CO}_2$  was cryogenically purified. The  $\text{CO}_2$  gas was then collected and was released directly into the VG Prism II dual inlet mass spectrometer and analyzed using standard analytical techniques. Analytical precision ( $2\sigma$  of 0.1‰) was estimated by analyzing a solution of  $\text{Na}_2\text{CO}_3$  (aq) with a known C isotopic composition and DIC concentrations similar to cave drip waters.

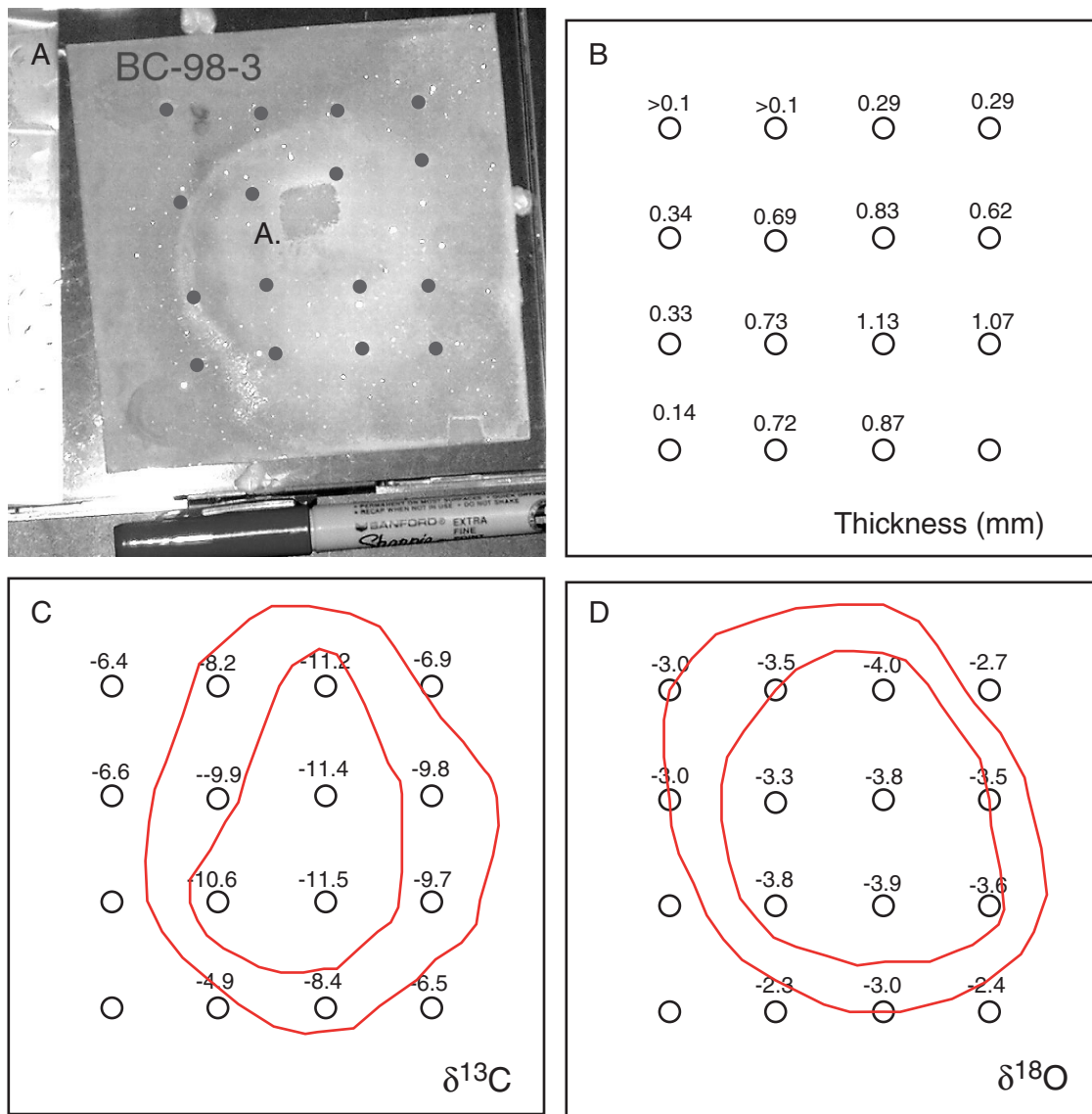


Figure 3.3. Spatial variations in glass plate BC-98-3 showing A) Photograph of glass plate BC-98-3. Approximately 1cm<sup>2</sup> area sampled to determine the temporal variability of calcite δ<sup>13</sup>C and δ<sup>18</sup>O values at A and small sample pits drilled on a 2 cm X 2 cm grid used to determine the special distribution of calcite δ<sup>13</sup>C and δ<sup>18</sup>O values. B) Distribution of calcite thickness. C) Distribution of δ<sup>13</sup>C values of calcite with -10‰ and -8‰ isopleths shown. D) Distribution of calcite δ<sup>18</sup>O values of calcite with the -3.5‰ and -3.0‰ isopleths.



## **FIELD CHEMISTRY**

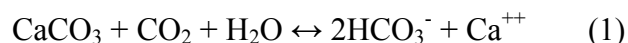
Water temperature and pH were measured in the cave at the time of water collection using a pH electrode and temperature probe. Two 40 ml amber VOA vials were collected for each water sample for alkalinity determination and  $\delta^{13}\text{C}$  of DIC. These samples were transported, in a dark and cool container, and alkalinities were determined at the end of each field day. Alkalinities were determined by titrating 25 ml of cave water to a pH of 4.5 using 0.1M HCl solution.

## **CATION ANALYSIS**

Major elemental concentrations were analyzed at the University of Minnesota using a ICP-MS (Perkin Elmer/Sciex Elan 5000). Approximately 15 ml of cave water was collected in an acid clean PP bottle and acidified using 1%  $\text{HNO}_3$  after returning to the University of Texas.

## **DETERMINATION OF POTENTIAL EXTENT OF DIC LOSS**

Calcite speleothem formation likely results when cave water that is in, or near, equilibrium with a high  $\text{P}_{\text{CO}_2}$  soil environment and calcite enters the cave environment with a lower  $\text{P}_{\text{CO}_2}$  (Hendy, 1971). The water will move towards chemical equilibrium with its new environment by degassing  $\text{CO}_2$  and the calcite precipitation/dissolution reaction (Eq. 1) depicted below will be driven to the right and calcite will precipitate.



As calcite precipitation driven by CO<sub>2</sub> degassing progresses, the HCO<sub>3</sub><sup>-</sup> reservoir, in the drip water, will undergo <sup>13</sup>C enrichment. The extent of <sup>13</sup>C enrichment is a function of the fractionation factors between the C species and the fraction of total inorganic carbon (DIC) lost to CO<sub>2</sub> degassing and CaCO<sub>3</sub> precipitation. The isotopic evolution may be modeled as a Rayleigh distillation process. This process was discussed in detail in Chapter 2. The size of the DIC reservoir was estimated by modeling the evolution of the geochemical composition of the cave water using PHREEQC<sup>TM</sup> (Parkhurst and Appelo, 1999) to constrain the potential chemical evolution of the cave water. Several assumptions are made in the modelling: 1) Upon entry into the cave environment and prior to CO<sub>2</sub> degassing, the water is in chemical equilibrium with a high P<sub>CO<sub>2</sub></sub> soil environment and calcite (Table 3.2b). To reach this end member, CO<sub>2</sub> was added to the solution, which was supersaturated with respect to calcite, to reach equilibrium with calcite. 2) The geochemical composition of the water collected in the cave has been altered since first entering the cave by CO<sub>2</sub> degassing, but not CaCO<sub>3</sub> precipitation, prior to measuring alkalinity, pH and DIC δ<sup>13</sup>C. 3) CO<sub>2</sub> degassing and CaCO<sub>3</sub> precipitation continue until the water is in chemical equilibrium with cave P<sub>CO<sub>2</sub></sub> and calcite (Table 3.2c). Assumptions 1 and 3 define two end member conditions where the differences in the modeled DIC concentrations define the possible extent of DIC loss. In this study, atmospheric P<sub>CO<sub>2</sub></sub> is used as the end member because cave P<sub>CO<sub>2</sub></sub> was not measured. This is a

conservative maximum estimate because natural cave environments have  $P_{\text{CO}_2}$  concentrations higher than atmospheric values.

### MAXIMUM MODELED $^{13}\text{C}$ ENRICHMENT.

An estimation of the maximum  $^{13}\text{C}$  enrichment in the  $\text{HCO}_3^-$  reservoir due to  $\text{CO}_2$  degassing and  $\text{CaCO}_3$  precipitation was made using a Rayleigh distillation model outlined in Chapter 2, published fractionation factors (outlined in Chapter 2), and the conservative upper limit estimation of DIC loss. The effects of Rayleigh distillation on the  $\delta^{13}\text{C}$  value of the  $\text{HCO}_3^-$  (aq) reservoir can be modeled by:

$$(\delta+1000)/(\delta_0+1000)=f^{(\alpha_{\text{p-r}}-1)} \quad (2)$$

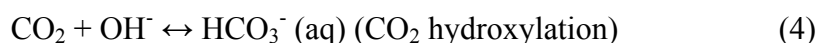
where  $\delta$  is the C isotopic composition of  $\text{HCO}_3^-$  (aq),  $\delta_0$  is the initial C isotopic composition of  $\text{HCO}_3^-$  (aq),  $f$  is the fraction of  $\text{HCO}_3^-$  (aq) remaining and  $\alpha_{\text{p-r}}$  is the equilibrium carbon isotope fractionation factor between  $\text{HCO}_3^-$  (aq) and a bulk product. The variable  $f$  was estimated by using the extent of DIC loss outlined in the *Potential extent of DIC loss determination* section with the results given in Table 3.2d. Because the C in  $\text{HCO}_3^-$  (aq) is evenly partitioned between  $\text{CaCO}_3$  and  $\text{CO}_2$  (g) during calcite precipitation, I define a fractionation factor between  $\text{HCO}_3^-$  (aq) and a bulk product such that  $\alpha_{(\text{bulk product} - \text{HCO}_3^-)}$  is  $1/2(\alpha_{\text{CO}_2-\text{HCO}_3^-}) + 1/2(\alpha_{\text{CaCO}_3-\text{HCO}_3^-})$ .

I modeled the oxygen isotope effects of  $\text{CO}_2$  degassing,  $\text{CaCO}_3$  precipitation and  $\text{H}_2\text{O}$  formation using an analogous Rayleigh distillation approach with the following assumptions: There is no oxygen isotope exchange between the DIC and the water, and the fractionation factor between bulk DIC

products and  $\text{HCO}_3^-$  (reactant) is  $2/6(\alpha_{\text{CO}_2-\text{HCO}_3^-}) + 3/6(\alpha_{\text{CaCO}_3-\text{HCO}_3^-}) + 1/6 (\alpha_{\text{H}_2\text{O}-\text{HCO}_3^-})$ , or in proportion to the oxygen in each of the three products. This approach is an end member calculation because it neglects  $\text{CO}_2$  hydration and hydroxylation reactions (eq. 3 and 4) which will buffer the isotopic composition of the  $\text{HCO}_3^-$  (aq) reservoir and reduce the magnitude of the isotope effects of  $\text{CO}_2$  degassing. The forward and backward reactions outlined in eq. 3 and 4, will result in the  $\text{HCO}_3^-$  acquiring an  $\delta^{18}\text{O}$  value closer to equilibrium with the large reservoir of O in  $\text{H}_2\text{O}$ .



and



This model of progressive loss of  $\text{HCO}_3^-$  during calcite precipitation (Eq. 1), while excluding O isotope exchange between DIC and  $\text{H}_2\text{O}$  (Eq. 3 and 4) will cause progressive  $^{18}\text{O}$  and  $^{13}\text{C}$  enrichment in the  $\text{HCO}_3^-$  reservoir as shown in Fig. 3.1B.

## RESULTS

The calcite grown on the glass plate was deposited much like a speleothem. The greatest calcite thickness was found where the cave drip fell on the plate, analogous to the component of maximum calcite growth along the speleothem growth axis (Figs. 3.3a and b). The calcite thickness decreased away from the growth axis from maximum thicknesses of 1.1 mm on plate BC-98-3 to a minimum value of less than 0.1 mm.

The spatial variability in  $\delta^{13}\text{C}$  and  $\delta^{18}\text{O}$  values of glass plate calcite show consistent trends. The  $\delta^{13}\text{C}$  values of the calcite from BC-98-1, BC-98-2 and BC-98-3 show progressive increases away from the growth axes; an example is given in Fig. 3.4C. In all three cases the  $\delta^{13}\text{C}$  values can be contoured, producing a “bull’s eye” pattern on the plate. The  $\delta^{13}\text{C}$  value of the calcite near the growth axes, the lowest values, is consistent with precipitation in C isotopic equilibrium with the DIC of the drip waters (Table 3.1).

The  $\delta^{18}\text{O}$  values of the calcite from the glass plates also increase progressively away from the growth axes (Fig. 3.4D). The magnitude of the  $^{18}\text{O}$  enrichment is not as large as the  $\delta^{13}\text{C}$  values. Only BC-98-3 exhibits  $\delta^{18}\text{O}$  enrichments away from the growth axis systematic enough to produce the “bull’s eye” pattern whereas the  $\delta^{18}\text{O}$  variability of BC-98-1 and BC-98-2 does not allow contouring. In all three plates the lowest  $\delta^{18}\text{O}$  value of the calcite is higher than equilibrium values by  $>2\text{‰}$ . Unlike the C isotopic system, the glass plate calcite is not deposited in O isotopic equilibrium near the center of the plate. The mechanisms responsible for the initial high  $\delta^{18}\text{O}$  values are outlined in Chapter 2. Briefly, the  $\delta^{18}\text{O}$  values of calcite exceeding that in O isotopic equilibrium with coexisting

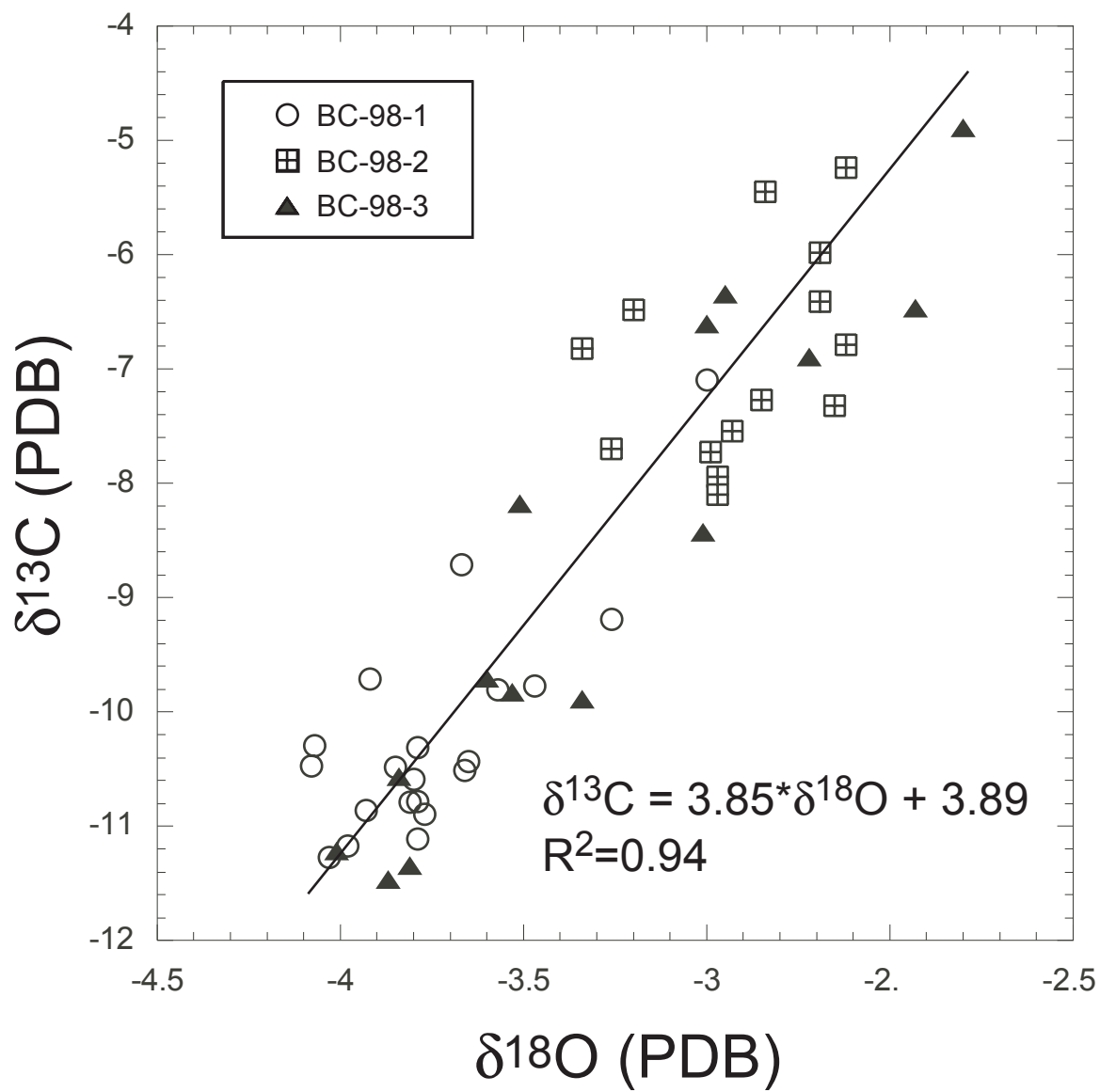


Figure 3.4.  $\delta^{13}\text{C}$  vs.  $\delta^{18}\text{O}$  plot of glass plate calcite sampled on a 2 cm x 2 cm grid to determine the spatial distribution of stable isotopes.

water likely results from the combination of direct incorporation of  $\text{HCO}_3^-$  into the calcite during rapid calcite precipitation and the evolution of the  $\text{HCO}_3^-$  reservoir during progressive calcite precipitation. This is modeled by Rayleigh distillation and outlined in the section “*Estimation of potential DIC loss and  $^{13}\text{C}$  enrichment in  $\text{HCO}_3^-$  reservoir*”

A plot of  $\delta^{13}\text{C}$  vs.  $\delta^{18}\text{O}$  values of the calcite from the three plates show strong positive correlation, characterized by the orthogonal regression line ( $\delta^{13}\text{C} = 4.21 + 3.87 * \delta^{18}\text{O}$ ) correlation coefficient of ( $R^2 = 0.84$ ), with minimum  $\delta^{13}\text{C}$  and  $\delta^{18}\text{O}$  values of -11.3‰ and -4.1‰ and maximum  $\delta^{13}\text{C}$  and  $\delta^{18}\text{O}$  values of -7.1‰ and -3.0‰ respectively (Fig. 3.4). BC-98-3 shows the largest  $^{13}\text{C}$  and  $^{18}\text{O}$  enrichments away from the growth axis of 6.6‰ and 1.7‰ respectively.

Calcite sampled vertically (and, thus, temporally) along the growth axis shows a similar trend. The  $\delta^{13}\text{C}$  vs.  $\delta^{18}\text{O}$  values of all three plates fall along the line  $\delta^{13}\text{C} = 3.89 + 3.85 * \delta^{18}\text{O}$ , correlation coefficient ( $R^2 = 0.94$ ) (Fig. 3.5). Individual plates sampled along the growth axis produced low isotopic variability. Only BC-98-3 produced a significant positive covariance ( $R^2 = 0.59$ ) between  $\delta^{18}\text{O}$  and  $\delta^{13}\text{C}$  values.

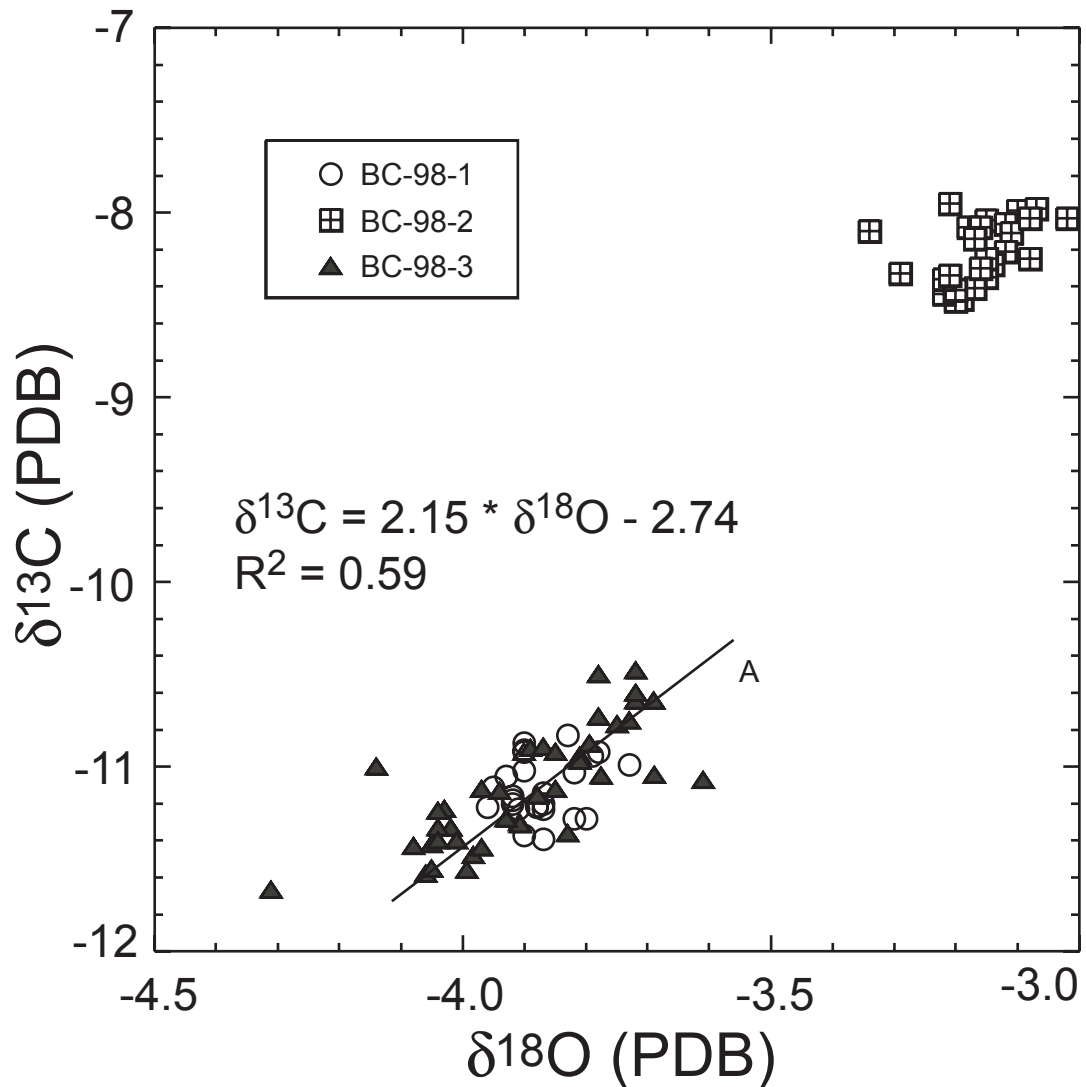


Figure 3.5.  $\delta^{13}\text{C}$  vs.  $\delta^{18}\text{O}$  plot of glass plate calcite sampled near the locus of precipitation to determine the temporal variation of stable isotopes. At sites BC-98-1 and BC-98-2 there is not enough variability to produce a significant trend in the data. BC-98-3 does show a positive correlation between  $\delta^{13}\text{C}$  and  $\delta^{18}\text{O}$  values, expressed as a line  $\delta^{13}\text{C} = -2.74 + 2.15 * \delta^{18}\text{O}$ , correlation coefficient ( $R^2 = 0.59$ ). Excluding the outliers with the two lowest and one highest  $\delta^{18}\text{O}$  values yields a slope of 2.57. Both of these regression lines are close to the values seen in the regression line through the spatial data (Fig. 3.4) suggesting the same mechanism is responsible for the positive covariation in  $\delta^{18}\text{O}$  and  $\delta^{13}\text{C}$  in space and time, likely Rayleigh distillation of the  $\text{HCO}_3^-$  reservoir.



## **ESTIMATION OF POTENTIAL DIC LOSS AND $^{13}\text{C}$ ENRICHMENT IN $\text{HCO}_3^-$ RESERVOIR**

The water collected at the drip sites was supersaturated with respect to calcite as calculated from pH, temperature and alkalinity data collected in the field and cation analysis (Table 3.2A). This suggests that degassing of  $\text{CO}_2$  prior to analysis altered the chemistry of the cave drip water. A maximum estimate of the possible extent of DIC losses, outlined in the methods section, is given in Table 3.2. These calculations suggest that between 72% and 83% of the DIC could have been lost to  $\text{CO}_2$  degassing and  $\text{CaCO}_3$  precipitation. My Rayleigh distillation model indicates that a loss of 72% to 83% of the DIC, in this model held as  $\text{HCO}_3^-$ , would result in a  $^{13}\text{C}$  enrichment of the  $\text{HCO}_3^-$  reservoir by 3.8 ‰ to 5.1 ‰. These are maximum estimates of the potential enrichments because the cave environment likely has a higher  $P_{\text{CO}_2}$  than atmospheric values. The maximum observed  $^{13}\text{C}$  enrichment, which occurred in plate BC-98-3, is 6.6 ‰, between 1.8 ‰ and 2.1 ‰ higher than the maximum conservative estimates.

## **DISCUSSION**

The study of modern speleothem calcite grown on glass plates can significantly increase our understanding of non-equilibrium isotope effects operating in cave systems. Sampling calcite near the locus of precipitation on the plates is analogous to sampling a speleothem along its growth axis. Sampling calcite on a transect away from the locus of precipitation is analogous to sampling

a speleothem along a growth layer. The O and C isotopic composition of the calcite can be directly compared to the O and C isotopic composition of the cave drip water, permitting quantification of the extent to which isotopic equilibrium is achieved. The magnitude and direction of isotopic offsets from equilibrium can allow the identification of specific isotope effects.

### **RAYLEIGH DISTILLATION MODEL**

The majority of C available for speleothem formation is held in the  $\text{HCO}_3^-$  reservoir and no other large source of C exists to buffer the  $\delta^{13}\text{C}$  value of calcite. As  $\text{CO}_2$  degassing and  $\text{CaCO}_3$  precipitation proceed there will be a progressive enrichment in the  $\delta^{13}\text{C}$  value of the  $\text{HCO}_3^-$  reservoir and the corresponding precipitated calcite. If  $\text{CO}_2$  hydration and hydroxylation reactions are sufficiently fast, relative to the rate of calcite precipitation, O isotopic equilibrium between  $\text{HCO}_3^-$  and  $\text{H}_2\text{O}$  will be maintained and there will be no change in the  $\delta^{18}\text{O}$  value of calcite during progressive  $\text{CO}_2$  degassing and  $\text{CaCO}_3$  precipitation. These processes will cause  $^{13}\text{C}$  enrichment in the speleothem calcite. On a  $\delta^{13}\text{C}$  vs.  $\delta^{18}\text{O}$  plot this will manifest itself as a trend with a vertical slope,  $\Delta^{13}\text{C}/\Delta^{18}\text{O} = \infty$  (Fig. 3.6, line A). If no  $\text{CO}_2$  hydration and hydroxylation reactions are operating to buffer the  $\delta^{18}\text{O}$  value of the  $\text{HCO}_3^-$  reservoir, a condition that will not occur in natural systems, then the isotopic

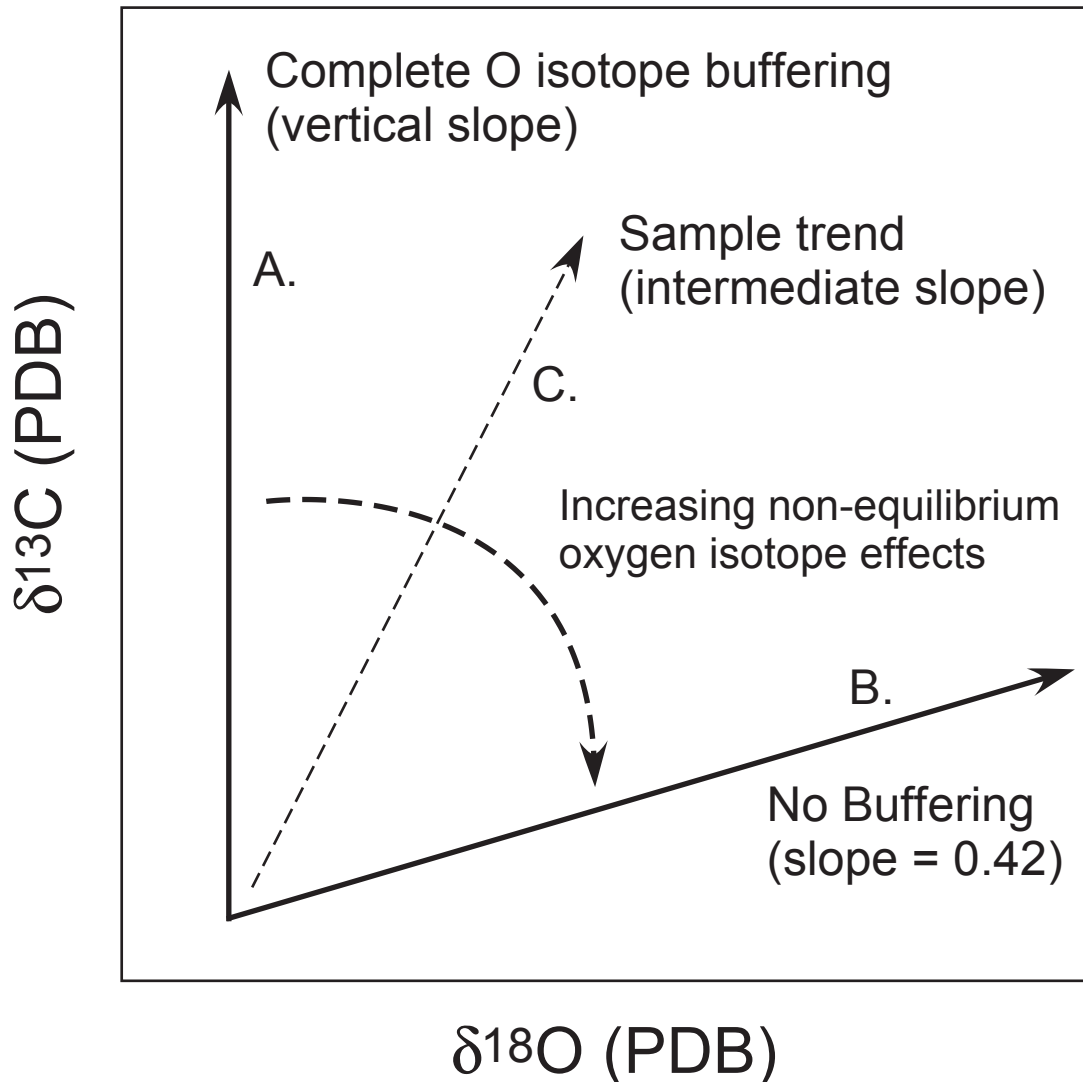
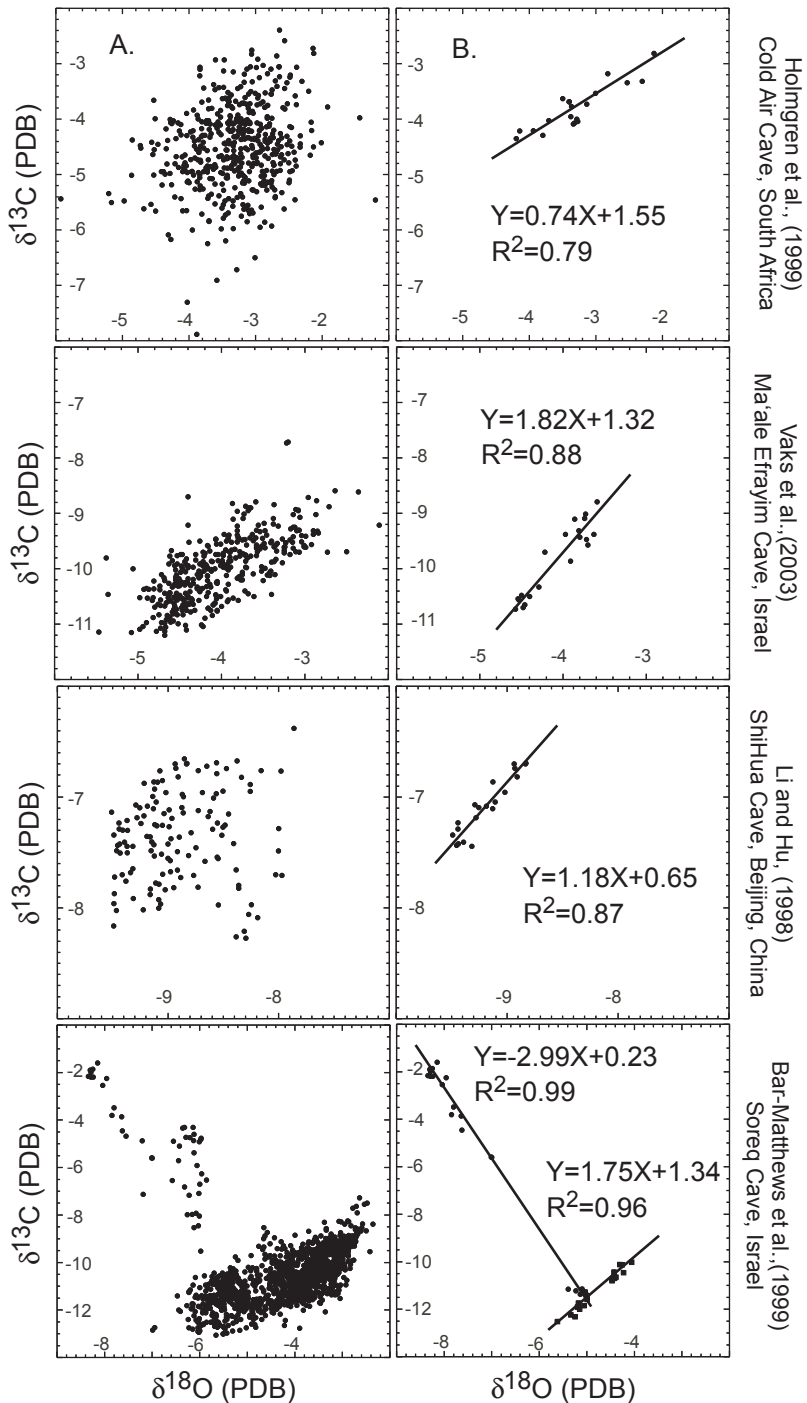


Figure 3.6. O and C isotope effects of progressive loss of  $\text{HCO}_3^-$  during  $\text{CO}_2$  degassing and calcite precipitation. If  $\text{CO}_2$  hydration/hydroxylation reactions proceed faster than  $\text{CO}_2$  degassing and  $\text{CaCO}_3$  precipitation, such that the  $\text{HCO}_3^-$  reservoir maintains O isotopic equilibrium with the water, the  $\delta^{13}\text{C}$  and  $\delta^{18}\text{O}$  composition of the speleothem calcite will evolve along line A. If no  $\text{CO}_2$  hydration/hydroxylation occurs, a situation that will not happen in natural systems, the  $\delta^{13}\text{C}$  and  $\delta^{18}\text{O}$  composition of the speleothem calcite will evolve along line B. These define two end member conditions that constrain the potential slope of the  $\delta^{13}\text{C}$  vs.  $\delta^{18}\text{O}$  values. If  $\text{CO}_2$  hydration/hydroxylation reaction operate, but not fast enough to buffer the O isotopic composition of the  $\text{HCO}_3^-$  reservoir, then the resulting speleothem calcite will evolve along a line of intermediate slope (Line C).

Figure 3.7.  $\delta^{13}\text{C}$  vs.  $\delta^{18}\text{O}$  plots for several speleothem studies from the literature where raw data was available. Column A. shows all of the data. Column B. shows the 20 consecutive samples with the highest correlation coefficient. The slope and y-intercept produced by an orthogonal regression and the correlation coefficients are included as an inset in the plot. In these studies, even when no positive correlation was evident in the complete data set, short segments of the record show high positive correlation. In Soreq Cave (Bar-Matthews et al., 1999) short segments of the complete record show highly positive and highly negative correlations and segments with a vertical  $\delta^{13}\text{C}$  vs.  $\delta^{18}\text{O}$  slope.



composition of the  $\text{HCO}_3^-$  reservoir and thus the calcite will evolve along a line with a slope of 0.42 at 26.6 °C (Fig. 3.6, line B). These two conditions represent the end members of a model that can be used to qualify the ability of  $\text{CO}_2$  hydration and hydroxylation reactions to buffer the  $\delta^{18}\text{O}$  values of the resulting calcite during progressive  $\text{CaCO}_3$  precipitation. A  $\delta^{13}\text{C}$  vs.  $\delta^{18}\text{O}$  trend with an intermediate slope, between  $\infty$  and 0.42, indicates  $\text{CO}_2$  hydration and hydroxylation reactions are too slow to maintain equilibrium yet not to slow such that no exchange occurs. A hypothetical example of a  $\Delta^{18}\text{O}/\Delta^{13}\text{C}$  slope of an intermediate value is given in Fig. 3.6, line C. Additional examples, taken from the literature, are given in Fig. 3.7 and Table 3.3.

## SPATIAL ISOTOPIC VARIABILITY

When considered individually, the three Upper Passage sites appear to each produce distinct  $\delta^{13}\text{C}$  and  $\delta^{18}\text{O}$  calcite compositions and variability. For instance, BC-98-3 shows the lowest  $\delta^{18}\text{O}$  and  $\delta^{13}\text{C}$  values and the greatest variability. BC-98-2 shows the highest isotopic compositions with the lowest variability. This may make it appear, even though the three stalagmites occupy an area of about 1 m<sup>2</sup> in the same cave environment, that each drip has its own unique isotopic and chemical composition (Tables 3.1 and 3.2). If these were ancient speleothems, one might infer distinct paleoenvironmental condition for each.

When considered as a single system, the  $\delta^{18}\text{O}$  and  $\delta^{13}\text{C}$  results from BC-98-1, 2 and 3 follow the same linear trends (Fig. 3.4), consistent with the model outlined in Fig. 3.6. Calcite precipitation and  $\text{CO}_2$  degassing may be proceeding

too fast for CO<sub>2</sub> hydration/hydroxylation reactions to buffer the O isotopic system. This manifests itself by producing a positive correlation between  $\delta^{18}\text{O}$  and  $\delta^{13}\text{C}$  calcite values, in this case with a slope of 3.87. It is likely that upon entry into the cave environment all three drips begin with similar DIC concentrations, DIC  $\delta^{13}\text{C}$  values and water  $\delta^{18}\text{O}$  values. BC-98-3 exhibits the lowest isotopic composition and the highest isotopic variability; it also has the smallest stalactite feeding drip water to the plate site. BC-98-2 exhibits the highest isotopic values but its drip flows over a much larger stalactite. BC-98-1 has an intermediate isotopic composition and isotopic variability and is fed by a stalactite of an intermediate size. The correspondence of higher isotopic values with larger stalactites and higher isotopic variability with shorter stalactites is consistent with progressive DIC loss by CO<sub>2</sub> degassing and calcite precipitation. There is a greater potential reaction progress along a longer stalactite prior to the cave water depositing calcite on the stalagmite, or the glass plate. As a result, calcite precipitated on a stalagmite, or a glass plate, under a relatively shorter stalactite would be expected to show greater isotopic variability and lower isotopic compositions near the locus of precipitation. The BC-98-3 plate, with its smaller stalactite, retains a greater proportion of its DIC for precipitation of calcite at the plate site and has the greatest potential for lower isotopic compositions and greater isotopic variability.

## **TEMPORAL ISOTOPIC VARIABILITY**

Analysis of glass plate calcite sampled temporally in progressive layers near the locus of precipitation is analogous to sampling a speleothem along its

growth axis. When plotted together, the  $\delta^{13}\text{C}$  vs.  $\delta^{18}\text{O}$  values of the temporal samples fall on a line with a slope (Fig. 3.5) very similar to the slope produced by glass plate calcite sampled spatially (along the growth layer, Fig. 3.4). Individual sites show relatively little O and C isotopic variability. The site with the largest temporal variability, BC-98-3, exhibits a positive  $\delta^{13}\text{C}$  vs.  $\delta^{18}\text{O}$  trend with a slope similar to glass plate calcite sampled spatially (along the growth layer). The small O and C isotopic variability seen in glass plate calcite sampled temporally, along the growth axis, may be controlled by the same mechanisms responsible for the isotopic variability seen along the growth layer. The extent that progressive  $\text{CaCO}_3$  precipitation and  $\text{CO}_2$  degassing alters the O and C isotopic composition of the  $\text{HCO}_3^-$  reservoir, and the calcite precipitated from it.

## **IMPLICATIONS FOR SPELEOTHEM BASED CLIMATE STUDIES**

My results indicate that progressive  $\text{CO}_2$  degassing and  $\text{CaCO}_3$  precipitation control the  $\delta^{13}\text{C}$  and  $\delta^{18}\text{O}$  values of calcite precipitated from cave drip water. This process manifests itself by producing a positive covariance between  $\delta^{13}\text{C}$  and  $\delta^{18}\text{O}$  values both along growth layers and along the growth axis. In this study, BC-98-3 shows the largest  $^{13}\text{C}$  and  $^{18}\text{O}$  enrichments along a growth layer, 6.6‰ and 1.7‰ respectively. This enrichment can be accounted for by Rayleigh distillation of the  $\text{HCO}_3^-$  reservoir combined with incomplete O isotopic equilibrium of the  $\text{HCO}_3^-$  reservoir with  $\text{H}_2\text{O}$ . These non equilibrium isotope effects may be influenced by climate. For example, increases in temperature will decrease  $\text{CO}_2$  solubility and increase chemical reaction rates that may influence the kinetic isotope effects identified in this paper. Predictions on

how climate change will influence these disequilibrium processes can not yet be made because the study area of Barbados experiences very little intra and inter-annual climate variability. Conducting a similar study in cave systems, with actively growing speleothems, that experience greater seasonality and inter annual climatic variability may document a climatic control on non-equilibrium isotope effects. Significantly more work needs to be done to calibrate isotopic shifts seen along the growth axis and growth layers to physical conditions in the cave environment such as temperature, drip rates, calcite precipitation rates, cave ventilation, etc.

The positive correlation between  $\delta^{13}\text{C}$  and  $\delta^{18}\text{O}$  values of speleothem calcite sampled along the growth axis is commonly explained by climate induced changes in vegetation type above the cave and temperature of speleothem formation. The results of this study offer an additional explanation for positive  $\delta^{13}\text{C}$  vs.  $\delta^{18}\text{O}$  covariation in speleothem calcite, providing support for the tests for equilibrium calcite precipitation (Hendy, 1971). Rather than assuming isotopic equilibrium when interpreting synchronous C and O isotopic shifts in speleothem records, the extent to which  $\text{CO}_2$  hydration/hydroxylation reactions buffer the O isotopic composition of the  $\text{HCO}_3^-$  reservoir along with the extent of Rayleigh distillation of the  $\text{HCO}_3^-$  reservoir should also be considered as an alternative explanation.

A simultaneous increase in  $\delta^{13}\text{C}$  and  $\delta^{18}\text{O}$  values of speleothem calcite has been identified by other researchers. Fornaca-Rinaldi, (1968) and Fantidis and Ehhalt (1970) suggested that  $\text{CO}_2$  degassing was responsible for  $^{13}\text{C}$  enrichments



but evaporation of the drip water was responsible for  $^{18}\text{O}$  enrichments. In my study, evaporative  $^{18}\text{O}$  enrichment of cave water was discounted as a method of producing  $^{18}\text{O}$  enrichments in calcite because of the high humidity experienced in the cave system ( $>98.2\%$ ), the short residence time of the cave water on the glass plates and the relatively large fraction of water that would have to be evaporated to produce the observed  $1.7\%$  calcite  $^{18}\text{O}$  enrichments. Equation 1 can be modified to estimate the fraction of  $\text{H}_2\text{O}$  evaporated ( $f$ ) needed to produce the  $1.7\%$  enrichment observed by using the fractionation factor,  $1000\ln\alpha_{\text{vapor-liquid}} = -8$  to  $-10$ . This suggests that between 16-19% of the water must be evaporated to produce the observed  $^{18}\text{O}$  enrichment, this is unlikely at such high humidity and short reaction times. Desmarchelier et al., (2000) measured the  $\delta^{18}\text{O}$  and  $\delta^{13}\text{C}$  values of the tips of actively growing soda straws from two locations in Victoria Fossil Cave, England along with current climatic conditions and the  $\delta^{18}\text{O}$  value of modern drip water and found only the stalactite samples with the lowest  $\delta^{18}\text{O}$  values were precipitated in O isotopic equilibrium. These samples plot on a line on a  $\delta^{13}\text{C}$  vs.  $\delta^{18}\text{O}$  graph with a slope of 3.3 and an  $R^2$  value of 0.98. Bard et al., (2002) included this line on a  $\delta^{13}\text{C}$  vs.  $\delta^{18}\text{O}$  plot, which they labeled kinetic fractionation slope, to show a lack of correlation in their data from along a speleothem growth axis. I agree with the interpretation in Desmarchelier et al., (2000) that the covariation in  $\delta^{18}\text{O}$  and  $\delta^{13}\text{C}$  values is caused by non-equilibrium isotope effects but the observed value of the slope is not critical. The slope will vary with the extent to which  $\text{CO}_2$  hydration/hydroxylation reactions buffer the  $\delta^{18}\text{O}$  value of the  $\text{HCO}_3^-$  reservoir.

## PREVALENCE OF $\delta^{18}\text{O}$ AND $\delta^{13}\text{C}$ COVARIATION IN SPELEOTHEM RECORDS

A literature search was performed to determine what percentage of speleothem stable isotopic studies produced results consistent with my proposed model (Table 3.3). These speleothems were broadly divided into three groups, those that show a positive  $\delta^{18}\text{O}$  and  $\delta^{13}\text{C}$  covariation, those that show no covariation and those that show a negative  $\delta^{18}\text{O}$  and  $\delta^{13}\text{C}$  covariation (Table 3.4). The majority, 61.7%, of studies that present the both  $\delta^{18}\text{O}$  and  $\delta^{13}\text{C}$  values of speleothem calcite sampled along growth axes exhibit positive  $\delta^{18}\text{O}$  and  $\delta^{13}\text{C}$  covariations. Whereas 34.0% of these speleothems show no correlation and only 4.3% show a negative  $\delta^{18}\text{O}$ - $\delta^{13}\text{C}$  correlation (Table 3.4). Even speleothem records that show no apparent  $\delta^{18}\text{O}$ - $\delta^{13}\text{C}$  covariation commonly contain shorter intervals that show strongly positive covariation, and less commonly strongly negative covariation and intervals that exhibit a vertical  $\delta^{13}\text{C}$  vs.  $\delta^{18}\text{O}$  slope (Fig. 3.7). This suggests that the influence of non equilibrium isotope effects on speleothem stable isotope records may be underestimated.

Certainly not all positive  $\delta^{18}\text{O}$  and  $\delta^{13}\text{C}$  covariations in speleothem records shown in Table 3.3 are the result of kinetic isotope effects brought on by  $\text{CO}_2$  degassing and  $\text{CaCO}_3$  precipitation that are independent of environmental conditions. For example the Pequin and Soreq Cave studies show striking isotopic shifts corresponding to global climate change but also manifest strong positive correlations in  $\delta^{18}\text{O}$  and  $\delta^{13}\text{C}$  values (Bar-Matthews et al., 1999; Bar-Matthews et al., 2003b). These studies, and others, show that some  $\delta^{18}\text{O}$  and  $\delta^{13}\text{C}$

speleothem records provide paleoclimatic information, even when strong positive covariation possibly due to non-equilibrium isotope effects is observed. Speleothem records may be influenced by kinetic isotope effects, outlined in this study, such that temperature controlled equilibrium fractionation models alone can not adequately explain the significance of the records.

## CONCLUSIONS

The analysis of glass plate calcite and the water from which that calcite precipitated can provide empirical evidence on the controls of  $\delta^{13}\text{C}$  and  $\delta^{18}\text{O}$  variations of ancient speleothems. A direct comparison between the  $\delta^{13}\text{C}$  and  $\delta^{18}\text{O}$  of glass plate calcite and its drip water allow the determination of the magnitude and direction of offsets from isotopic equilibrium and the non-equilibrium isotope effects operating in the cave.

The spatial distribution of  $\delta^{18}\text{O}$  and  $\delta^{13}\text{C}$  values of glass plate calcite exhibits a strong positive correlation.  $\text{CO}_2$  degassing and  $\text{CaCO}_3$  precipitation may lead to progressive  $^{13}\text{C}$  and  $^{18}\text{O}$  enrichment in the speleothem calcite due to Rayleigh distillation of the isotopic composition of the  $\text{HCO}_3^-$  reservoir. The  $\delta^{13}\text{C}$  vs.  $\delta^{18}\text{O}$  slope may be controlled by the ability of  $\text{CO}_2$  hydration/hydroxylation reaction to buffer the O isotopic composition of the  $\text{HCO}_3^-$  reservoir. The correlation of glass plate  $\delta^{18}\text{O}$  and  $\delta^{13}\text{C}$  values with stalactite length is consistent with this conclusion. It may be important to consider both the O and C isotopic composition of the calcite as a single system in order to identify the non-equilibrium isotope effects operating in the system.

The mechanisms identified in this study can account for the positive correlation between  $\delta^{13}\text{C}$  and  $\delta^{18}\text{O}$  values of glass plate calcite in Barbados and may have implications for other speleothem studies. A compilation of speleothem stable isotope records from the literature shows that the majority of records exhibit positive  $\delta^{18}\text{O}$ - $\delta^{13}\text{C}$  covariation. Positive correlation between  $\delta^{13}\text{C}$  and  $\delta^{18}\text{O}$  values seen in ancient speleothem studies may be influenced by the non-equilibrium processes outlined in this study. Therefore, direct application of equilibrium fractionation factors in analyzing speleothem stable isotope records may be unwarranted. Proper interpretation of these records may require that the non-equilibrium isotope effects causing  $\delta^{13}\text{C}$  and  $\delta^{18}\text{O}$  variability in speleothems be calibrated to physical condition in the cave, such as temperature and  $\text{P}_{\text{CO}_2}$ , drip rates and calcite precipitation rates.

Table 3.1. Calcite and water stable isotopic compositions

Site	Max. Calcite Thickne ss (mm)	Plate calcite $\delta^{13}\text{C}$ value (PDB)		Range in DIC $\delta^{13}\text{C}$ value (PDB)		Calcite in C isotopic equilibrium with DIC @ 26.6° C (PDB)		Plate calcite $\delta^{18}\text{O}$ value (PDB)		Calcite in O isotopic equilibrium with cave drip water @ 26.6°C (PDB)	
		Min.	Max.	Min.	Max.	Min.	Max.	Min.	Max.	Min.	Max.
BC-98-1	0.8	-11.3	-7.1	-13.4	-11.5	-11.4	-9.5	-4.1	-3.0	-6.0	-5.4
BC-98-2	0.7	-8.1	-5.2	-11.4	-9.8	-9.4	-7.8	-3.3	-2.6	-6.0	-5.4
BC-98-3	1.1	-11.5	-4.9	-13.5	-10.9	-11.5	-8.9	-4.0	-2.3	-6.0	-5.4

Table 3.2. Harrison's Cave water chemistry

Chemistry of water collected in the cave											
Site	Date	pH	Ca <sup>2</sup> (x10 <sup>-3</sup> )	Concentration (mmol/L)					Fraction of DIC		
				DIC (x10 <sup>-3</sup> )	CO <sub>2</sub> <sup>*</sup> (x10 <sup>-4</sup> )	HCO <sub>3</sub> <sup>-</sup> (x10 <sup>-3</sup> )	CO <sub>3</sub> <sup>-2</sup> (x10 <sup>-5</sup> )	CO <sub>2</sub> <sup>*</sup>	HCO <sub>3</sub> <sup>-</sup>	CO <sub>3</sub> <sup>-2</sup>	SI
BC-98-1	2/1/99	7.8	2.18	4.41	1.29	4.14	1.72	0.03	0.94	0.00	0.76
	7/1/00	8.1	1.83	4.19	0.64	3.98	3.08	0.02	0.95	0.01	0.93
BC-98-2	2/1/00	8.1	1.84	4.07	0.60	3.85	3.18	0.01	0.95	0.01	0.97
	7/1/00	8.1	1.49	3.01	0.49	2.87	2.08	0.02	0.95	0.01	0.71
BC-98-3	2/1/99	7.7	2.14	4.36	1.59	4.08	1.35	0.04	0.93	0.00	0.66
	7/1/00	8.1	1.96	4.24	0.69	4.02	2.92	0.02	0.95	0.01	0.94
Calculated chemistry of water in equilibrium with theorized high CO <sub>2</sub> environment and calcite with no calcite precipitation											
Site	Date	pH	Ca <sup>2</sup> (x10 <sup>-3</sup> )	Concentration (mmol/L)					Fraction of DIC		
				DIC (x10 <sup>-3</sup> )	CO <sub>2</sub> <sup>*</sup> (x10 <sup>-4</sup> )	HCO <sub>3</sub> <sup>-</sup> (x10 <sup>-3</sup> )	CO <sub>3</sub> <sup>-2</sup> (x10 <sup>-6</sup> )	CO <sub>2</sub> <sup>*</sup>	HCO <sub>3</sub> <sup>-</sup>	CO <sub>3</sub> <sup>-2</sup>	
BC-98-1	2/1/99	7.0	2.18	5.10	7.75	4.22	2.98	0.15	0.83	0.00	
	7/1/00	7.1	1.83	4.81	6.07	4.12	3.50	0.13	0.86	0.00	
BC-98-2	2/1/99	7.1	1.84	4.72	6.24	4.01	3.32	0.13	0.85	0.00	
	7/1/00	7.4	1.49	3.27	2.65	2.95	4.06	0.08	0.90	0.00	
BC-98-3	2/1/99	7.0	2.14	4.99	7.52	4.14	2.96	0.15	0.83	0.00	
	7/1/00	7.1	1.96	4.89	6.50	4.15	3.33	0.13	0.85	0.00	

Calculated chemistry of water in equilibrium with atmospheric CO<sub>2</sub> and calcite allowing calcite precipitation

Site	Date	pH	Ca <sup>2</sup> (x10 <sup>-4</sup> )	Concentration (mmol/L)				Fraction of DIC		
				DIC (x10 <sup>-3</sup> )	CO <sub>2</sub> * (x10 <sup>-5</sup> )	HCO <sub>3</sub> <sup>-</sup> (x10 <sup>-4</sup> )	CO <sub>3</sub> <sup>-2</sup> (x10 <sup>-5</sup> )	CO <sub>2</sub> *	HCO <sub>3</sub> <sup>-</sup>	CO <sub>3</sub> <sup>-2</sup>
BC-98-1	2/1/99	8.3	4.53	0.87	8.31	0.84	1.02	0.01	0.96	0.01
	7/1/00	8.4	3.03	1.14	8.98	1.10	1.58	0.01	0.97	0.01
BC-98-2	2/1/00	8.4	3.14	1.03	8.23	1.00	1.44	0.01	0.97	0.01
	7/1/00	8.3	4.56	0.93	8.98	0.90	1.06	0.01	0.97	0.01
BC-98-3	2/1/99	8.2	4.87	0.94	10.39	0.91	0.95	0.01	0.97	0.01
	7/1/00	8.4	3.64	1.04	8.98	1.00	1.31	0.01	0.97	0.01

Potential <sup>13</sup>C enrichment due to Rayleigh distillation

Site	Date	Fractional loss			Ca <sup>2</sup>
		DIC	HCO <sub>3</sub> <sup>-</sup>	Ca <sup>2</sup>	
BC-98-1	2/1/99	0.83	0.80	0.79	5.1
	7/1/00	0.76	0.73	0.83	4.1
BC-98-2	2/1/00	0.78	0.75	0.83	4.4
	7/1/00	0.72	0.70	0.69	3.7
BC-98-3	2/1/99	0.81	0.78	0.77	4.8
	7/1/00	0.79	0.76	0.81	4.5

Table 3.3 Compilation of published  $\delta^{18}\text{O}$  and  $\delta^{13}\text{C}$  speleothem records

Ref.	Speleothem Name	Type	slope \$	R ‡	#
<b>North America/Caribbean</b>					
(Denniston et al., 1999)	CC-A	S	X		
(Denniston et al., 1999)	MC-28	S	X		
(Denniston et al., 1999)	SV-1	S	+		
(Denniston et al., 1999)	SV-2	S	X		
Denniston 01Paleo3	ON-3B	S	+		
(Denniston et al., 2001)	ON-3	S	+		
(Denniston et al., 2001)	BCC1-1	S	+		
(Denniston et al., 1999)	CWC-3L	S	X		
(Denniston et al., 1999)	CWC-2SS	S	X		
(Dorale et al., 1992)	CWC-1S	S	1.9	0.39*	30
(Dorale et al., 1992) <sup>§</sup>	CWC-1Sseg1	S	1.0	0.67	5
(Dorale et al., 1992) <sup>§</sup>	CWC-1Sseg2	S	-5	-0.39	9
(Dorale et al., 1992) <sup>§</sup>	CWC-1Sseg3	S	3	0.67**	16
(Dorale et al., 1998)	CC\DBL	S	+		
(Dorale et al., 1998)	CC\E	S	+		
(Dorale et al., 1998)	CC\C	S	X		
(Gascoyne et al., 1981)	75123	S	X, -		
(Gascoyne et al., 1981)	75125	Sc/F	X		
(Gonzalez and Gomez, 2002)	VCZ-1	S	+		
(Harmon et al., 1978a)	72041	S	X		
(Lauriol et al., 1997)	TITC/GB	F	2.1		8
(Lauriol et al., 1997)	TTH12-3	F	X		12
(Mickler, 2004)	AH-L	S	3.3	0.45**	33



Ref.	Speleothem Name	Type §	slope §	R ‡	#
(Mickler, 2004)	AH-M	S	2.6	0.88**	20
(Mickler, 2004)	AH-S	S	2.1	0.57*	15
(Mickler, 2004)	51-38	Sc-F	1.2	0.141	9
(Mickler, 2004)	25	S	2.2	0.36	7
(Mickler, 2004)	25	S	4	0.19	7
(Mickler, 2004)	BC-53	S	3.5	0.29	30
(Mickler, 2004)	BC-61	S	2.7	0.70**	46
(Banner et al., 1994)	IS-LM	F	1.74	0.13	12
(Banner et al., 1994)	ISS2	S	1.9	0.44**	157
(Banner et al., 1994)	IS-ST	F	1.35	0.57	11
(Banner et al., 1994)	DDS2	S	1.2	0.58**	217
(Banner et al., 1994)	KCS2	F	0.84	0.92**	6
(Banner et al., 1994)	KCS1	F	1.5	0.96**	9
(Banner et al., 1994)	KCS3	F	0.97	0.69*	10
(Banner et al., 1994)	CWN4	S	1.22	0.53**	40
(Banner et al., 1994)	NBSwall	F	1.7	0.60**	20
(Banner et al., 1994)	NBSwhite	F	4.1	0.84**	10
(Serefiddin et al., 2004)	RC2	S	X		
(Serefiddin et al., 2004)	RC20	S/F	X		
(Thompson et al., 1976)	NB10	S	X		44
(Thompson et al., 1976)	NB11	S	X		11
(Thompson et al., 1976)	NB4	S	+		30
(Thompson et al., 1976)	GV2		+		28
(van Beynen et al., 2004)	MF1	S	X		
<b>Europe</b>					
(Bard et al., 2002)	Stalagmite I	S	X		
(Duplessy et al., 1971)	d'Ornac unnamed	S	X		

Ref.	Speleotheom Name	Type §	slope §	R ±	#
(Duplessy et al., 1969)	T	S	X		
(Duplessy et al., 1969)	G	S	1.4		
(Fornaca-Rinaldi et al., 1968)	Sarteano	S	X		41
(Fornaca-Rinaldi et al., 1968)	Montecello	Sc	3.71	0.97**	6
(Fornaca-Rinaldi et al., 1968)	S. Lucia	Sc	6.12	0.89*	6
(Gascoyne, 1992)	76127	F	++		
(Gascoyne, 1992)	77143B	F	+		
(Gascoyne, 1992)	77162	F	++		
(Gascoyne, 1992)	79151	F/S	X,+		
(Gascoyne, 1992)	79158	S	X		
[Schwarcz, 1996 #346]	unnamed	S	-, +		
(Genty et al., 2003)	Vil9	S	2.7	0.59**	299
(Genty et al., 2003) <sup>ss</sup>	Vil9,D2-	S	0.91	0.51**	25
(Genty et al., 2003) <sup>ss</sup>	Vil9,D2-D3	S	1.1	0.58**	61
(Genty et al., 2003) <sup>ss</sup>	Vil9,D3-D4	S	3.4	0.50**	40
(Genty et al., 2003) <sup>ss</sup>	Vil9,D4-D6	S	1.9	0.63**	127
(Genty et al., 2003) <sup>ss</sup>	Vil9,D6-	S	2.7	0.61**	46
(Genty et al., 1998)	Han-stm5b	S	1.2	0.35	10
(Gewelt, 1981)	RSM V	S	1.3	0.33	15
(Horvatincic et al., 2003)	Pos CG-85	S	0.43	0.83**	10
(Jimenez de Cisneros et al., 2003)	ET	Sc	2.2	0.94**	18
(Kacanski et al., 2001)	Cermosjna	S	3.8	0.81	5
(Kadlec et al., 1996)	Zazdiná	F	X		
(Kadlec et al., 1996)	Holstenjnská	F	1.2		
(Labonne et al., 2002)	Altamira	F	X		
(Lauritzen and Onac, 1999)	LFG-2	S	X		

Ref.	Speleothem Name	Type	slope	R	#
(Lauritzen and Lundberg, 2004)	LP6	F	+	±	
	S-88-17	F	+		
	S-88-17seg1	F	++		
	S-88-17seg2	F	+,X		
	FM-2	F	2.9++	++	
	FM3		5.6		
	L-03		3.4		
	Ham85-2	S	+		
	SG92-1		X		
	SG93	S	- +		
	SG95	S	X		
	SG92-4	S	+		
	SG92-2	S	2.5	0.34**	232
	ER76	S	X		
	CC3	S	X		
	CL26	S	X		
	Cla4	S	2.4	0.73**	75
	Cla4A	S	4.7	0.67*	11
	Cla4B	S	8	0.22	21
	Cla4C	S	10	0.2	10
	Cla4D	S	-5	0.35	15
	Cla4E	S	2.9	0.92**	10
	Cla4F	S	-4	0.44	8
	Stal-B7-1	S	>1	0.63**	98
	Stal-B7-5	S	>1	0.55**	50
	Stal-B7-7	S	>1	0.63**	228
	(Lauritzen, 1995)				
	(Lauritzen, 1995) <sup>*</sup>				
	(Lauritzen, 1995) <sup>*</sup>				
	(Lauritzen, 1995)				
	(Linge et al., 2001)				
	(Linge et al., 2001)				
	(Linge et al., 2001)				
	(Linge et al., 2001)				
	(Linge et al., 2001)				
	(Linge et al., 2001)				
	(Linge et al., 2001)				
	(Berstad et al., 2002)				
	(McDermott et al., 1999)				
	(McDermott et al., 1999)				
	(McDermott et al., 1999)				
	(Plagnes et al., 2002)				
	(Plagnes et al., 2002) <sup>*</sup>				
	(Plagnes et al., 2002) <sup>*</sup>				
	(Plagnes et al., 2002) <sup>*</sup>				
	(Plagnes et al., 2002) <sup>*</sup>				
	(Plagnes et al., 2002) <sup>*</sup>				
	(Plagnes et al., 2002) <sup>*</sup>				
	(Niggemann et al., 2003b)				
	(Niggemann et al., 2003b)				
	(Niggemann et al., 2003b)				

Ref.	Speleothem Name	Type	slope	R	#
(Niggemann et al., 2003a)	AH-1	S	+	‡	384
(Onac et al., 2002)	Pu2	S	X	0.37**	
(Pazdur et al., 1995)	JWi2	S	0.9	0.81**	53
(Spötl et al., 2001)	OBI1 12	S	+		
(Verheyden et al., 2000)	Père Noël	S	+		
<b>Middle East</b>					
(Bar-Matthews et al., 2003b)	Peqin	S's	1.1	0.53**	483
(Bar-Matthews et al., 2003b) <sup>g</sup>	Peqin	S's	-1.5	-	568
(Bar-Matthews et al., 2003b) <sup>g</sup>	Peqin	S's	1.1	0.27**	239
(Bar-Matthews et al., 2003b) <sup>g</sup>	Peqin	S's	X	0.55**	
(Bar-Matthews et al., 2003b) <sup>g</sup>	Peqin	S's	1.1	0.57**	237
(Bar-Matthews et al., 2003b) <sup>g</sup>	Soreq	S's	1.4	0.04	1387
(Bar-Matthews et al., 2003b) <sup>g</sup>	Soreq	S's	0.93	0.67**	1340
(Bar-Matthews et al., 2003b) <sup>g</sup>	Soreq	S's	1.3	0.34**	1149
(Bar-Matthews et al., 2003b) <sup>g</sup>	Soreq	S's	-3.5	-	18
(Bar-Matthews et al., 2003b) <sup>g</sup>	Soreq	S's	0.72	0.94**	221
(Burns et al., 2002)	S3	S	+	0.41**	
(Frumkin et al., 2000)%	AF12	S	-		
(Frumkin et al., 2000)%	AF12	S	+		
(Frumkin et al., 1999)	NQ38	S	+		
(Vaks et al., 2003)	ME12+ME5	S's	1.4	0.55**	389
<b>China</b>					
(Hou et al., 2003)	LS9602	S	X		
(Hou et al., 2003)	TS9701	S	X		
(Li et al., 1998)	S312	S	1	0.44**	133
(Tan et al., 1998)	TS9501	S	+	0.4**	52

Ref.	Speleothem Name	Type	slope	R	#
(Huang, 1992)	Shiquan	S	\$	±	8
(Huang et al., 2001)	HS-2	S	2.18285167 ++	0.2	
(KDL)	Shuinan	S	++		
(KDL)	Xiangshuiyan	S	+		
(Li et al., 1996)	A	S	+,X		
(Ma et al., 2003)	ZFFS-1	S	+		
(Paulsen et al., 2003) <sup>%</sup>	SF-1	S	++	0.82**	
(Paulsen et al., 2003) <sup>%</sup>	SF-1	S	+		
(Wang, 1986)	82-29	S	+		6
(Wang, 1986)	GL	S	+		16
(Wang et al., 2001) <sup>&amp;∞</sup>	Composite	S	-0.13	-	1652
(Wang et al., 2001) <sup>&amp;</sup>	MSD	S	-1.23	-	268
(Wang et al., 2001) <sup>&amp;</sup>	MSL	S	-1.93	-	285
(Wang et al., 2001) <sup>&amp;</sup>	PD	S	1	0.62**	149
(Wang et al., 2001) <sup>&amp;</sup>	YT	S	-0.42	0.53**	338
(Wang et al., 2001) <sup>&amp;</sup>	H82	S	-0.21	-	612
(Wang et al., 1998) <sup>&amp;</sup>	Hulu/unnamed	S	+	0.12**	32
(Zhao et al., 2003) <sup>&amp;</sup>	996182	S	X		
(Wang et al., 1995)	BZ4	S	+	0.68*	9
(Wang et al., 1995)	BZ4'	S	+	0.36	10
(Zhang et al., 2004)	Q2	S	+		45
(Zhang et al., 2004)	D3	S	2.22	0.52**	118
(Zhang et al., 2004) <sup>∞</sup>	D3*	S	5.55	0.37**	74
(Zhang et al., 2004) <sup>∞</sup>	D3*	S	1.47	0.37**	44

Ref.	Speleotheom Name	Type	slope \$	R ±	#
(Zhang et al., 2004)	D4	S	3.22	0.32**	527
(Zhang et al., 2004) <sup>∞</sup>	D4*	S	3.7	0.39**	115
(Zhang et al., 2004) <sup>∞</sup>	D4*	S	11.1	0.06	280
(Zhang et al., 2004) <sup>∞</sup>	D4*	S	1.85	0.67**	59
(Zhang et al., 2004) <sup>∞</sup>	D4*	S	2.94	0.30**	84
<b>Australia/New Zealand</b>					
(Desmarchelier et al., 2000)	SC-S11	S	1.9	0.77**	90
(Fischer et al., 1996)	FSDC	S	++		
(Goede et al., 1986)	LT	S	X		
(Goede and Vogel, 1991)	LC	S	+	0.73**	40
(Xia et al., 2001)	LYN	S	++,X		
(Goede et al., 1990)	FC	S	X-	-0.19	36
(Goede, 1994)	FT	S	-	-0.089	170
(Goede et al., 1996)	RO	S	X+		
(Hellstrom et al., 1998)	ED1	F	+		
(Hellstrom et al., 1998)	MD3	F	+		
(Williams et al., 1999)	Max's	S	X		56
(Williams et al., 1999)	GG1	S	X		42
(Williams et al., 1999)	GG2	S	X		63
(Williams et al., 1999)	Waipuna-1	Sc	+	0.37**	51
<b>Africa</b>					
(Holmgren et al., 1995)	LII4	S	X		
(Holmgren et al., 2003)	T7	S	1.3	0.23**	480
(Holmgren et al., 2003)	T8	S	X,+		
(Repinski et al., 1999)	T5	S	+		
(Talma and Vogel, 1992)	V3	S	X		
(Talma et al., 1974)	T24	S	-,X		

Ref.	Age Range ka	G.R.^ cm/ka	T °C	Elev. m	Location
<b>North America/Caribbean</b>					
(Denniston et al., 1999)	3-0	11	9		N45° W92°
(Denniston et al., 1999)	7.5-0	4	8.7	396	N44° W92°
(Denniston et al., 1999)	8.6-0	7.5	8		N44° W92°
(Denniston et al., 1999)	6.6-1.8	11.5	8		N44° W92°
Denniston 01Paleo3	13.3-12.4	9.33	14		N38° W91°
(Denniston et al., 2001)	10-2.5	2.66	14		N38° W91°
(Denniston et al., 2001)	10-0	0.81	18		N36° W93°
(Denniston et al., 1999)	8.6-2	4.2	8.8	320	N43° W92°
(Denniston et al., 1999)	7.5-1	1.01	8.8	320	N43° W92°
(Dorale et al., 1992)	7.7-1.15	1.99	8.8	320	N43° W92°
(Dorale et al., 1992) <sup>8</sup>	7.7-5.9	3.02	8.8	320	N43° W92°
(Dorale et al., 1992) <sup>8</sup>	5.9-3.6	1.59	8.8	320	N43° W92°
(Dorale et al., 1992) <sup>8</sup>	3.6-1.15	1.9	8.8	320	N43° W92°
(Dorale et al., 1998)	65-25	1.34			N38° W90°
(Dorale et al., 1998)	70-35	0.29			N38° W90°
(Dorale et al., 1998)	75-25	0.37			N38° W90°
(Gascoyne et al., 1981)	55-50		4	365	N49° W125°
(Gascoyne et al., 1981)	64-28	0.23	4	365	N49° W125°
(Gonzalez and Gomez, 2002)	12-0				N11° W70°
(Harmon et al., 1978a)	230-100	0.22	13.5	160	N38° W86°
(Lauriol et al., 1997)	>350		~0	990	N66° W141°
(Lauriol et al., 1997)	81		~0	1219	N66° W141°
(Mickler, 2004)	11.6-8.4		26.6	250	N13° W60°
(Mickler, 2004)	93.5-66.6		26.6	250	N13° W60°
(Mickler, 2004)	23.1-22.1		26.6	250	N13° W60°
(Mickler, 2004)	51-38		26.6	250	N13° W60°

Ref.	Age Range ka	G.R. <sup>Δ</sup> cm/ka	T °C	Elev. m	Location
(Mickler, 2004)	25		26.6	250	N13° W60°
(Mickler, 2004)	25		26.6	250	N13° W60°
(Mickler, 2004)	34.4-0		26.6	250	N13° W60°
(Mickler, 2004)	53.9-0		26.6	250	N13° W60°
(Banner et al., 1994)	35.5-1.8	1.2	22		N30°W98°
(Banner et al., 1994)	71.2-13.9	0.05-8	22		N30°W98°
(Banner et al., 1994)	27.6-13.2	8.3	22		N30°W98°
(Banner et al., 1994)	69.6-15.3	0.08-10			N30°W98°
(Banner et al., 1994)	>350-29			600	N29°W100°
(Banner et al., 1994)	>350-20.4	0.25		600	N29°W100°
(Banner et al., 1994)	229.9-11.9	0.16		600	N29°W100°
(Banner et al., 1994)	38.5-7.7	0.05-8	19		N30°W99°
(Banner et al., 1994)	16.8-11	14.3	21		N30°W98°
(Banner et al., 1994)	11.5-8.1	3.9	21		N30°W98°
(Serefiddin et al., 2004)	82-24	1.65	8	1400	N44°W104°
(Serefiddin et al., 2004)	62-50	0.22	8	1400	N44°W104°
(Thompson et al., 1976)	200-165	2	11	655	N38° W81°
(Thompson et al., 1976)	0-2	10	11	655	N38° W81°
(Thompson et al., 1976)			11	655	N38° W81°
(Thompson et al., 1976)			11	715	N38° W81°
(van Beynen et al., 2004)	180-145, 125-62 7.6-0	0.2 103-2	7.3	430	N38°W91°
<b>Europe</b>					
(Bard et al., 2002)	190-142	0.25	15.8	<40m	N42° E11°
(Duplessy et al., 1971)	130-90	6	12.6		France
(Duplessy et al., 1969)			12.6		France
(Duplessy et al., 1969)					France
(Fornaca-Rinaldi et al., 1968)					Italy



Ref.	Age Range ka	G.R. <sup>^</sup> cm/ka	T °C	Elev. m	Location
(Fornaca-Rinaldi et al., 1968)					Italy
(Fornaca-Rinaldi et al., 1968)					Italy
(Gascoyne, 1992)	238-225				N54° W2°
(Gascoyne, 1992)	126-108				N54° W2°
(Gascoyne, 1992)	114-98	0.75			N54° W2°
(Gascoyne, 1992)	290-210,320-250	0.3			N54° W2°
(Gascoyne, 1992)	180-170	2			N54° W2°
(Schwarcz, 1986)]	290-190	0.3			N54° W2°
(Genty et al., 2003)	83.1-31.8	2.89	11		N46° E0°
(Genty et al., 2003) <sup>ss</sup>	83-79	3.75	11		N46° E0°
(Genty et al., 2003) <sup>ss</sup>	76-67	3.11	11		N46° E0°
(Genty et al., 2003) <sup>ss</sup>	61-56	2.05	11		N46° E0°
(Genty et al., 2003) <sup>ss</sup>	52-40	7.4	11		N46° E0°
(Genty et al., 2003) <sup>ss</sup>	40-32	0.99	11		N46° E0°
(Genty et al., 1998)	0.045-0	8.8	8.9	180	N50° E5°
(Gewelt, 1981)	11-5		9		N50° E5°
(Horvatincic et al., 2003)	Holocene		8	529	N46° E14°
(Jimenez de Cisneros et al., 2003)	190-160		20		N37° W4°
(Kacanski et al., 2001)	2.3-0	6.36	11.6	530	N45° E21°
(Kadlec et al., 1996)	100, 124-114.4				
(Kadlec et al., 1996)	114.4 to 99.9				
(Labonne et al., 2002)	22-10.7	2.2	18		N42° E3°
(Lauritzen and Onac, 1999)	131-58	0.67		545	N47° E23°
(Lauritzen and Lundberg, 2004)	424-392	.25 to .66			N66° E14°
(Lauritzen, 1995)	118-6	3.5		920	N68° E16°
(Lauritzen, 1995) <sup>ss</sup>	8-6	3.5		920	N68° E16°

Ref.	Age Range ka	G.R.^ cm/ka	T °C	Elev. m	Location
(Lauritzen, 1995) <sup>8</sup>	118-106			920	N68° E16°
(Lauritzen, 1995)	145-80	0.21		160	N67° E14°
(Linge et al., 2001)		3.41		160	N67° E14°
(Linge et al., 2001)	200				N66° E13°
(Linge et al., 2001)	123-73	4.6	3.5	220	
(Linge et al., 2001)	Eemian		2.8	280	N67° E13°
(Linge et al., 2001)	140-10		2.8	280	N67° E13°
(Linge et al., 2001)	4.2-0	3.46	2.8	280	N67° E13°
(Linge et al., 2001)	8-4.5		2.8	280	N67° E13°
(Berstad et al., 2002)	630-330	0.08	2.8	280	N67° E13°
(McDermott et al., 1999)	12-0	4	6.6	1165	N45° E12°
(McDermott et al., 1999)	9-0	4.04	10.4	60	N52° W9°
(McDermott et al., 1999)	11.5-0	4.3	14.5	75	N44° E4°
(Plagnes et al., 2002)	189-74	0.2-10	14.5	75	N44° E4°
(Plagnes et al., 2002) <sup>8</sup>	75.7-74.5	6	14.5	75	N44° E4°
(Plagnes et al., 2002) <sup>8</sup>	83.4-82.4	20	14.5	75	N44° E4°
(Plagnes et al., 2002) <sup>8</sup>	112.5-99.1	0.2	14.5	75	N44° E4°
(Plagnes et al., 2002) <sup>8</sup>	128-118	3	14.5	75	N44° E4°
(Plagnes et al., 2002) <sup>8</sup>	170-160	1	14.5	75	N44° E4°
(Plagnes et al., 2002) <sup>8</sup>	189-188	10	14.5	75	N44° E4°
(Niggemann et al., 2003b)	12.5-6	12.5-6	9.4	185	N49° E7°
(Niggemann et al., 2003b)	9-5.5	9-5.5	9.4	185	N49° E7°
(Niggemann et al., 2003b)	18-17, 9.5-5.2, 2-0	1.8-26	9.4	185	N49° E7°
(Niggemann et al., 2003a)	6-0.8	7.01	9.4	308	N49° E7°
(Onac et al., 2002)	8-1	3.1	9.8	482	N47° E23°
(Pazdur et al., 1995)	28-18.9	3.1	1100	385	N51° E19°
(Spötl et al., 2001)	8-0	3.9	5.4		N47° E15°

Ref.	Age Range ka	G.R.^ cm/ka	T °C	Elev. m	Location
(Verheyden et al., 2000)	13-1.8	5.8	8.9?	203	N50° E5°
<b>Middle East</b>					
(Bar-Matthews et al., 2003b)	250-0		16	650	N33° E35°
(Bar-Matthews et al., 2003b) <sup>8</sup>	250-0		16	650	N33° E35°
(Bar-Matthews et al., 2003b) <sup>8</sup>	120-14		16	650	N33° E35°
(Bar-Matthews et al., 2003b) <sup>8</sup>	120-131		16	650	N33° E35°
(Bar-Matthews et al., 2003b) <sup>8</sup>	250-135		16	650	N33° E35°
(Bar-Matthews et al., 2003b) <sup>8</sup>	184-0	1.5 100	22.5	400	N31° E35°
(Bar-Matthews et al., 2003b)	184-0 Excl7-7.5,119-128	1.5 100	22.5	400	N31° E35°
(Bar-Matthews et al., 2003b) <sup>8</sup>	118-0	1.5 100	22.5	400	N31° E35°
(Bar-Matthews et al., 2003b) <sup>8</sup>	128-118		22.5	400	N31° E35°
(Bar-Matthews et al., 2003b) <sup>8</sup>	184-128		22.5	400	N31° E35°
(Burns et al., 2002)	0.740-0	31			Oman
(Frumkin et al., 2000)%	170-65	1	17	730	N32° E35°
(Frumkin et al., 2000)%	45-0	2	17	730	N32° E35°
(Frumkin et al., 1999)	6-0	4.4	19	600	N32° E35°
(Vaks et al., 2003)	67-16.6	2to100	21.5	250	N32° E35°
<b>China</b>					
(Hou et al., 2003)	1-0	15	15	200	N40°E116°
(Hou et al., 2003)	2.2-0	8.7	15	200	N40°E116°
(Li et al., 1998)	0.486-0	100	15	200	N40°E116°
(Tan et al., 1998)			15	200	N40°E116°
(Huang, 1992)	16.5-3	1			Hubei
(Huang et al., 2001)	20.2-10.5	5		205	N31°E111°
(KDL)	190-90	2.46			N26°E106°
(KDL)	44-0	4.27			N26°E106°

Ref.	Age Range ka	G.R.^ cm/ka	T °C	Elev. m	Location
(Li et al., 1996)	36.4-326.3-1.1		19.5	200	N39°E115°
(Ma et al., 2003)	3-0	1	13	100	N40°E117°
(Paulsen et al., 2003) <sup>%</sup>	0-150	1.38	14	500	N34°E109°
(Paulsen et al., 2003) <sup>%</sup>	150-1230	1.38	14	500	N34°E109°
(Wang, 1986)	>350-112				250
(Wang, 1986)	385-267	2.7			250
(Wang et al., 2001) <sup>&amp;∞</sup>	75-11		15.4	80	N32°E119°
(Wang et al., 2001) <sup>&amp;</sup>	54-19	1	15.4	80	N32°E119°
(Wang et al., 2001) <sup>&amp;</sup>	75-31	1.16	15.4	80	N32°E119°
(Wang et al., 2001) <sup>&amp;</sup>	19-11	0.84	15.4	80	N32°E119°
(Wang et al., 2001) <sup>&amp;</sup>	17-14.5	4.1	15.4	80	N32°E119°
(Wang et al., 2001) <sup>&amp;</sup>	16-11	2.99	15.4	80	N32°E119°
(Wang et al., 1998) <sup>&amp;</sup>	380-170	0.34	15.4	80	N32°E119°
(Zhao et al., 2003) <sup>&amp;</sup>	17-10		15.4	80	N32°E119°
(Wang et al., 1995)	76-55	1.1			near Beijing
(Wang et al., 1995)	158-74	0.53			near Beijing
(Zhang et al., 2004)	152-122	7.4	15.8		N26°E108°
(Zhang et al., 2004)	164-91.5	0.15-19	15.6	680	N25°E108°
(Zhang et al., 2004) <sup>∞</sup>	<124	5.4	15.6	680	N25°E108°
(Zhang et al., 2004) <sup>∞</sup>	>124	0.72	15.6	680	N25°E108°
(Zhang et al., 2004)	155-0.09	1.1-49	15.6	680	N25°E108°
(Zhang et al., 2004) <sup>∞</sup>	<9.3	18	15.6	680	N25°E108°
(Zhang et al., 2004) <sup>∞</sup>	16-9.3	4.5	15.6	680	N25°E108°
(Zhang et al., 2004) <sup>∞</sup>	66-42	1.7	15.6	680	N25°E108°
(Zhang et al., 2004) <sup>∞</sup>	>113	1.6	15.6	680	N25°E108°
<b>Australia/New Zealand</b>					
(Desmarchelier et al., 2000)	190-152	0.83	16.8	70	N37°E141°

Ref.	Age Range ka	G.R.^ cm/ka	T °C	Elev. m	Location
(Fischer et al., 1996)	55-18,2.6-0				S20°E140°
(Goede et al., 1986)	110-72	4.05	9.5	460	S42°E146°
(Goede and Vogel, 1991)	15-11.7	22.2	9.5	300	S42°E146°
(Xia et al., 2001)	9.9-5.1	26.9	9.5	300	S42°E146°
(Goede et al., 1990)	4.25-2.9	26.7	8.3	360	S43°E146°
(Goede, 1994)	98-55	1.99	8.3	360	S43°E146°
(Goede et al., 1996)	2, 13.2-10.9	2.2	15	80	S37°E148°
(Hellstrom et al., 1998)	17-0	0.12	7	685	S41°E173°
(Hellstrom et al., 1998)	31-0	2to 5	5	390	S41°E172°
(Williams et al., 1999)	3.9-0	8.1	11.5	325	S38°
(Williams et al., 1999)	10.22-0	3.3	13.3	100	S38°
(Williams et al., 1999)	10.52-0	7.5	13.3	100	S38°
(Williams et al., 1999)	0.1-0		11.5	320	S38°
<b>Africa</b>					
(Holmgren et al., 1995)	51-43,38-35,28-21	0.86	20.6	1128	S25° E26°
(Holmgren et al., 2003)	6.4-0	18.5	18	400	S24° E29°
(Holmgren et al., 2003)	24.4-12.7,10.2-0	2,11	18	400	S24° E29°
(Repinski et al., 1999)	4.4-4.0,8-0	50	18	400	S24° E29°
(Talma and Vogel, 1992)	45-12,5-0		17.5		S33° E22°
(Talma et al., 1974)			21	486	S24° E30°

- § Speleothems are designated with a slope of  $\delta^{18}\text{O}$  vs.  $\delta^{13}\text{C}$  (X vs. Y) graph for those studies providing either raw data, regressions, or graphs. When data were available, these slopes were determined by orthogonal regression. We categorized those speleothem studies that provide spatial or temporal variations in  $\delta^{18}\text{O}$  and  $\delta^{13}\text{C}$  values into 5 qualitative categories, corresponding to synchronous positive (+) or negative (-) co-variation in  $\delta^{18}\text{O}$  and  $\delta^{13}\text{C}$  values, as indicated by coincident minima or maxima and overall temporal trends. Those with no apparent co-variation are designated as “X”, and those with exceptional co-variation are designated “+ +” or “- -”. Some speleothems display discrete portions with positive, negative or non-correlation, and are designated accordingly (e.g. +X).
- ‡ The linear correlation coefficient, R, between  $\delta^{18}\text{O}$  and  $\delta^{13}\text{C}$  values, is designated as significant with \* (>95% confidence), or highly significant with \*\* (>99% confidence). The lack of either \* or \*\* indicates a correlation without rigorous significance.
- § Type of speleothems are designated as: S=stalagmite, F=flowstone, Sc=stalactite, with composite stalagmite records designated “S,S”.
- ^ Average or range of speleothem growth rates.
- ∞ Indicates portions of speleothems or composite speleothem records that are excluded from the compilation in table 4.
- % These two segments of a single speleothem were merged as one item for Table 5.
- & All of these speleothems are from the Hulu/Tangshan cave. Presumably for an unknown environmental reason most of these speleothems have negative correlations between  $\delta^{18}\text{O}$  and  $\delta^{13}\text{C}$  values, comprising 5 of 6 speleothems with negative correlations in Table 4.

\$ The correlation between  $\delta^{18}\text{O}$  and  $\delta^{13}\text{C}$  values of speleothem calcite are designated as in Table 3, with qualitative categories + and – corresponding to positive and negative co-variation in  $\delta^{18}\text{O}$  and  $\delta^{13}\text{C}$  and + + and - - indicating strong positive and negative co-variation. X indicates no systematic co-variation in  $\delta^{18}\text{O}$  and  $\delta^{13}\text{C}$  values. Those speleothems with correlation coefficients which are significant (>95% confidence) or highly significant (>99% confidence) are also designated with + +, or - -.

Table 3.4 Summary of speleothem records with  $\delta^{18}\text{O}$  and  $\delta^{13}\text{C}$  value correlations

Category	statistical descriptor	#	%	
- -	>99% confidence	4	2.8	Negative Correlation
-	<95% confidence	2	1.4	4.3%
- , X		5	3.5	
X	no correlation	37	25.9	No Correlation
+ , X		6	4.2	33.6%
+		26	18.2	
+	<95% confidence	17	11.9	Positive Correlation
+ +	High confidence	7	4.9	62.2%
+ +	>95% confidence	5	3.5	
+ +	>99% confidence	34	23.8	
Total		143		



## **CHAPTER 4: APPLICATION OF HIGH-RESOLUTION X-RAY COMPUTED TOMOGRAPHY IN DETERMINING THE SUITABILITY OF SPELEOTHEMS FOR USE IN PALEOCLIMATIC, PALEOHYDROLOGIC RECONSTRUCTIONS**

### **ABSTRACT**

The isotopic and elemental compositions of speleothems can be used as proxies to elucidate past climate changes. Speleothem material is precious, however, and its use in such climate studies must be balanced against the need to preserve fragile cave environments. Accordingly, accurate assessment of the internal speleothem stratigraphy can provide insight into: 1) Overall sample quality for paleoclimate studies, and 2) the position of the central growth axis of the sample prior to destructive sample preparation, which involves bisecting by sawing the sample along its growth axis. Chemical and isotopic samples taken along the growth axis have the greatest potential to reflect the composition of the water from which the speleothem precipitated. The growth axis of speleothems cannot be reliably determined by visual inspection of uncut specimens, and incorrect bisections may compromise their applicability as geochemical climate proxies.

High-resolution X-ray computed tomography (HRXCT) is a non-destructive technique that can identify the position of the growth axis in speleothems by detecting subtle changes in calcite density between growth bands. HRXCT imagery of these variations can be animated as ‘stacks’ of slices and rendered in three dimensions. Such imagery can be used to identify the best plane along which the speleothem should be sectioned for sampling. These images may also reveal

samples that have been extensively altered during their history, making them unsatisfactory for climatic studies. Additionally, HRXCT imagery can be used to determine the volume and location of large fluid inclusions for use in reconstructing the H and O isotopic composition of paleoprecipitation.

## **INTRODUCTION**

The use of isotopic and trace element compositions of speleothems (i.e., secondary cements found in caves such as flowstones, stalagmites, and stalactites), has grown with the increased interest in climate change studies. Speleothems are effective proxies in paleoclimate studies for several reasons, including the following: 1) they contain trace element and isotopic tracers that have been used to infer changes in paleotemperature, paleovegetation and paleoprecipitation (Hendy and Wilson, 1968; Dorale et al., 1992; Winograd et al., 1992; Banner et al., 1996; Baker et al., 1998a; Genty et al., 1998); 2) they may be continuously deposited over thousands of years and have thin growth bands that can be precisely dated using U series dating methods (Musgrove et al., 2001); 3) growth rates of these bands may provide proxies for environmental parameters such as aquifer recharge rates (Proctor et al., 2000; Polyak and Asmerom, 2001; Tan et al., 2003), and 4) speleothems form in a wide variety of locations where other high-resolution climate records may be absent. Although the potential value of speleothems in climate studies is clear, geochemical sampling is destructive, such that speleothem use should be balanced with the need to conserve fragile cave environments and material.

A speleothem is usually prepared for sampling by slicing the specimen, with a rock saw, along the growth axis and polishing the slabbed surface. The elemental and isotopic composition of speleothems may change away from the growth axis due

to changes in water chemistry caused by progressive CO<sub>2</sub> degassing, evaporation and calcite precipitation (Hendy and Wilson, 1968; Hendy, 1971; Gonzalez and Lohmann, 1988). Specifically, off-axis samples are more subject to non-equilibrium fractionation effects that are not regular or predictable. In addition, recent studies have attributed paleoenvironmental significance to changes in speleothem growth band thickness (Proctor et al., 2000; Polyak and Asmerom, 2001; Tan et al., 2003). Growth bands in speleothems thin away from the growth axis. For these reasons, acquisition of the most reliable paleoenvironmental information requires that speleothems be sectioned to intersect the growth axis. Unfortunately, the growth history of speleothems is often complex (Fig. 4.1), making external visual identification of the growth axis difficult or impossible. A mistake during slabbing wastes valuable speleothem material and may limit data quality.

Computed tomography (CT) is a non-destructive technique for creating images of the interior of solid opaque objects (Ketcham and Carlson, 2001). Rather than conventional X-radiography, in which an X-ray cone beam is projected through an entire sample onto film, CT images are created by directing a planar fan beam at an object from multiple angular orientations. The resulting images are termed slices because they correspond to what would be observed if the object were cut open along the image plane. The grayscales in these images correspond to relative X-ray attenuation, which is a function of elemental composition and density. By obtaining a series of contiguous slices for an object, a complete three-dimensional volume can be imaged. Because the fan beam has a thickness determined by the X-ray spot size and detector vertical pitch or collimation, the pixels in CT images are called voxels, or volume elements. Resolution in CT images is partly determined by the voxel dimensions, and partly by properties of the features being imaged.

High-resolution X-ray CT (HRXCT) is an industrial adaptation of standard medical CT or CAT scan. It differs in that it can use higher-energy X-rays, finer detectors, and longer imaging times, allowing it to penetrate denser objects and achieve 1-3 orders of magnitude better resolution than medical devices (Ketcham and Carlson, 2001). The scanner at The University of Texas at Austin can image objects up to 500 mm in diameter, with a height of up to 1500 mm. Slice thickness on large objects (in excess of 75 mm in diameter or 150 mm high) can be as low as 0.25 mm. For smaller objects, the minimum slice thickness is approximately 1/1000 of the cross-sectional diameter, and can be as low as 5  $\mu\text{m}$ .

HRXCT provides a non-destructive means to image the internal stratigraphy of speleothems, as it can detect density contrasts within the calcite growth bands. CT slices of these ‘stratigraphic’ variations can be animated as ‘stacks’ of slices, as well as rendered as a three-dimensional (3D) volume. The resulting imagery can serve as a guide to determine the most appropriate plane for sample sectioning and the overall suitability of the sample for study.

## **MATERIALS AND METHODS**

### **Specimens**

Stalagmite AH-M was collected at the Apes Hill Quarry, Barbados, West Indies (Fig. 4.1 and 4.2). The stalagmite was unearthed from a cavity during quarry operations and subsequently donated to the University of Texas as part of an ongoing study of paleoclimatic and paleohydrologic reconstruction. The stalagmite is approximately 24 cm in height and 12 cm in diameter and consists of dense, optically

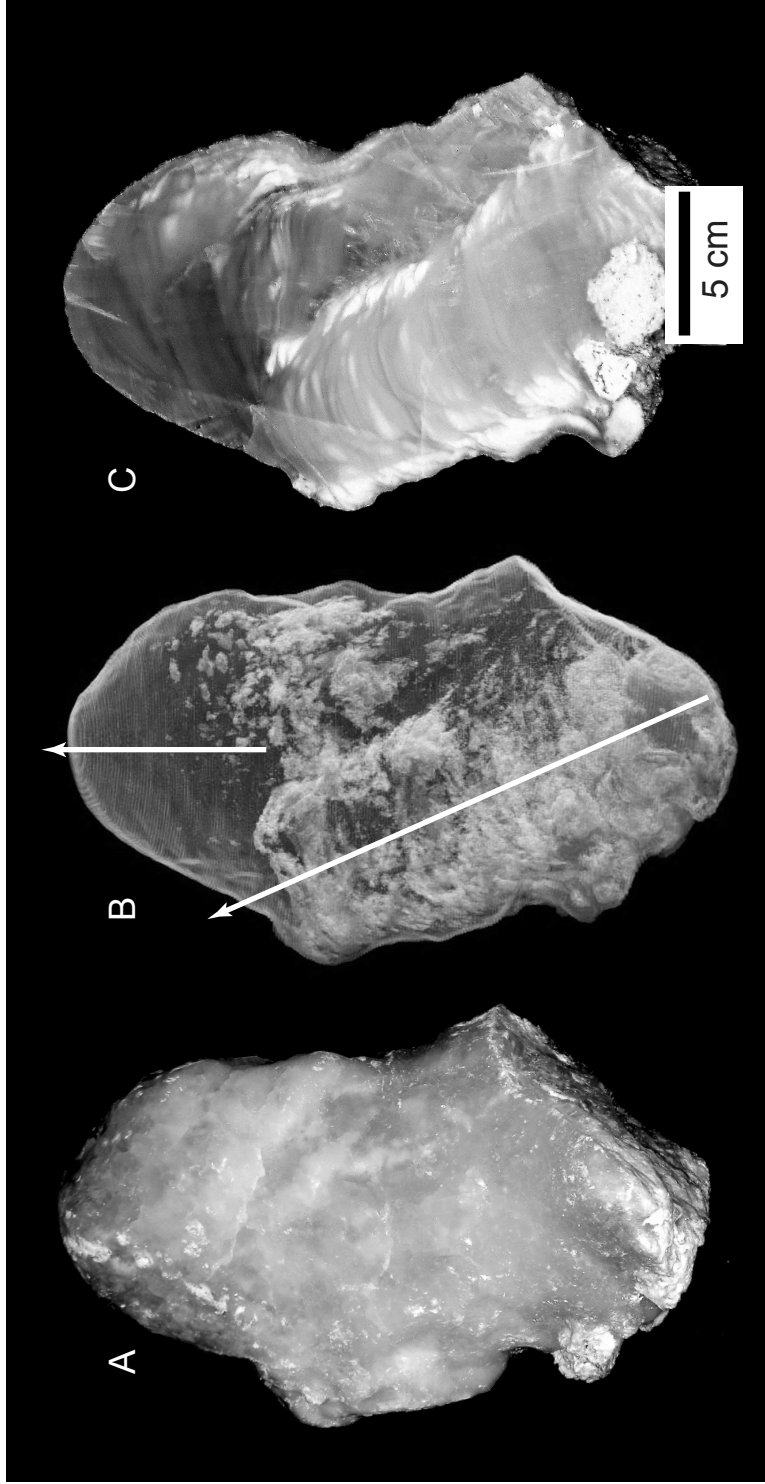


Figure 4.1 A. Photograph of the unsliced, unpolished side of stalagmite sample AH-M. Note that no internal structure is visible. B. Three-dimensional volume rendering of AH-M with solid material rendered transparent and inclusions rendered in lighter grays. Solid arrows indicate two different growth axes easily visible in the HRXCT data. The speleothem apparently leaned to one side during its growth, shifting the locus and apparent direction of precipitation. These images are available as a complete animation at: <http://www.crlab.geo.utexas.edu/pubs/mickleretal/mickleretal.htm> C. Photograph of the sliced and polished stalagmite AH-M. Note how the internal stratigraphy identified by HRXCT scanning prior to the slicing of the sample matches the stratigraphy of the polished specimen. The scan was used to identify the plane that intersected both growth axes.

clear calcite crystals. Like most speleothems, its shape and texture do not allow its internal stratigraphy to be ascertained.

Stalagmite ANY-01 (Fig. 4.3) was collected from Anyway Cave, Hays County, Texas for use in an ongoing study of paleoclimatic and paleohydrologic reconstruction. The stalagmite is approximately 33 cm in height and 20 cm in diameter. Dark staining on the outside of the stalagmite, plus the reasons given above for AH-M, made determination of the internal stratigraphy impossible. Both stalagmite samples were CT scanned prior to sample preparation.

### **CT scanning**

This section on CT scanning, and other information in this chapter specifically pertaining to the technical aspects of the CT process, have been written by Dr. Richard Ketcham and Dr. Matthew Colbert. This information was compiled for publication in the *Journal of Caves and Karst Studies* (Mickler et al., 2004). The speleothem specimens were scanned at the High-Resolution X-ray Computed Tomography (CT) Facility at The University of Texas at Austin (UTCT). The facility and typical scanning procedures and parameters are described in detail by Ketcham and Carlson (2001). Scanning parameters were optimized for fast acquisition of slices, to minimize scanning time and costs. For sample AH-M, X-ray energy was set to 420 kV and 4.7 mA, with a focal spot size of 1.8 mm. X-rays were pre-filtered to reduce beam-hardening artifacts (artificial brightening of the edges compared to the center of the images caused by preferential attenuation of soft X-rays through dense objects) using two brass plates with a total thickness of 3.175 mm. X-ray intensities were measured using a 512-channel cadmium-tungstate solid-state linear array, with a horizontal channel pitch of 0.31 mm. Each slice was

acquired using 808 views (angular orientations), each view having an acquisition time of 32 ms. The resulting acquisition time was approximately 34 seconds per slice. The speleothem was scanned in a 160% offset mode (Ketcham and Carlson, 2001), with a slice thickness and inter-slice spacing of 1.0 mm. The image field of reconstruction was 180 mm, and the reconstructed image was created as a 512x512 16-bit TIFF file, resulting in an in-plane pixel resolution of 0.35 mm. Image reconstruction parameters were calibrated to maximize usage of the 12-bit range of grayscales available in the output images. 239 images were obtained, with a total scanning time of approximately 2.25 hours.

For sample ANY-01, scanning parameters were changed slightly to accommodate the different sample dimensions. The differences were that the offset mode was 130%, there were 1000 views per slice, slice thickness and spacing were 2.0 mm and the field of reconstruction was 155 mm. 153 slices were acquired, and the total scan time was approximately 1.75 hours.

Overall costs were \$200-\$300 per sample scanned. While not trivial, such amounts are small compared to the time and expense of field work and geochemical analysis, in addition to the larger issues of data quality and preservation of cave material. It should also be emphasized that data with better clarity and resolution than that presented here can be obtained with the equipment used for this study, if greater detail is required for a particular research objective.

### **Image processing**

Animations of the original CT serial sections were made using QuickTime™. Two techniques were used to study the data in 3D. First, images were ‘resliced’ along orthogonal planes using ImageJ© creating a series of images that can be

animated. This software program can be downloaded from the National Institutes of Health (NIH) web site (<http://rsb.info.nih.gov/ij/>). Second, a technique known as volume rendering was used to create visualizations of the entire data volume in 3D. Volume rendering consists of allocating to each voxel grayscale value a color and opacity, allowing some materials to be transparent while leaving others partially or fully opaque, while also retaining the density information in the images. The entire data set can be rendered, or a part can be cut away along an arbitrary plane to reveal any internal surface. These renderings were accomplished using VG Studio Max™ software (Volume Graphics GmbH, Heidelberg, Germany).

## **RESULTS AND DISCUSSION**

CT scanning of the speleothems reveals complex internal stratigraphies that can not be identified by visual inspection of the uncut specimens. For sample AH-M, CT scanning revealed that the locus of deposition changed significantly at least three times as the stalagmite leaned to one side during its growth (Fig. 4.1). This stratigraphy likely resulted from deposition on a soft substrate that settled during formation of the stalagmite. Similar to AH-M, CT scanning of ANY-01 reveals that the latest stage of growth took place off the main axis (Fig. 4.3). Additionally, the late stage calcite is denser than the previously deposited calcite and formed a drape on the outside of the stalagmite, which obscures the porous nature of the underlying calcite. CT scanning reveals the multiple growth axes of these stalagmites and the planes that intersect these axes (Fig. 4.2).

In addition to aiding in the identification of the growth axes, CT scanning also reveals the volume and location of large voids within the stalagmite, which may be filled with air or water (Fig. 4.2). Researchers have recently analyzed water from



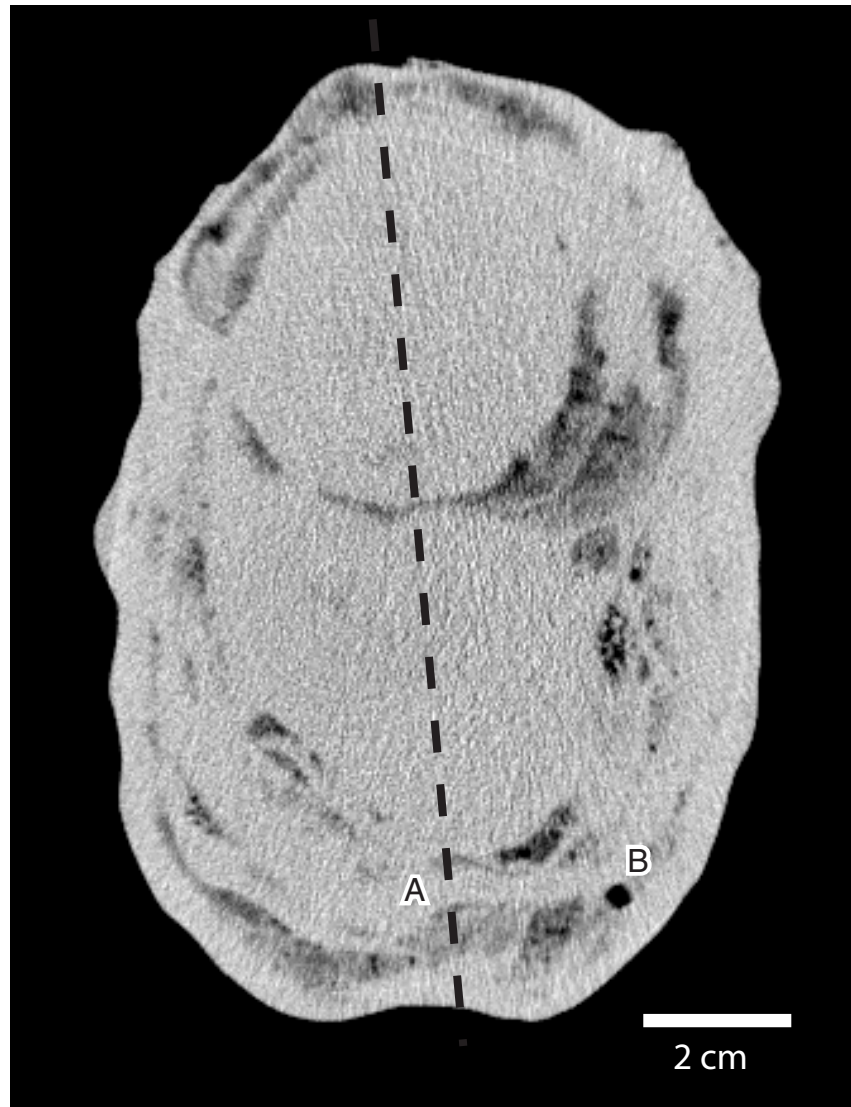


Figure 4.2. HRXCT slice through AH-M showing density variations. Higher densities are indicated by lighter gray scale values. Two sets of concentric growth bands are visible. The upper set was apparently deposited before subsidence of the speleothem. The lower set indicates the location of the new growth axis on the flanks of the previously deposited speleothem material. A plane that bisects both growth axes is easily determined (dashed line A). A large void, near B, may be filled with air or the water from which this speleothem precipitated.



Figure 4.3. Volume renderings of ANY-01. Cutaways reveal a late shift in the primary growth axis and significant internal porosity around the growth axis. Calcite deposited after the shift in the growth axis has a significantly lower porosity and higher density than calcite near the core of the speleothem. This calcite drape further complicates the visual inspection of the speleothem by obscuring the highly porous central core.

large fluid inclusions in speleothems for use in paleoprecipitation stable-isotope reconstructions (Genty et al., 2002). The dramatic density contrast between calcite and pore space (either water or air filled) allows easy identification of voids that fall within the scan's scale of resolution. A more time-intensive scanning protocol with detailed calibration could potentially allow discrimination between fluid-filled and air-filled voids, although this was not undertaken in this study because the primary objective was inexpensive inspection for growth axis determination.

The scanning reveals that AH-M is comprised of dense calcite with an occasional isolated void. In contrast, the calcite around the primary growth axis of ANY-01 varies greatly in density and contains many large and small voids (Fig. 4.3). Porous calcite around the growth axis of a speleothem may allow both post-depositional alteration of calcite through isotopic and elemental exchange with cave water and emplacement of pore filling calcite cements. Such processes will alter the primary isotopic and elemental composition of a speleothem, rendering it unsuitable for paleoclimate studies. For these reasons, ANY-01 was not sliced for sampling. Where feasible such samples can be returned to the location with the cave from which they were collected.

Another feature of CT imagery is that it can be easily disseminated via the Internet, both as a record of the work done and potentially as an educational or archival resource. Web based images allow remote users to view CT data animations, isolate individual slices and view rendered 3D volumes from any orientation. Scans and image processing of the samples used in this study are available on the World Wide Web at:

(<http://www.ctlab.geo.utexas.edu/pubs/mickleretal/mickleretal.htm>).

## **CHAPTER 5: BARBADOS SPELEOTHEM STABLE ISOTOPE RECORD**

### **INTRODUCTION**

Temporal variations in the  $\delta^{18}\text{O}$  and  $\delta^{13}\text{C}$  composition of ancient speleothems have been used to elucidate past climate change. A summary the significance of speleothem  $\delta^{18}\text{O}$  and  $\delta^{13}\text{C}$  records is given in the introductions to chapter 1, 2 and 3 of this document as well as the references discussed therein. In order to use equilibrium controlled fractionation factors to evaluate ancient speleothem records, the speleothem calcite must be precipitated in O and C isotopic equilibrium with its corresponding drip water, to be used reliably. Many studies of ancient speleothems assume that the speleothem calcite is precipitated in C and O isotopic equilibrium and the isotopic records are evaluated accordingly.

This study differs from many other speleothem-based climate studies because it first determines the extent to which equilibrium calcite precipitation is achieved in the modern system. Also, the kinetic isotope effects that cause deviations from equilibrium are identified and outlined in Chapters 2 and 3. In brief, speleothem calcite  $^{13}\text{C}$  depletions and  $^{18}\text{O}$  enrichment are likely caused by kinetically driven departures in the fractionation between  $\text{HCO}_3^-$  (aq) and  $\text{CaCO}_3$ . Also, speleothem calcite  $^{13}\text{C}$  and  $^{18}\text{O}$  enrichments can be accounted for by Rayleigh distillation of the  $\text{HCO}_3^-$  (aq) reservoir during degassing of  $\text{CO}_2$ . These kinetic isotope effects are considered when interpreting the temporal  $\delta^{18}\text{O}$  and  $\delta^{13}\text{C}$  trends of ancient speleothems from Barbados, West Indies.

## **SITE AND SAMPLE DESCRIPTION**

Five speleothems were collected from Barbados that collectively grew over the time interval from 11,573 to 0 yr. Sample locations are identified in Fig. 5.1. Two speleothems, BC-53 and BC-61, were collected from the Upper Passage in Harrison's Cave, a site that was also used in the study of modern speleothems outlined in Chapters 2 and 3. An image of BC-53 is given in Fig. 5.2; no high resolution image of BC-61 is available. Speleothem BC-61 was collected by Dr. Larry Edwards (University of Minnesota) and analyzed by Dr. Yemane Asmeron at the University of Minnesota. Three speleothems, AH-L, AH-M and AH-S, (Figs. 5.3, 5.4, 5.5 and 5.6) were collected from the Apes Hill quarry after the speleothems were unearthed during quarry operation. Speleothem AH-M was the focus of the CT imaging study outlined in chapter 4. Because the speleothems were collected from quarry tailings, detailed cave environmental conditions could not be collected. The Harrison's Cave sample locations have been discussed in chapter 2.

## **METHODS**

Speleothems were prepared for sampling by slicing the speleothem along its growth axis using a water saw. The location of the growth axis was determined prior to slicing using the methods outlined in Chapter 4 for the Apes Hill speleothems. The freshly slabbed surface was polished on a 12 inch flat lap using distilled water as a cooling agent. Coarse polishing was done on a 20  $\mu\text{m}$  metal bonded diamond lap and fine polishing was done using a progressively finer, 30, 10 and 2  $\mu\text{m}$ , resin bonded diamond laps. The laps were dedicated to speleothem sample preparation to avoid contamination issues. The speleothems were then gently washed using a dilute micro cleaning solution followed by ultrasonic cleaning in de-ionized water.

Calcite samples were collected for O and C isotopic analysis using a binocular microscope and a hand held dental drill with a 0.4mm drill bit. The sample site was prepared by removing the top most layer of calcite using the dental drill. The resulting powder was discarded and the drill bit cleaned using a weak HCl solution and visually inspected under a binocular microscope. Approximately 2-3 mg of calcite were removed from the prepared surface and transferred to a sample vial.

Calcite  $\delta^{18}\text{O}$  and  $\delta^{13}\text{C}$  values were determined at the University of Texas at Austin. Approximately 200-350  $\mu\text{g}$  of calcite was reacted with 100%  $\text{HPO}_4$  at  $90^\circ\text{C}$  using a Micromass Multiprep system. The resulting  $\text{CO}_2$  gas was analyzed on a Prism II dual inlet mass spectrometer. Detailed analytical procedures are outlined in the methods sections of chapters 2 and 3. C and O isotopic analysis of BC-61 were analyzed at The University of Minnesota, where 100 to 200  $\mu\text{g}$  of  $\text{CaCO}_3$  were reacted with 100%  $\text{H}_3\text{PO}_4$ , cryogenically purified and analyzed on a Finnigan MAT delta E triple-collector mass spectrometer, method modified after McCrea (1950). Precision ( $2\sigma$ ) was reported by the University of Minnesota as 0.2‰ for  $\delta^{18}\text{O}$  and 0.13‰ for  $\delta^{13}\text{C}$ .

Samples were taken from the speleothems for U-series dating by drilling trenches approximately 5mm in width along discrete growth layers. Roughly 1 gram of calcite powder was collected for the procedure. The results of the U series dating are given in Table 5.3.

Uranium and thorium isotopic analysis was performed at the University of Texas using a Finnigan Mat 261 thermal ionization mass spectrometer upgraded with an ion counting system using a MasCom secondary electron multiplier. Samples were dissolved in  $\text{HNO}_3$  acid and spiked with a tracer of  $^{229}\text{Th}$ ,  $^{233}\text{U}$  and  $^{236}\text{U}$  with

known concentrations. After the sample and tracer were equilibrated, U and Th were coprecipitated using Fe and  $\text{NH}_4\text{OH}$ . The Fe coprecipitate was dissolved in 6N  $\text{HNO}_3$  and the U and Th were then separated using ion exchange resin chemistry. The U and Th aliquots were analyzed on single zone refined rhenium filaments loaded with colloidal graphite. Detailed procedures utilized at the University of Texas at Austin are outlined in Musgrove (2000). Standard values are outlined in Table 3. Procedural blanks for  $^{238}\text{U}$  and  $^{232}\text{Th}$  are approximately 1.9 and 2.2 pg respectively.

## RESULTS

The U-series dating of the speleothems allowed the speleothem calcite  $\delta^{18}\text{O}$  and  $\delta^{13}\text{C}$  values to be put in a chronostratigraphy (Figs. 5.7 and 5.8 respectively). The five speleothems produced a nearly continuous record from 11573 to 0 yr; the interval from 6655 to 5388 was not represented in the speleothem  $\delta^{18}\text{O}$  and  $\delta^{13}\text{C}$  records. The speleothem  $\delta^{18}\text{O}$  and  $\delta^{13}\text{C}$  values are given in Table 5.4 along with stratigraphic position and interpolated ages. Age errors associated with the dated horizons are given in Table 3.

The speleothems studied exhibit relatively larger  $\delta^{13}\text{C}$  variations, between -14‰ and -8 ‰ PDB, relative to the  $\delta^{18}\text{O}$  variability, between -4.5‰ and -2‰ PDB. Of the speleothems studied, four out of the five speleothems analyzed (AH-L, AH-M, AH-S and BC-61) exhibit a highly significant positive correlation between  $\delta^{18}\text{O}$  and  $\delta^{13}\text{C}$  values. The significance of strong positive correlations is outlined in Chapter 3. In the modern system, large  $^{13}\text{C}$  enrichments, relative to dripwater DIC and within individual glass plates, were caused by progressive calcite precipitation and  $\text{CO}_2$  degassing from the speleothem's drip water (Ch. 2 and 3). An extent of

reaction can be modeled using equilibrium fractionation factors and a Rayleigh distillation approach, outlined in chapter 3. The speleothems BC-53, BC-61, AH-L, AH-M and AH-S have a range in  $\delta^{13}\text{C}$  values of 3.85‰, 3.29‰, 4.88‰, 5.03‰ and 4.75‰ respectively. If the observed range of  $\delta^{13}\text{C}$  values were solely due to the progressive loss of  $\text{CO}_2$  and calcite precipitation then this would require a loss of DIC between 39% and 53%. Variations in the extent of reaction this large would result in extreme variations in calcite precipitation rates that are not recorded in these speleothems.

## DISCUSSION

The speleothems from Harrison's Cave, BC-53 and BC-61, exhibit similar O and C isotopic compositions and temporal trends (Fig. 5.7 and 5.8). Between approximately 5388 and 3000 yr the  $\delta^{18}\text{O}$  and  $\delta^{13}\text{C}$  values increase. The speleothem AH-M continues these trends, with a similar change in both  $\delta^{13}\text{C}$  and  $\delta^{18}\text{O}$  from approximately 9793 to 6655 yr. Despite the intriguing similarity in the temporal changes in both  $\delta^{13}\text{C}$  and  $\delta^{18}\text{O}$  between BC-53, BC-61 and AH-M, placing environmental significance on the  $\delta^{18}\text{O}$  and  $\delta^{13}\text{C}$  record is problematic.

I conclude that the ancient speleothems used in this study were not precipitated in O and C isotopic equilibrium with their corresponding drip water for several reasons: 1) The positive covariation between  $\delta^{18}\text{O}$  and  $\delta^{13}\text{C}$  values of four of five ancient speleothems studied is consistent with the non equilibrium isotope effects identified in modern speleothem calcite (Fig. 5.9). Because the ancient speleothem calcite was not directly compared to the stable isotopic composition of the water from which it precipitated, an absolute test for equilibrium calcite precipitation could not be made. An estimate of the  $\delta^{18}\text{O}$  value of the water a



speleothem precipitates from can be made by analyzing the H and O isotopic composition of fluid inclusion held in the speleothem (Matthews et al., 2000; Dennis et al., 2001; Genty et al., 2002). This was not done in this study. 2) The tip of BC-53 was actively growing when the speleothem was collected but the youngest calcite sampled on the speleothem was not in O isotopic equilibrium with the modern groundwater system. 3) It's unlikely that environmental factors alone could cause the high frequency variations seen in the  $\delta^{18}\text{O}$  and  $\delta^{13}\text{C}$  values of ancient speleothems. For example, AH-L shows a 5‰ shift in  $\delta^{13}\text{C}$  and a 1.5‰ shift in  $\delta^{18}\text{O}$  values of speleothem calcite in a 2000 year time interval. If these shifts were interpreted using equilibrium fractionation factors, a large shift in the proportion of C3 and C4 plants as well as a temperature shift of 3 to 4°C, or a change in the O isotopic composition of average rainfall on Barbados of 1.5‰ would be required to justify the isotopic shifts observed. Large environmental fluctuations are not likely to have occurred in the tropics over the Holocene.

The non-equilibrium isotope effects outlined in chapter 2 and 3 suggest changes in the calcite precipitation rates may effect the  $\delta^{18}\text{O}$  and  $\delta^{13}\text{C}$  composition of the ancient speleothem calcite. Both BC-53 and BC-61 exhibit synchronous shifts in both  $\delta^{18}\text{O}$  and  $\delta^{13}\text{C}$  values yet they show no significant change in growth rate. Although more detailed chronology needs to be done, the only large shift in growth rate recorded, from 35 cm/ky to 2.2 cm/ky, occurs at the top of AH-L, synchronous with the change in calcite transparenence seen at the top of the speleothem (Fig. 5.3). This decrease in growth rate is accompanied by an increase in the  $\delta^{13}\text{C}$  values of the calcite in AH-L but no corresponding shift in O isotopes is seen. Also, the shift in  $\delta^{13}\text{C}$  values seems to be in the opposite direction than predicted; slower precipitation

rates should favor equilibrium calcite precipitation accompanied by C isotope equilibrium and lower  $\delta^{13}\text{C}$  values.

In addition, the  $\delta^{18}\text{O}$  and  $\delta^{13}\text{C}$  values of the speleothem calcite show no correlation with other paleoenvironmental records from the area. The temporal  $^{87}\text{Sr}/^{86}\text{Sr}$  variations in samples BC-53 and BC-61 were used to reconstruct the paleoprecipitation amounts on Barbados from 5388 to 0 yr (Banner et al., 1996). In this study the  $^{87}\text{Sr}/^{86}\text{Sr}$  ratio of speleothems from Harrison's Cave, including BC-53 and BC-61, were analyzed. It is hypothesized that periods of decreased rainfall on Barbados would increase groundwater residence times in the limestone aquifer and the water would obtain a  $^{87}\text{Sr}/^{86}\text{Sr}$  value close to the limestone. With increasing rainfall amounts, diffuse flowpaths are exceeded and the water utilizes faster conduit flow paths and the water retains a higher  $^{87}\text{Sr}/^{86}\text{Sr}$  value closer of the soil zone. The speleothems in Harrison's Cave are precipitated from this water and the speleothems retain the  $^{87}\text{Sr}/^{86}\text{Sr}$  values of the water.

In the modern system, changes in cave drip rate produced strong positive correlation in calcite  $\delta^{18}\text{O}$  and  $\delta^{13}\text{C}$  values in modern speleothems at the Spur 1 locality in Harrison's Cave (Chapter 2). Changes in recharge rates feeding water to the speleothem precipitation sites should cause synchronous changes in the  $\delta^{18}\text{O}$  and  $\delta^{13}\text{C}$  of the calcite precipitated at that site. There does not appear to be a correlation between the  $\delta^{18}\text{O}$  and  $\delta^{13}\text{C}$  values of the Harrison's cave speleothems with the  $^{87}\text{Sr}/^{86}\text{Sr}$  composition of those same speleothems. Therefore, the stable isotopic composition of Harrison's Cave speleothems do not show a correlation with the environmental fluctuations identified using Sr isotopes and other climatic and archeological records identified in Banner et al. (1996).

The  $\delta^{18}\text{O}$  and  $^{87}\text{Sr}/^{86}\text{Sr}$  values of fossil and living corals, from the island of Barbados, have been used to reconstruct the O isotopic composition and sea surface temperatures of the ocean around Barbados over the last 20,000 yr. (Fairbanks, 1989; Guilderson et al., 1994). This is significant to our study because the temperature and isotopic composition of the tropical Atlantic, the ultimate source of the water feeding the cave drip sites, will likely influence the  $\delta^{18}\text{O}$  value of the cave drip waters on Barbados and the speleothems precipitated from that drip water. The coral record does not match the Barbados speleothem record. The  $\delta^{18}\text{O}$  variability seen in the coral record, approximately 0.6‰, is much smaller than that seen in the speleothem record, approximately 2.3‰, over the last 12,000 yr. Also, the coral record does not show the high resolution-high frequency variations seen in the speleothem record. The coral record may be buffered by the relatively constant temperature and O isotopic composition of the ocean water relative to precipitation. In addition, few data points are represented in the coral record over the Holocene.

Holocene climate variations recorded in lake deposits have been used to reconstruct Caribbean climatic variability over the Holocene (Curtis, 1997). This study utilized lake cores from five lakes in the circum-Caribbean region; Punta Laguna and Coba (Yucatan Peninsula), Chichancanab (Yucatan Peninsula), Peten-Itza (Guatemala), Valencia (Venezuela) and Miragoane (Haiti). The compilation of the climatic records obtained from the analyses of these lake cores was used to produce a general Holocene climate record for the circum-Caribbean region. Prior to 10,500  $^{14}\text{C}$  yr BP the lake basins were dry indicating high evaporation/precipitation (E/P) ratios. The lakes began filling with water between 10,500 and 7,600  $^{14}\text{C}$  yr BP indicating lowering e/p ratios. High lake levels existed between approximately 8,500

and 3,000  $^{14}\text{C}$  yr BP indicating relatively moist conditions with low e/p ratios. Between 3,000  $^{14}\text{C}$  yr BP to present the lakes began to lower and higher  $\delta^{18}\text{O}$  values of lake cores suggest a gradual climatic drying.

If the ancient speleothem record was controlled by the same environmental factors that influenced the lake core record then I would expect to see relatively consistent  $\delta^{18}\text{O}$  and  $\delta^{13}\text{C}$  values in speleothem calcite deposited between 8500 and 3000 yr BP. Variable  $\delta^{18}\text{O}$  and  $\delta^{13}\text{C}$  values of speleothem calcite deposited before 10,500 yr and after 3000 yr BP should show the highest variability. The ancient speleothem  $\delta^{18}\text{O}$  and  $\delta^{13}\text{C}$  values do not conform to these assumptions.

## **FUTURE WORK**

This study quantified the magnitude and direction of non equilibrium isotope effects seen in the stable isotopic compositions of modern speleothems from Barbados. In addition, we proposed mechanisms responsible for those offsets. Unfortunately, changes in water chemistry due to  $\text{CO}_2$  degassing and calcite precipitation were not modeled as precisely as possible. We may not have accurately determined the chemistry of the water as it first entered the cave environment, before  $\text{CO}_2$  degassing and calcite precipitation altered that water chemistry. In addition, lack of data on the cave atmospheric  $\text{CO}_2$  concentration did not allow the chemistry of the cave water, in equilibrium with the cave environment, to be determined. Future work will concentrate on constraining changes in water chemistry through speleothem formation. The extent of TIC loss can then be compared to observed changes in speleothem  $\delta^{18}\text{O}$  and  $\delta^{13}\text{C}$  values to determine observed fractionation factors. These observed fractionation factors may be more applicable in explaining

the observed  $\delta^{18}\text{O}$  and  $\delta^{13}\text{C}$  values of ancient speleothems than experimentally determined equilibrium fractionation factors.

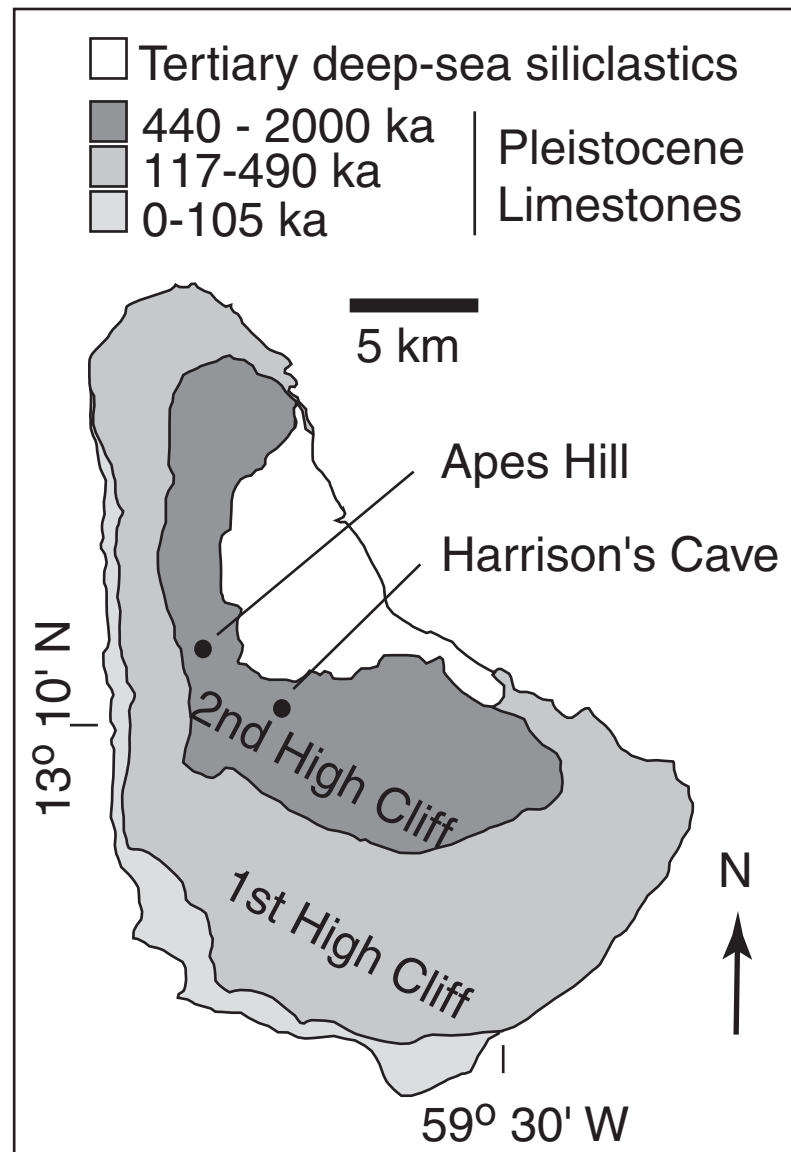
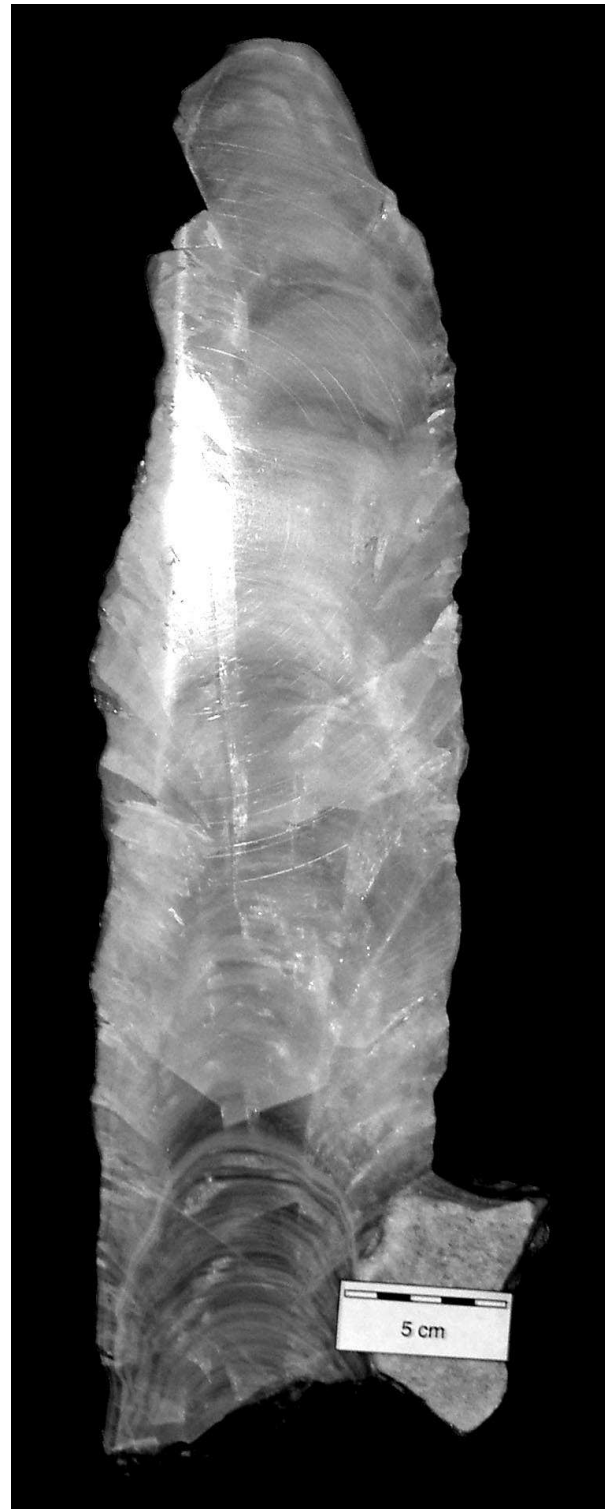


Figure 5.1 Map of Barbados, West Indies, showing the location of Harrison's Cave and Apes Hill quarry.

Figure 5.2 Speleothem BC-53 collected from Harrison's Cave. This speleothem is composed of transparent dense columnar calcite crystals. A block of country rock can be seen cemented into the lower portion of the speleothem below scale.



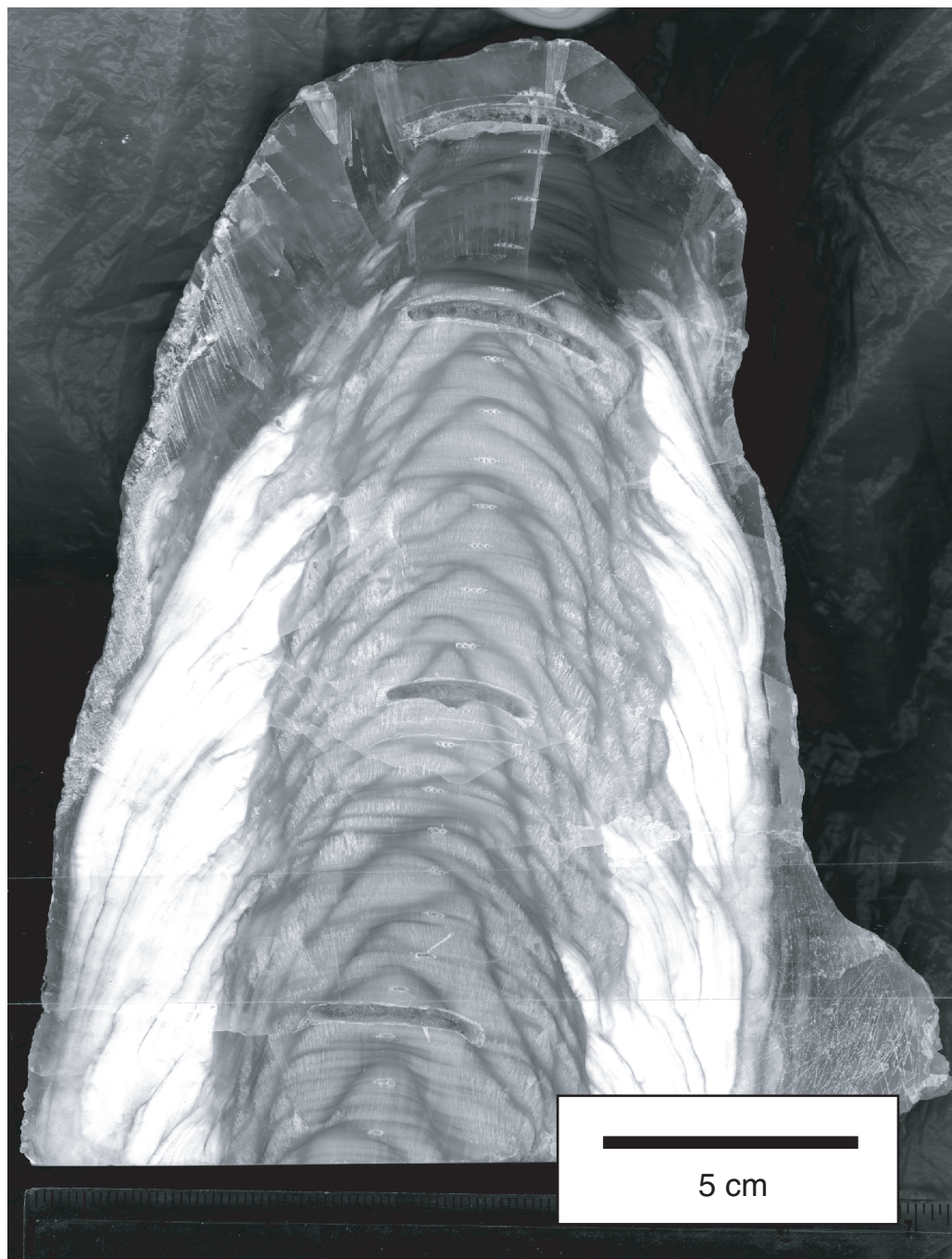


Figure 5.3 Speleothem AH-L top collected from Apes Hill quarry. Speleothem AH-L was too large to prepare for geochemical sampling. It was sawed roughly in half prior to polishing. The lower half of this sample is AH-L bottom. This speleothem is composed of transparent dense columnar calcite crystals. Fluid/gas inclusions increase in density to the sides of the growth axis producing the white calcite.



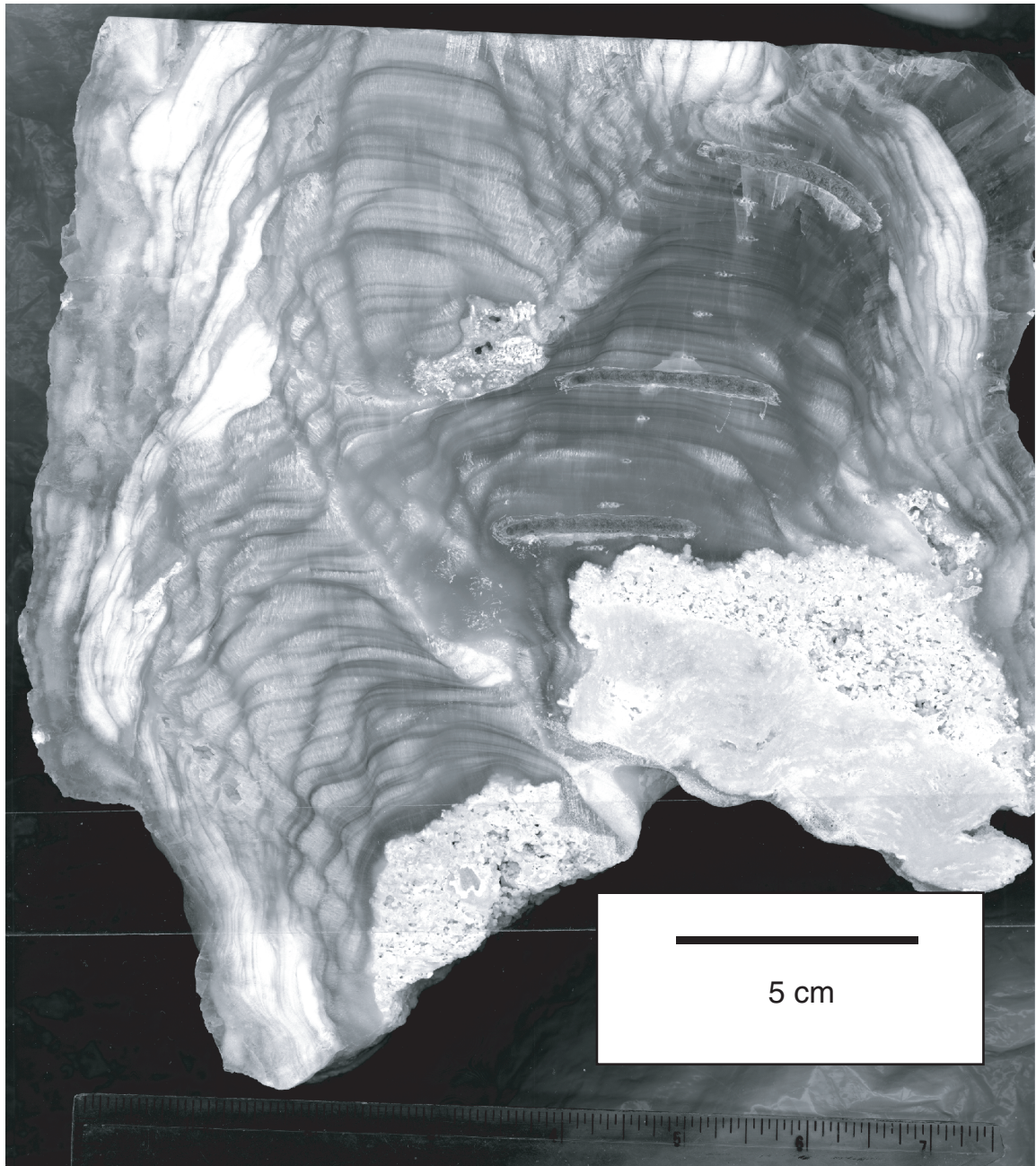


Figure 5.4 Speleothem AH-L bottom collected at Apes Hill Quarry. This speleothem is composed of transparent dense columnar calcite crystals. This speleothem formed by the coalescence of two neighboring speleothems. Internal stratigraphy was simpler in the section to the right of the image so this was chosen for geochemical sampling. Host limestone material can be seen cemented into the bottom of the speleothem.

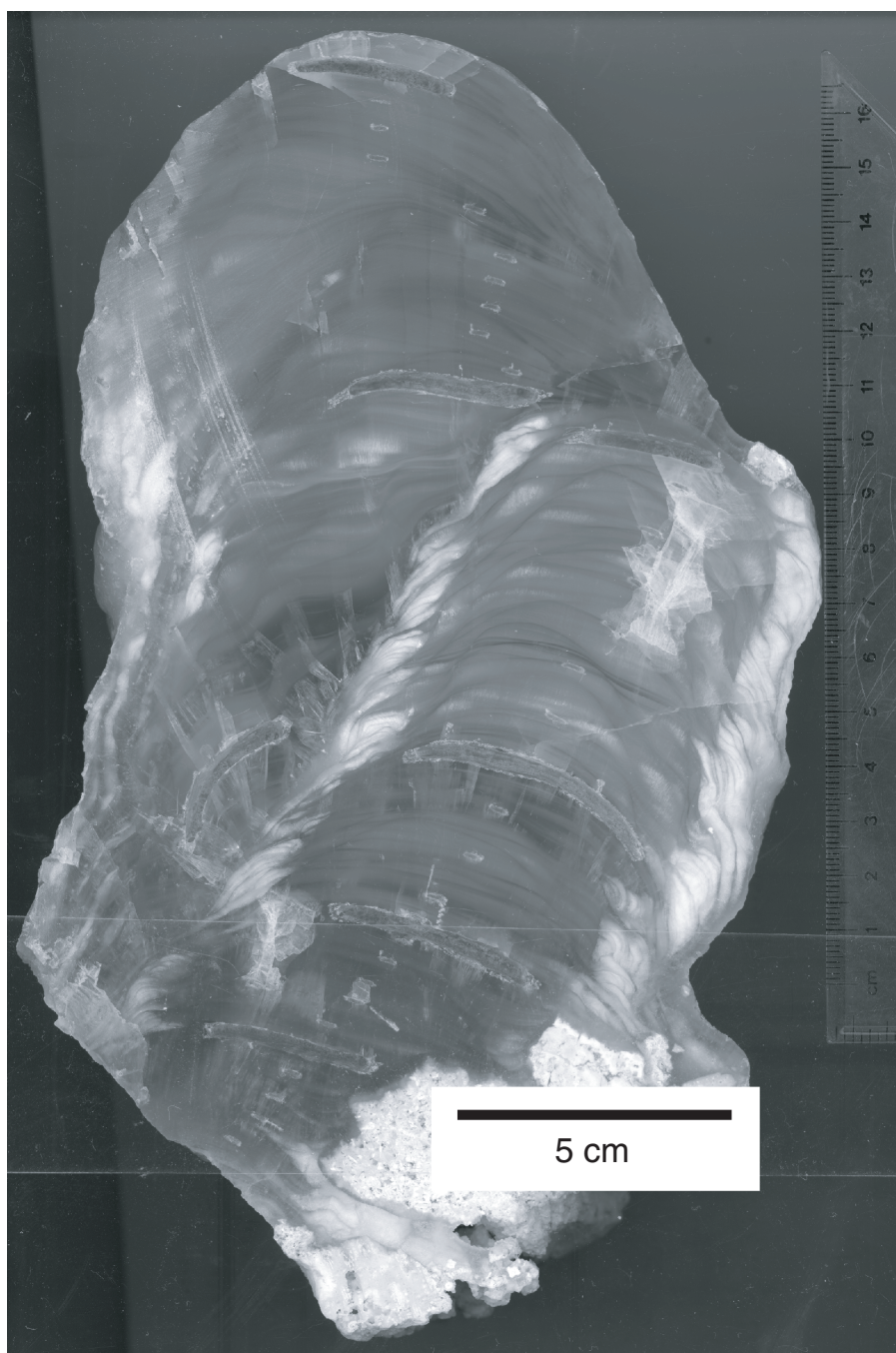


Figure 5.5 Speleothem AH-M collected at Apes Hill quarry. This speleothem is composed of transparent dense columnar calcite crystals. AH-M has a complex growth history which was the subject of further analysis in chapter 4. The speleothem was likely deposited on a soft substrate and it settled to one side during deposition. This changed the direction of the growth axis.



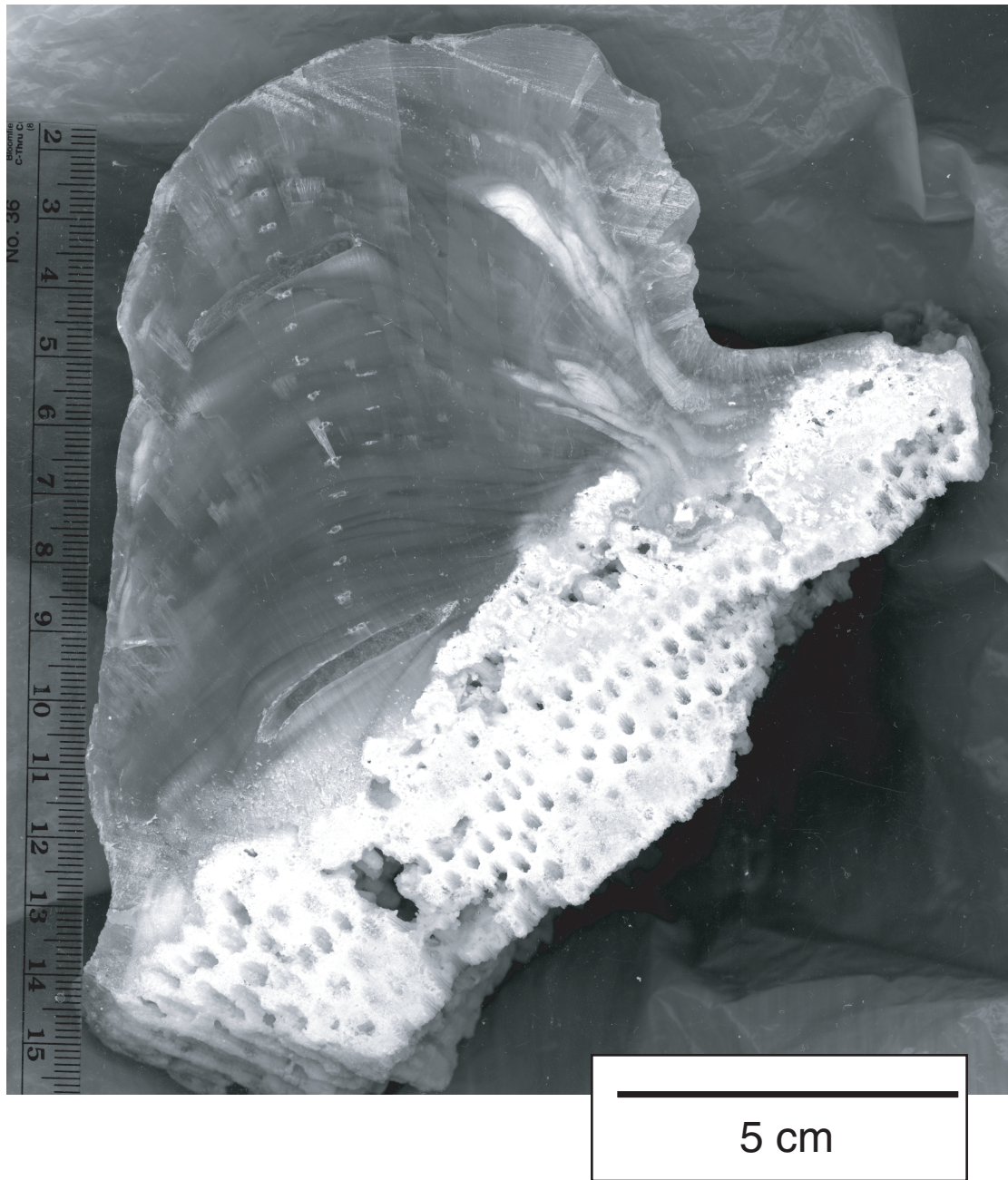
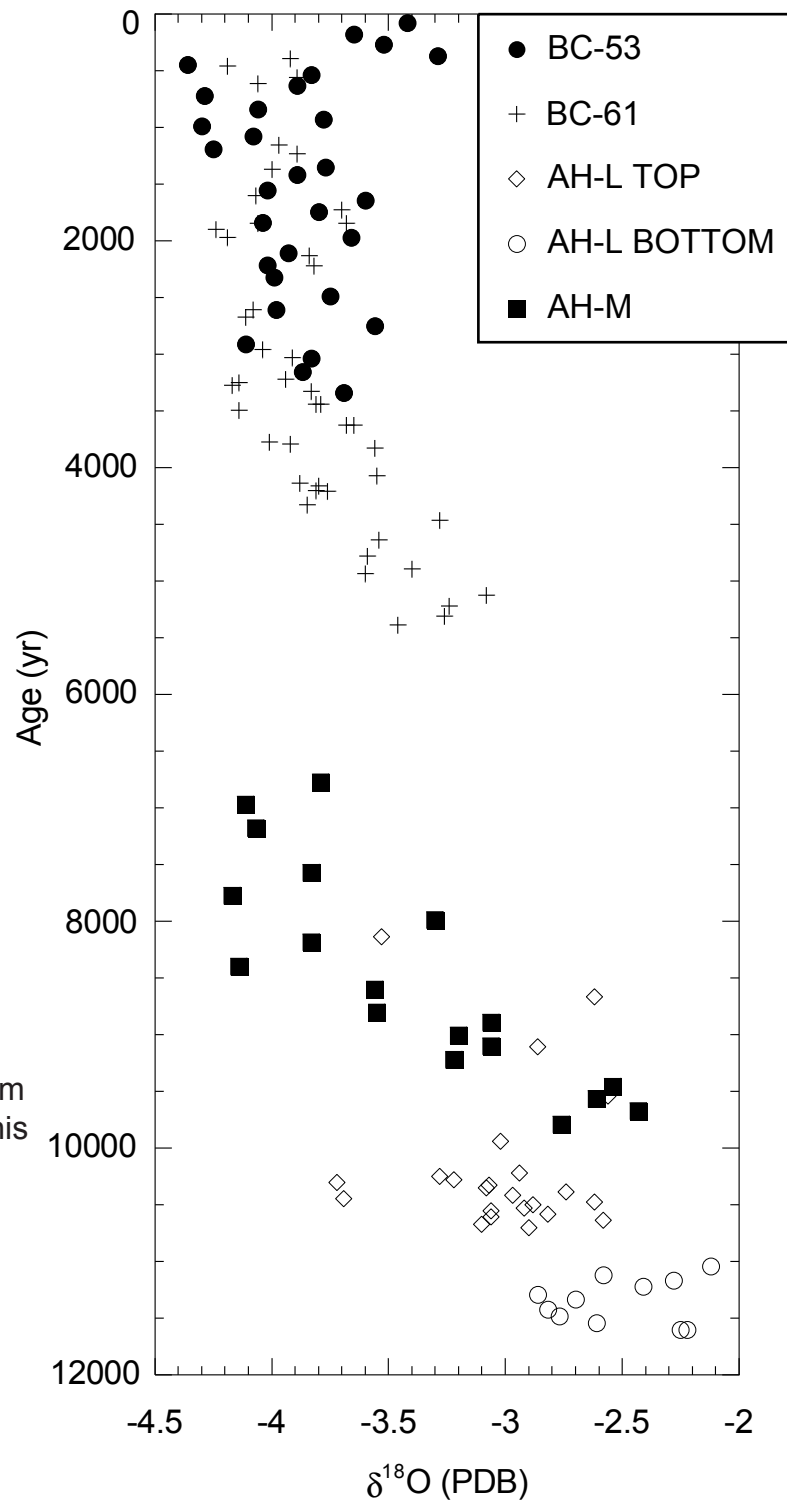


Figure 5.6 Speleothem AH-S collected at Apes Hill quarry. This stalagmite is composed of transparent dense columnar calcite crystals. The U-Th dates on this speleothem produced an age reversal. The sample that is stratigraphically higher, and thus younger, produced an age older than the underlying sample. The sample was not considered in the long term stable isotopic record.

Fig. 5.7 Temporal  $\delta^{18}\text{O}$  trend of the Barbados speleothems. Speleothem AH-S is not included in this trend because U-series dating produced an age reversal and the speleothem could not be placed into the chronostratigraphy.



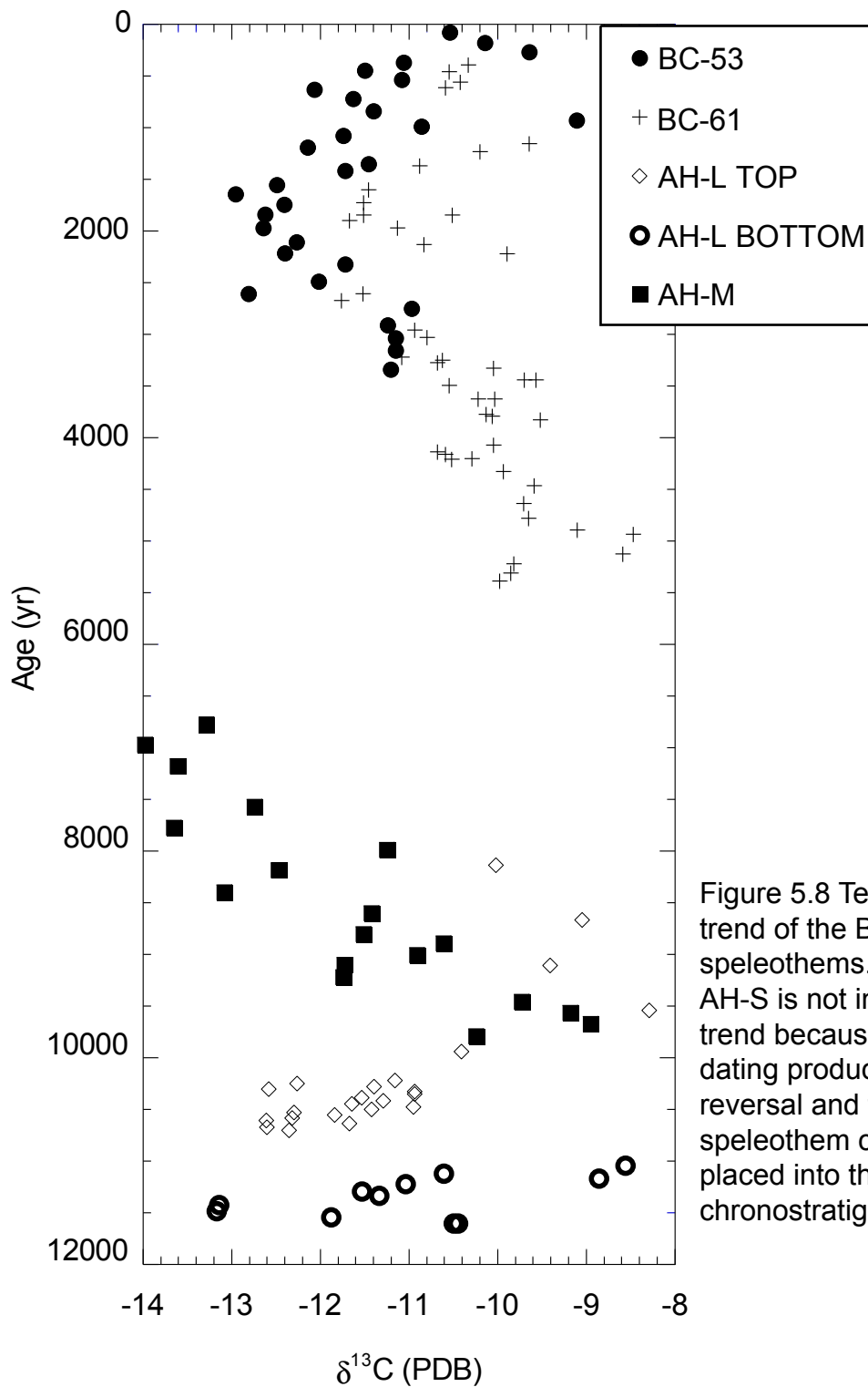


Figure 5.8 Temporal  $\delta^{13}\text{C}$  trend of the Barbados speleothems. Speleothem AH-S is not included in this trend because U-series dating produced an age reversal and the speleothem could not be placed into the chronostratigraphy.

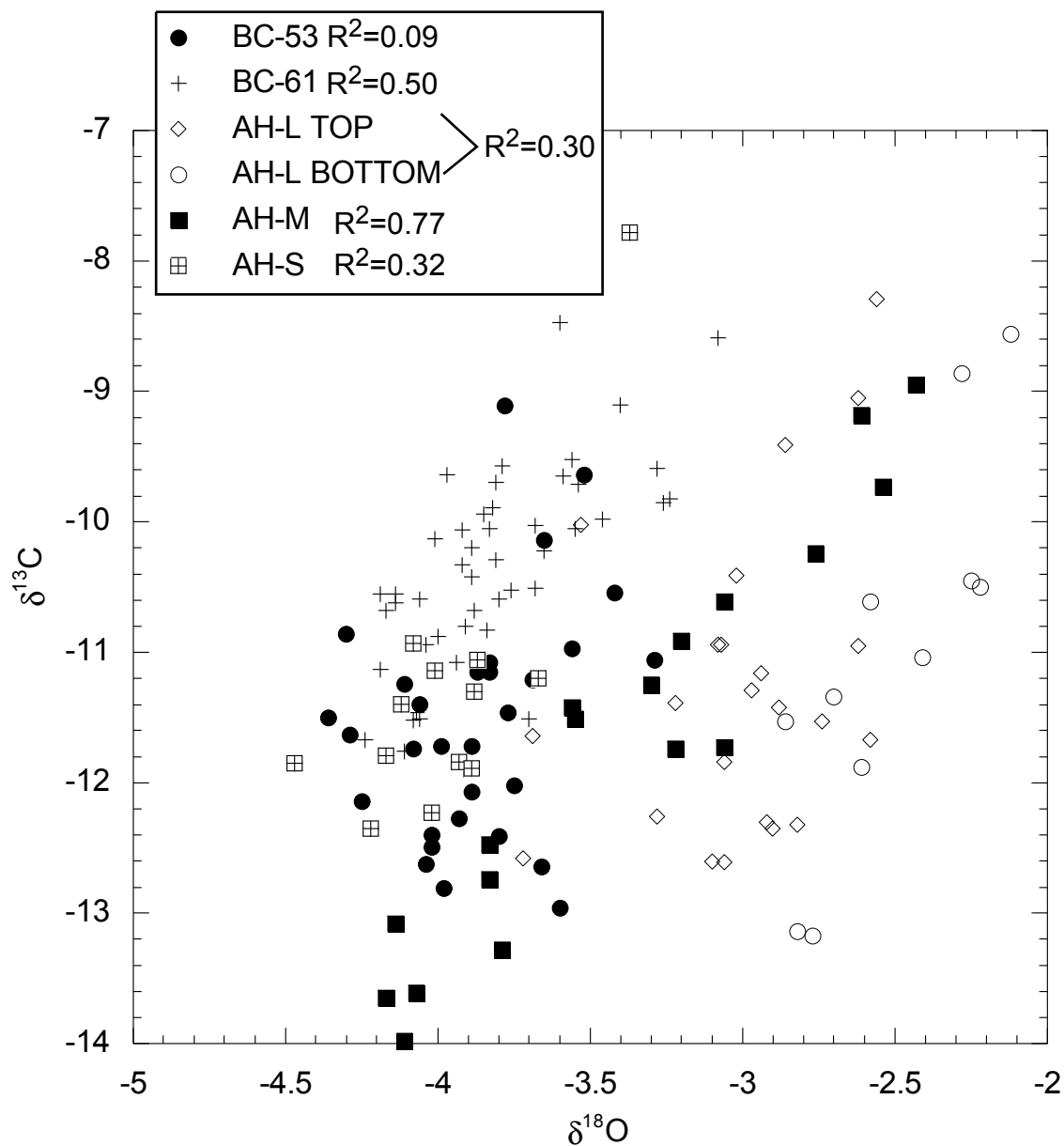


Figure 5.9  $\delta^{13}\text{C}$  vs.  $\delta^{18}\text{O}$  plot of ancient speleothem calcite. Correlation coefficients are included in the legend. Speleothem AH-L was sawed in half and the data collected from each half is plotted using separate symbols. Because AH-L top and AH-L bottom are the same speleothem the correlation coefficient included all the data. Out of the 5 speleothems studied only BC-53 lacked a significant positive  $\delta^{18}\text{O}$  vs.  $\delta^{13}\text{C}$  covariation.

## APPENDICES

### APPENDIX 1. GLASS PLATE CALCITE FROM HARRISON'S CAVE SAMPLED ALONG THE GROWTH AXIS

BC-98-1 Placed between 7/11/98 and 2/1/99

11 samples collected

Plate site	Sample number	Estimated time of deposition  (calendar year)	$\delta^{13}\text{C}$  (PDB)	$\delta^{18}\text{O}$  (PDB)
BC-98-1	1	1999.09	-12.26	-4.09
BC-98-1	3	1998.99	-12.44	-4.20
BC-98-1	4	1998.93	-12.16	-4.05
BC-98-1	5	1998.88	-12.23	-4.16
BC-98-1	6	1998.83	-12.12	-4.11
BC-98-1	7	1998.78	-12.25	-4.18
BC-98-1	8	1998.73	-12.02	-4.20
BC-98-1	9	1998.68	-12.10	-4.23
BC-98-1	10	1998.63	-11.55	-4.06
BC-98-1	11	1998.58	-11.94	-4.19

BC-98-1 Placed between 2/1/99 and  
7/1/00

32 samples collected

Plate site	Sample number	Estimated time of deposition  (calendar year)	$\delta^{13}\text{C}$  (PDB)	$\delta^{18}\text{O}$  (PDB)
BC-98-1	1	2000.50	-11.37	-3.90
BC-98-1	2	2000.45	NA	NA
BC-98-1	3	2000.41	-11.39	-3.87
BC-98-1	4	2000.37	NA	NA
BC-98-1	5	2000.32	-11.28	-3.82
BC-98-1	6	2000.28	NA	NA
BC-98-1	7	2000.23	-11.14	-3.87
BC-98-1	8	2000.19	NA	NA
BC-98-1	9	2000.15	-11.28	-3.80

BC-98-1	10	2000.10	NA	NA
BC-98-1	11	2000.06	-11.20	-3.87
BC-98-1	12	2000.01	-11.20	-3.92
BC-98-1	13	1999.97	-11.22	-3.96
BC-98-1	14	1999.93	-11.22	-3.88
BC-98-1	15	1999.88	-11.23	-3.87
BC-98-1	16	1999.84	-11.23	-3.91
BC-98-1	17	1999.79	-11.18	-3.92
BC-98-1	18	1999.75	-11.21	-3.88
BC-98-1	19	1999.70	-11.16	-3.92
BC-98-1	20	1999.66	-11.11	-3.95
BC-98-1	21	1999.62	NA	NA
BC-98-1	22	1999.57	NA	NA
BC-98-1	23	1999.53	-10.87	-3.90
BC-98-1	24	1999.48	-11.05	-3.93
BC-98-1	25	1999.44	-11.02	-3.90
BC-98-1	26	1999.40	-10.92	-3.90
BC-98-1	27	1999.35	-10.91	-3.90
BC-98-1	28	1999.31	-10.83	-3.83
BC-98-1	29	1999.26	-11.03	-3.82
BC-98-1	30	1999.22	-10.92	-3.78
BC-98-1	31	1999.18	-10.99	-3.73
BC-98-1	32	1999.13	-10.94	-3.79

BC-98-2 Placed between 7/11/98 and 2/1/99  
11 samples collected

Plate site	Sample number	Estimated time of deposition (calendar year)	$\delta^{13}\text{C}$ (PDB)	$\delta^{18}\text{O}$ (PDB)
BC-98-2	1	1999.09	-10.29	-3.81
BC-98-2	2	1999.04	-10.31	-3.85
BC-98-2	3	1998.99	-9.90	-3.74
BC-98-2	4	1998.93	-10.02	-3.75
BC-98-2	5	1998.88	-10.22	-3.80
BC-98-2	6	1998.83	-10.24	-3.76
BC-98-2	7	1998.78	-10.23	-3.71
BC-98-2	8	1998.73	-10.32	-3.74
BC-98-2	9	1998.68	-9.99	-3.68
BC-98-2	10	1998.63	-10.12	-3.78
BC-98-2	11	1998.58	-9.92	-3.70



BC-98-2 Placed between 2/1/99 and 7/1/00  
27 samples collected

Plate site	Sample number	Estimated time of deposition (calendar year)	$\delta^{13}\text{C}$ (PDB)	$\delta^{18}\text{O}$ (PDB)
BC-98-2	1	2000.50	-7.95	-3.21
BC-98-2	2	2000.45	-8.33	-3.29
BC-98-2	3	2000.39	-8.04	-3.15
BC-98-2	4	2000.34	-7.99	-3.10
BC-98-2	5	2000.29	-8.06	-3.12
BC-98-2	6	2000.24	-8.08	-3.18
BC-98-2	7	2000.19	-7.98	-3.07
BC-98-2	8	2000.13	-8.08	-3.16
BC-98-2	9	2000.08	-8.11	-3.11
BC-98-2	10	2000.03	-8.21	-3.12
BC-98-2	11	1999.98	-8.25	-3.08
BC-98-2	12	1999.92	-8.28	-3.14
BC-98-2	13	1999.87	-8.35	-3.15
BC-98-2	14	1999.82	-8.47	-3.19
BC-98-2	15	1999.77	-8.03	-3.08
BC-98-2	16	1999.71	-8.48	-3.20
BC-98-2	17	1999.66	-8.44	-3.22
BC-98-2	18	1999.61	-8.41	-3.17
BC-98-2	19	1999.56	-8.42	-3.20
BC-98-2	20	1999.51	-8.36	-3.22
BC-98-2	21	1999.45	-8.25	-3.15
BC-98-2	22	1999.40	-8.10	-3.34
BC-98-2	23	1999.35	-8.14	-3.17
BC-98-2	24	1999.30	NA	NA
BC-98-2	25	1999.24	-8.03	-3.02
BC-98-2	26	1999.19	-8.30	-3.16
BC-98-2	27	1999.14	-8.34	-3.21

BC-98-3 Placed between 7/11/98 and  
2/1/99

13 samples collected

Plate site	Sample number	Estimated time of deposition (calendar year)	$\delta^{13}\text{C}$ (PDB)	$\delta^{18}\text{O}$ (PDB)
BC-98-3	1	1999.09	-11.76	-4.04
BC-98-3	2	1999.04	-11.84	-4.09
BC-98-3	3	1999.00	-11.68	-4.08
BC-98-3	4	1998.96	-11.61	-4.08
BC-98-3	5	1998.91	-11.64	-4.11
BC-98-3	6	1998.87	-11.87	-4.09
BC-98-3	7	1998.83	-11.84	-4.13
BC-98-3	8	1998.79	-11.83	-4.05
BC-98-3	9	1998.74	-11.84	-4.07
BC-98-3	10	1998.70	-11.79	-4.19
BC-98-3	11	1998.66	-11.65	-3.97
BC-98-3	12	1998.61	-11.20	-4.00
BC-98-3	13	1998.57	-10.87	-3.87

BC-98-3 Placed between 2/1/99 and  
7/1/00

47 samples collected

Plate site	Sample number	Estimated time of deposition (calendar year)	$\delta^{13}\text{C}$ (PDB)	$\delta^{18}\text{O}$ (PDB)
BC-98-3	1	2000.50	-10.92	-3.90
BC-98-3	2	2000.47	NA	NA
BC-98-3	3	2000.44	-10.73	-3.78
BC-98-3	4	2000.41	NA	NA
BC-98-3	5	2000.38	-10.94	-3.81
BC-98-3	6	2000.35	NA	NA
BC-98-3	7	2000.32	-11.12	-3.97
BC-98-3	8	2000.29	NA	NA
BC-98-3	9	2000.26	-11.13	-3.94
BC-98-3	10	2000.23	-11.23	-4.03
BC-98-3	11	2000.20	-11.33	-4.02

BC-98-3	12	2000.17	-11.40	-4.01
BC-98-3	13	2000.14	-11.24	-4.04
BC-98-3	14	2000.11	-11.33	-4.04
BC-98-3	15	2000.08	NA	NA
BC-98-3	16	2000.05	-11.42	-4.05
BC-98-3	17	2000.02	-11.43	-4.08
BC-98-3	18	1999.99	-11.40	-4.04
BC-98-3	19	1999.96	NA	NA
BC-98-3	20	1999.93	-11.58	-4.06
BC-98-3	21	1999.90	-11.55	-4.05
BC-98-3	22	1999.87	-11.666	-4.311
BC-98-3	23	1999.84	-11.479	-3.983
BC-98-3	24	1999.81	-11.438	-3.970
BC-98-3	25	1999.78	-11.301	-3.908
BC-98-3	26	1999.75	-11.313	-3.907
BC-98-3	27	1999.72	-11.049	-3.775
BC-98-3	28	1999.69	-11.557	-3.993
BC-98-3	29	1999.66	-11.153	-3.879
BC-98-3	30	1999.63	-11.043	-3.689
BC-98-3	31	1999.60	-10.875	-3.795
BC-98-3	32	1999.57	-11.36	-3.83
BC-98-3	33	1999.54	-10.48	-3.72
BC-98-3	34	1999.51	-10.50	-3.78
BC-98-3	35	1999.48	-10.64	-3.72
BC-98-3	36	1999.45	-10.64	-3.69
BC-98-3	37	1999.42	-10.60	-3.72
BC-98-3	38	1999.39	-10.77	-3.75
BC-98-3	39	1999.36	-10.90	-3.89
BC-98-3	40	1999.33	-10.75	-3.73
BC-98-3	41	1999.30	-10.89	-3.87
BC-98-3	42	1999.27	-11.28	-3.93
BC-98-3	43	1999.24	-10.92	-3.85
BC-98-3	44	1999.21	-11.00	-4.14
BC-98-3	45	1999.18	-11.07	-3.61
BC-98-3	46	1999.15	-11.12	-3.85
BC-98-3	47	1999.12	-10.97	-3.81

Spur 1 Placed between 7/11/98 and 2/1/99  
15 samples collected

Plate site	Sample number	Estimated time of deposition (calendar year)	$\delta^{13}\text{C}$ (PDB)	$\delta^{18}\text{O}$ (PDB)
------------	---------------	---	--------------------------------	--------------------------------

---

Spur 1	1	1999.09	-3.68	-4.66
Spur 1	2	1999.05	-3.67	-4.66
Spur 1	3	1999.01	-3.84	-4.82
Spur 1	4	1998.98	-3.14	-4.51
Spur 1	5	1998.94	-2.89	-4.40
Spur 1	6	1998.90	-3.01	-4.47
Spur 1	7	1998.86	-3.29	-4.48
Spur 1	8	1998.83	-3.47	-4.44
Spur 1	9	1998.79	-3.79	-4.51
Spur 1	10	1998.75	-4.23	-4.58
Spur 1	11	1998.71	-4.26	-4.71
Spur 1	12	1998.68	-4.59	-4.69
Spur 1	13	1998.64	-5.14	-4.77
Spur 1	14	1998.60	-5.57	-4.79
Spur 1	15	1998.56	-3.69	-4.61

## APPENDIX 2. GLASS PLATE CALCITE FROM HARRISON'S CAVE SHOWING SPATIAL VARIABILITY.

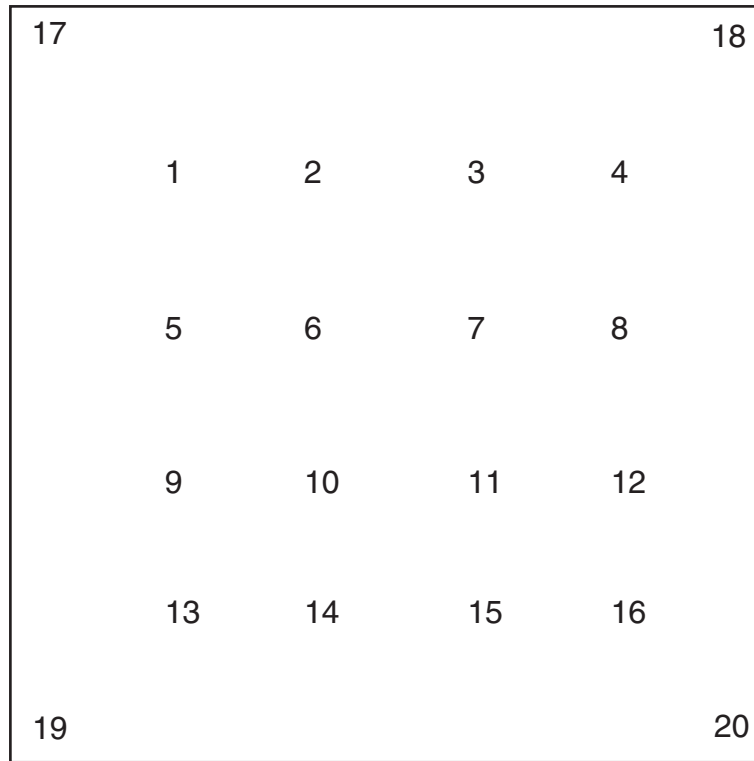
Placed between 7/11/98 and  
2/1/99

Plate site	Sample number	$\delta^{13}\text{C}$ (PDB)	$\delta^{18}\text{O}$ (PDB)
BC-98-1	1	-10.29	-4.07
BC-98-1	2	-10.47	-4.08
BC-98-1	3	-10.59	-3.80
BC-98-1	4	-10.86	-3.93
BC-98-1	5	-10.48	-3.85
BC-98-1	6	-10.78	-3.79
BC-98-1	7	-11.11	-3.79
BC-98-1	8	-11.27	-4.03
BC-98-1	9	-10.31	-3.79
BC-98-1	10	-10.89	-3.77
BC-98-1	11	-11.17	-3.98
BC-98-1	12	-10.79	-3.81
BC-98-1	13	-9.77	-3.47
BC-98-1	14	-10.51	-3.66
BC-98-1	15	-10.43	-3.65
BC-98-1	16	-9.19	-3.26
BC-98-1	17	-9.71	-3.92
BC-98-1	18	-9.80	-3.57
BC-98-1	19	-8.71	-3.67
BC-98-1	20	-7.09	-3.00
BC-98-2	1	-5.98	-2.69
BC-98-2	2	-6.48	-3.20
BC-98-2	3	NA	NA
BC-98-2	4	NA	NA
BC-98-2	5	-6.41	-2.69
BC-98-2	6	-7.94	-2.97
BC-98-2	7	-6.79	-2.62
BC-98-2	8	-5.24	-2.62
BC-98-2	9	-7.54	-2.93
BC-98-2	10	-8.10	-2.97
BC-98-2	11	-7.32	-2.65
BC-98-2	12	-5.45	-2.84
BC-98-2	13	-7.70	-3.26

BC-98-2	14	-7.73	-2.99
BC-98-2	15	-7.27	-2.85
BC-98-2	16	-6.82	-3.34

Placed between 7/11/98 and  
2/1/99

Plate site	Sample number	$\delta^{13}\text{C}$	$\delta^{18}\text{O}$
		(PDB)	(PDB)
BC-98-3	1	NA	NA
BC-98-3	2	NA	NA
BC-98-3	3	-6.61	-3.00
BC-98-3	4	-6.35	-2.95
BC-98-3	5	-4.89	-2.30
BC-98-3	6	-10.57	-3.84
BC-98-3	7	-9.89	-3.34
BC-98-3	8	-8.18	-3.51
BC-98-3	9	-8.43	-3.01
BC-98-3	10	-11.47	-3.87
BC-98-3	11	-11.35	-3.81
BC-98-3	12	-11.22	-4.01
BC-98-3	13	-6.47	-2.43
BC-98-3	14	-9.71	-3.60
BC-98-3	15	-9.83	-3.53
BC-98-3	16	-6.90	-2.72



Glass plates calcite on glass plates BC-98-1, 2 and 3 were sampled on a grid. The glass plates measured roughly 10 cm X 10 cm and the samples were taken on a grid approximately 2cm X 2cm. These results are given in Appendix 2. The location of the sample on the glass plate, corresponding to the sample number, is given in the accompanying diagram. Only glass plate BC-98-1 had samples taken from locations 17 through 20.

### APPENDIX 3. U-TH SYSTEMATICS

Sample name	Age (yr)	Error (+) (yr)	Error (-) (yr)	<sup>230</sup> Th (ppm)	Error (ppm)	<sup>232</sup> Th (ppm)	Error (ppm)	<sup>238</sup> U (ppm)	Error (ppm)	$\delta^{234}\text{U}$ (initial)	Error	$\delta^{234}\text{U}$ (present)	Error
<b>Apes Hill Speleothems</b>													
AH-S top	2306	323	322	0.0374	0.0052	5.6	6.6	104.8	0.12	40.2	1.5	40	1.5
AH-S base	2211	305	304	0.0316	0.0043	6.5	2.7	92.49	0.1	39.3	1.5	39.1	1.5
AH-M T-2	2752	324	323	0.0399	0.0046	11.8	28.2	93.76	0.09	38.7	1.4	38.4	1.4
AH-M B-2	6549	630	626	0.0534	0.0049	22.6	23.7	54.2	0.05	28.6	1.6	28.1	1.5
AH-M top	6655	397	396	0.0983	0.0057	8.3	3.9	98.74	0.09	27.3	1.4	26.8	1.4
AH-M base	9345	469	467	0.095	0.0046	-1.8	1.9	69.09	0.07	24.6	1.6	23.9	1.6
AH-L Top T-1	8428	441	439	0.0276	0.001	64	1.9	21.19	0.03	35.9	3.4	35	3.3
AH-L Top B-3	10198	106	106	0.1214	0.0012	8.8	1.6	81.1	0.09	24.7	1.7	24	1.6
AH-L Top B-1	10626	129	128	0.1206	0.0012	32	1.9	76.58	0.21	34.5	3	33.5	2.9
AH-L Base R Top	11068	145	145	0.0786	0.001	6.4	1.9	48.29	0.06	30.9	2.6	30	2.5
AH-L R-B-1	11573	92	92	0.2081	0.0015	10.6	1.6	121.6	0.19	39.8	2.1	38.5	2.1
<b>Harrison's Cave Speleothems</b>													
BC-53 Tip	23	13	13	0.0039	0.001	135.5	6.19	734.3	1.63	34	1.6	34	1.6
BC-53 5*	773	15	15	0.1011	0.002	32	2.8	843.2	4.52	35	4.2	35	4.2
BC-53 13.1	1738	29	29	0.1951	0.003	63.8	3.54	727.1	1.18	35	1.3	35	1.3
BC-53 7.1	2352	1192	1180	0.329	0.005	11036	61.76	609.7	0.87	33	1.5	32	1.4
BC-53 2.1	3496	270	270	0.2602	0.004	1808	9.29	533.8	2.66	-121	2.9	-119	2.8



# **APPENDIX 4. ANCIENT SPELEOTHEM GEOCHEMISTRY FROM HARRISON'S CAVE AND APES HILL QUARRY**

<u>Speleothem</u>	<u>Sample Number</u>	<u>Stratigraphic location</u>	<u>U-Th Age</u>	<u>Age error</u>	<u>Estimated Age</u>	<u>δ<sup>13</sup>C</u>	<u>δ<sup>18</sup>O</u>
		<u>Distance from tip</u>					
		<u>(cm)</u>					
BC-53	6*	41.2	(ya) 3440	(yr) 64	(ya) 3440.0	(PDB) -11.21	(PDB) -3.69
BC-53	1	40.5			3341.6	-11.15	-3.87
BC-53	2	39.0			3157.2		
BC-53	2.1	38.8	3496	399	3132.3	-11.15	-3.83
BC-53	3	38.0			3034.3	-11.24	-4.11
BC-53	4	37.0			2914.9	-10.97	-3.56
BC-53	5	35.6			2753.2	-12.81	-3.98
BC-53	6	34.3			2608.6		
BC-53	7.1	33.4	2352	1778	2511.6	-12.02	-3.75
BC-53	7	33.2			2490.4	-11.72	-3.99
BC-53	8	31.6			2324.7	-12.4	-4.02
BC-53	9	30.5			2215.0	-12.27	-3.93
BC-53	10	29.4			2108.5	-12.64	-3.66
BC-53	11	28.0			1972.9	-12.62	-4.04
BC-53	12	26.5			1837.9	-12.41	-3.8
BC-53	13	25.4			1746.6		
BC-53	13.1	25.3	1738	29	1738.0	-12.96	-3.6
BC-53	14	24.2			1645.1	-12.49	-4.02
BC-53	15	23.1			1554.7	-11.72	-3.89
BC-53	16	21.4			1419.7	-11.46	-3.77
BC-53	17	20.6			1354.1	-12.14	-4.25
BC-53	18	18.4			1193.6		

<u>Speleothem</u>	<u>Sample Number</u>	<u>Stratigraphic location</u> <u>Distance from tip</u> <u>(cm)</u>	<u>U-Th Age</u> <u>(ya)</u>	<u>Age error</u> <u>(yr)</u>	<u>Estimated Age</u> <u>(ya)</u>	<u><math>\delta^{13}\text{C}</math></u> <u>(PDB)</u>	<u><math>\delta^{18}\text{O}</math></u> <u>(PDB)</u>
BC-53	19	16.8			1078.8	-11.74	-4.08
BC-53	20	15.5			988.1	-10.86	-4.3
BC-53	21	14.7			929.8	-9.11	-3.78
BC-53	22	13.3			839.1	-11.4	-4.06
BC-53	5*	12.3	773	15	773.0		
BC-53	25	8.6			535.7	-11.08	-3.83
BC-53	26	7.2			448.1	-11.5	-4.36
BC-53	27	5.9			367.5	-11.06	-3.29
BC-53	28	4.3			268.9	-9.64	-3.52
BC-53	29	2.9			179.9	-10.14	-3.65
BC-53	30	1.3			81.6	-10.54	-3.42
BC-53	Tip	0.3	23	19	23.0		

<u>Speleothem</u>	<u>Sample Number</u>	<u>Stratigraphic location</u> <u>Distance from tip (cm)</u>	<u>U-Th Age</u> <u>(ya)</u>	<u>Age error</u> <u>(yr)</u>	<u>Estimated Age</u> <u>(ya)</u>	<u><math>\delta^{13}\text{C}</math></u> <u>(PDB)</u>	<u><math>\delta^{18}\text{O}</math></u> <u>(PDB)</u>
BC-61	Straw						
BC-61	yng	0.25	395	45	1900	-11.67	-4.24
BC-61	a2	2	459	46	395	-10.33	-3.92
BC-61	a4	4.25			459	-10.55	-4.19
BC-61	a6	5.5			562	-10.42	-3.89
BC-61	a10	17.25			619	-10.59	-4.06
BC-61	a15	19			1155	-9.64	-3.97
BC-61	a20	22	1372	37	1235	-10.2	-3.89
BC-61	a22	25.25			1372	-10.88	-4.00
BC-61	a24	27			1601	-11.46	-4.07
BC-61	a26a	28.75			1725	-11.51	-3.7
BC-61	a26b	28.75			1849	-11.51	-4.06
BC-61	a28	30.5			1849	-10.51	-3.68
BC-61	a30	32.75			1973	-11.13	-4.19
BC-61	ax2	34	2220	52	2132	-10.83	-3.84
BC-61	a32	35.5			2220	-9.89	-3.82
BC-61	ax1	35.75	2676	69	2611	-11.52	-4.08
BC-61	b1	36.5	2956	580	2676	-11.76	-4.11
BC-61	b2	38.5	3033	28	2956	-10.94	-4.04
BC-61	b5-d	41			3033	-10.8	-3.91
BC-61	b6	41.5			3218	-11.08	-3.94
BC-61	b6-d	41.75			3255	-10.62	-4.14
BC-61	b7-d	42.5			3273	-10.68	-4.17
BC-61	b8	44			3329	-10.05	-3.83
BC-61	b8-d	44			3440	-9.70	-3.81
BC-61		44			3440	-9.57	-3.79

<u>Speleothem</u>	<u>Sample Number</u>	<u>Stratigraphic location</u>	<u>U-Th Age</u>	<u>Age error</u>	<u>Estimated Age</u>	<u><math>\delta^{13}\text{C}</math></u>	<u><math>\delta^{18}\text{O}</math></u>
		<u>Distance from tip (cm)</u>	<u>(ya)</u>	<u>(yr)</u>	<u>(ya)</u>	<u>(PDB)</u>	<u>(PDB)</u>
BC-61	b8.5d	44.75			3495	-10.55	-4.14
BC-61	b10	46.5			3625	-10.03	-3.68
BC-61	b10-d	46.5			3625	-10.22	-3.65
BC-61	b-x1	49.25	3828	72	3828	-9.52	-3.56
BC-61	c-1	50	4072	206	4072	-10.05	-3.55
BC-61	c6	52.75			4139	-10.68	-3.88
BC-61	c8	53.75			4164	-10.59	-3.8
BC-61	c10	55.5			4207	-10.29	-3.81
BC-61	c15	55.75	4213	137	4213	-10.52	-3.76
BC-61	c18	57.25			4330	-9.94	-3.85
BC-61	c24	59			4467	-9.59	-3.28
BC-61	c26	61.25			4642	-9.71	-3.54
BC-61	c28	63			4779	-9.65	-3.59
BC-61	c30	64.5			4896	-9.10	-3.40
BC-61	c20	65	4935	210	4935	-8.47	-3.60
BC-61	d2	69.5			5124	-8.59	-3.08
BC-61	d4	71			5218	-9.82	-3.24
BC-61	chip	72.5	5312	67	5312	-9.85	-3.26
BC-61	d6	72.75	5388	159	5388	-9.98	-3.46

<u>Speleothem</u>	<u>Sample Number</u>	<u>Stratigraphic location</u> <u>Distance from base</u> <u>(cm)</u>	<u>U-Th Age</u> <u>(ya)</u>	<u>Age error</u> <u>(yr)</u>	<u>Estimated Age</u> <u>(ya)</u>	<u><math>\delta^{13}\text{C}</math></u> <u>(PDB)</u>	<u><math>\delta^{18}\text{O}</math></u> <u>(PDB)</u>
AH-L Top	1	0.625			10704	-12.35	-2.90
AH-L Top	2	1.65			10671	-12.60	-3.10
AH-L Top	3	2.55			10641	-11.67	-2.58
AH-L Top	Top B-1	3	10626	129	10626		
AH-L Top	4	3.5			10610	-12.61	-3.06
AH-L Top	5	4.25			10585	-12.32	-2.82
AH-L Top	6	5.075			10558	-11.84	-3.06
AH-L Top	7	5.9			10530	-12.30	-2.92
AH-L Top	8	6.75			10502	-11.42	-2.88
AH-L Top	9	7.5			10478	-10.95	-2.62
AH-L Top	10	8.45			10446	-11.64	-3.69
AH-L Top	11	9.3			10418	-11.29	-2.97
AH-L Top	Top B-2	9.55	10410	664	10410		
AH-L Top	12	10.45			10385	-11.53	-2.74
AH-L Top	13	11.55			10353	-10.94	-3.08
AH-L Top	14	12.45			10328	-10.94	-3.07
AH-L Top	15	13.225			10306	-12.58	-3.72
AH-L Top	16	14.15			10279	-11.39	-3.22
AH-L Top	17	15.125			10252	-12.26	-3.28
AH-L Top	18	16.175			10222	-11.16	-2.94
AH-L Top	Top B-3	17	10198	106	10198		
AH-L Top	19	17.55			9946	-10.41	-3.02
AH-L Top	20	18.425			9543	-8.29	-2.56
AH-L Top	21	19.375			9107	-9.41	-2.86
AH-L Top	Top T-1	20.85	8428	441	8428		

<u>Speleothem</u>	<u>Sample Number</u>	<u>Stratigraphic location</u> Distance from base (cm)	<u>U-Th Age</u> (ya)	Age error (yr)	Estimated Age (ya)	<u>δ13C</u> (PDB)	<u>δ18O</u> (PDB)
AH-L Top	22	20.325			8670	-9.05	-2.62
AH-L Top	23	21.475			8141	-10.02	-3.53
<u>Speleothem</u>	<u>Sample Number</u>	<u>Stratigraphic location</u> Distance from base (cm)	<u>U-Th Age</u> (ya)	Age error (yr)	Estimated Age (ya)	<u>δ13C</u> (PDB)	<u>δ18O</u> (PDB)
AH-L bottom	1	0			11603	-10.50	-2.22
AH-L bottom	1	0			11603	-10.45	-2.25
AH-L bottom	R-B-1	0.5	11573	92	11573		
AH-L bottom	2	0.975			11544	-11.88	-2.61
AH-L bottom	3	1.975			11483	-13.17	-2.77
AH-L bottom	4	2.925			11425	-13.14	-2.82
AH-L bottom	5	4.4			11335	-11.34	-2.70
AH-L bottom	6	5.1			11292	-11.53	-2.86
AH-L bottom	7	6.25			11222	-11.04	-2.41
AH-L bottom	8	7.125			11169	-8.86	-2.28
AH-L bottom	9	7.9			11121	-10.61	-2.58
AH-L bottom	Base R						
AH-L bottom	Top	8.8	11067	145	11067		
AH-L bottom	10	9.2			11042	-8.56	-2.12

<u>Speleothem</u>	<u>Sample Number</u>	<u>Stratigraphic location Distance from base (cm)</u>	<u>U-Th Age (ya)</u>	<u>Age error (yr)</u>	<u>Estimated Age (ya)</u>	<u><math>\delta^{13}\text{C}</math> (PDB)</u>	<u><math>\delta^{18}\text{O}</math> (PDB)</u>
AH-M	1	0.6			9793	-10.24	-2.76
AH-M	2	1.2			9671	-8.95	-2.43
AH-M	3	1.7			9569	-9.18	-2.61
AH-M	4	2.25			9457	-9.73	-2.54
AH-M	5	2.575			9391		
AH-M	Base	2.8			9345		
AH-M	6	3.4	9345	468	9223	-11.74	-3.22
AH-M	7	4			9100	-11.73	-3.06
AH-M	8	4.45			9009	-10.91	-3.2
AH-M	9	5			8897	-10.61	-3.06
AH-M	10	5.45			8805	-11.51	-3.55
AH-M	11	6.45			8601	-11.42	-3.56
AH-M	12	7.425			8402	-13.08	-4.14
AH-M	13	8.475			8188	-12.47	-3.83
AH-M	14	9.45			7990	-11.25	-3.3
AH-M	15	10.5			7776	-13.65	-4.17
AH-M	16	11.5			7572	-12.74	-3.83
AH-M	17	12.5			7368		
AH-M	18	13.425			7180	-13.61	-4.07
AH-M	19	14.425			6976	-13.98	-4.11
AH-M	20	15.4			6777	-13.28	-3.79
AH-M	Top	16	6655	397	6655		

<u>Speleothem</u>	<u>Sample Number</u>	<u>Stratigraphic location</u> <u>Distance from base (cm)</u>	<u>U-Th Age</u> <u>(ya)</u>	<u>Age error</u> <u>(yr)</u>	<u>Estimated Age</u> <u>(ya)</u>	<u><math>\delta^{13}\text{C}</math></u> <u>(PDB)</u>	<u><math>\delta^{18}\text{O}</math></u> <u>(PDB)</u>
AH-S	Base	0.9	2211	305	NA	-12.35	-4.22
AH-S	1	1.7			NA	-11.30	-3.88
AH-S	2	2.9			NA	-11.40	-4.12
AH-S	3	3.85			NA	-12.53	-5.78
AH-S	4	4.8			NA	-11.90	-3.89
AH-S	5	5.75			NA	-11.84	-3.93
AH-S	6	6.7			NA	-11.89	-3.89
AH-S	7	7.75			NA	-11.06	-3.87
AH-S	8	8.75			NA	-11.20	-3.67
AH-S	9	9.8			NA	-12.23	-4.02
AH-S	10	10.8			NA	-11.79	-4.17
AH-S	11	11.8			NA		
AH-S	Top	12.4	2306	323	NA	-11.14	-4.01
AH-S	12	12.9			NA	-11.85	-4.47
AH-S	13	13.85			NA	-10.93	-4.08
AH-S	14	14.8			NA	-7.78	-3.37
AH-S	15	15.85			NA		

Estimated age was calculated by assuming a linear growth rate between dated intervals. The samples stratigraphic location, relative to the stratigraphic location of the nearest dated intervals, was used to place the sample in a chronostratigraphic framework. BC speleothems were collected from Harrison's Cave and AH speleothems were collected from Apes Hill Quarry.



## APPENDIX 5. BC-61 ELEMENTAL GEOCHEMISTRY

<u>Sample Name</u>	<u>Sample Number</u>	<u>Stratigraphic Location</u> Distance from tip (cm)	<u>Estimated Age</u> (ya)	<u>δSr</u>	<u>Mg</u> (ppm)	<u>Al</u> (ppm)	<u>Si</u> (ppm)	<u>P</u> (ppm)
BC-61	yn9	0.25	395	26.86	468.1	30	237.8	336.9
BC-61	a2	2	459	26.59	418.7	18	184.3	347.5
BC-61	a6	5.5	619	26.72	390	52	243.8	360.4
BC-61	a10	17.25	1155	26.81	473.4	21	332.3	151.1
BC-61	a15	19	1235	26.9	431.3	35	315	246
BC-61	a20	22	1372	26.78	438.8	13	197.7	273
BC-61	a24	27	1725	26.72	449.4	21	205.6	262.1
BC-61	a26a	28.75	1849	26.72	498.8	18	251.9	357.9
BC-61	a26b	28.75	1849	27.11	531.1	19	266.3	223.3
BC-61	a30	32.75	2132		572.8	15	156	276.9
BC-61	a32	35.5	2611	26.7	472.3	37	255.6	330.8
BC-61	ax1	35.75	2676	26.67	446.9	541	306.6	338.4
BC-61	b2	38.5	3033	26.88	522	32	381.9	266.8
BC-61	b6	41.5	3255	26.64	517.1	637	441.9	283.6
BC-61	b8	44	3440	26.98	584.9	20	265.9	239.2
BC-61	b10	46.5	3625	27.11	533.3	28	229.2	274.6
BC-61	b12	48.75	3791	26.86	530	26	252.1	288.7
BC-61	b-x1	49.25	3828	27.24	564.2	32	220.7	265.8

<u>Sample Name</u>	<u>Sample Number</u>	<u>Stratigraphic location</u> Distance from tip (cm)	<u>Estimated Age</u> (ya)	<u>δSr</u>	<u>Mg</u> (ppm)	<u>Al</u> (ppm)	<u>Si</u> (ppm)	<u>P</u> (ppm)
BC-61	c-1	50	4072	27.25	516.6	29	219	296.7
BC-61	c8	53.75	4164	26.99	479.1	564	286.2	284.1
BC-61	c10	55.5	4207	26.98	495.9	24	217	273.1
BC-61	c15	55.75	4213	27.03	510	29	349.1	275.4
BC-61	c24	59	4467	27.52	539.4	49	219.2	212.8
BC-61	c26	61.25	4642	27.26	546.9	40	238.2	310.4
BC-61	c28	63	4779	27.21	493.1	55	307.5	317.8
BC-61	c30	64.5	4896	27.39	489.8	37	254.7	273.4
BC-61	c20	65	4935	27.2	508.1	37	188.3	246.2
BC-61	d2	69.5	5124	27.72	648.2	15	236.2	128.6
BC-61	d4	71	5218	27.56	544.4	16	164.7	231.8
BC-61	chip	72.5	5312	27.54	453.3	40	342.2	304.3
BC-61	D6	7275	5388	27.34	442.5	56	225.3	218.6
Detection Limit					0.25	0.01	0.3	0.05

<u>Sample Name</u>	<u>Sample Number</u>	<u>Stratigraphic location</u> Distance from tip (cm)	<u>Estimated Age</u> (ya)	<u>Fe</u> (ppm)	<u>Mn</u> (ppm)	<u>Sr</u> (ppm)	<u>Ba</u> (ppm)	<u>U</u> (ppm)
BC-61	yng	0.25	395	58.5	1.78	49.3	1.62	0.77
BC-61	a2	2	459	39.7	0.5	45.2	1.48	0.74
BC-61	a6	5.5	619	39.1	0.54	41.4	1.09	0.63
BC-61	a10	17.25	1155	78.2	0.85	50.1	1.25	0.47
BC-61	a15	19	1235	42.7	0.56	52.5	1.34	0.52
BC-61	a20	22	1372	33.9	0.38	53.9	1.6	0.51
BC-61	a24	27	1725	34.6	0.82	46	1.27	0.71
BC-61	a26a	28.75	1849	35.6	0.65	47.6	1.57	0.62
BC-61	a26b	28.75	1849	22.3	0.39	42.5	0.92	0.44
BC-61	a30	32.75	2132	24.9	0.37	58.3	1.49	0.57
BC-61	a32	35.5	2611	59.5	1.17	47.3	1.38	0.7
BC-61	ax1	35.75	2676	40.7	0.65	48.5	1.56	0.67
BC-61	b2	38.5	3033	47.1	1.05	53.7	1.72	0.84
BC-61	b6	41.5	3255	106.9	1.83	54.3	1.68	0.59
BC-61	b8	44	3440	25.2	3	50.7	1.28	0.58
BC-61	b10	46.5	3625	44.9	29.71	42.9	1.53	0.7
BC-61	b12	48.75	3791	26.4	0.63	45.7	1.36	0.79
BC-61	b-x1	49.25	3828	39.9	0.35	45.8	1.31	0.68
BC-61	c-1	50	4072	42.8	0.63	49	2.29	0.71
BC-61	c8	53.75	4164	37.2	1.44	54.3	1.45	0.66
BC-61	c10	55.5	4207	112.8	1.2	53	1.47	0.62
BC-61	c15	55.75	4213	181.7	1.83	50.1	1.42	0.62
BC-61	c24	59	4467	22.1	0.32	55.5	1.36	0.54

<u>Sample Name</u>	<u>Sample Number</u>	<u>Stratigraphic location</u> Distance from tip (cm)	<u>Estimated Age</u> (ya)	<u>Fe</u> (ppm)	<u>Mn</u> (ppm)	<u>Sr</u> (ppm)	<u>Ba</u> (ppm)	<u>U</u> (ppm)
BC-61	c26	61.25	4642	85.8	0.82	46.4	1.19	0.68
BC-61	c28	63	4779	1151.4	9.6	47.9	1.3	0.74
BC-61	c30	64.5	4896	59.4	1.46	49.9	2	0.65
BC-61	c20	65	4935	68.7	2.87	49.9	1.58	0.51
BC-61	d2	69.5	5124	17.6	0.29	48.6	3.26	0.42
BC-61	d4	71	5218	21.2	0.31	49.1	1.15	0.69
BC-61	chip	72.5	5312	62.9	1.46	57.7	1.66	0.58
BC-61	d6	72.75	5388	23	0.59	56	1.23	0.48
Detection Limit				0.03	0.001	0.0025	0.0007	0.000075

149 Elemental analyses were performed in the laboratory of Rick Knurr at the University of Minnesota. Detection limits were reported by Musgrove (2000) on similar speleothem samples from central Texas.

## BIBLIOGRAPHY

- Baker A., Genty D., Dreybrodt W., Barnes W. L., Mockler N. J., and Grapes J. (1998a) Testing theoretically predicted stalagmite growth rate with recent annually laminated samples; implications for past stalagmite deposition. *Geochim. Cosmochim. Acta* **62**(3), 393-404.
- Baker R. G., Gonzalez L. A., Raymo M., Bettis E. A., III, Reagan M. K., and Dorale J. A. (1998b) Comparison of multiple proxy records of Holocene environments in the Midwestern United States. *Geol.* **26**(12), 1131-1134.
- Banner J. L., Musgrove M., Asmerom Y., Edwards R. L., and Hoff J. A. (1996) High-resolution temporal record of Holocene ground-water chemistry; tracing links between climate and hydrology. *Geol.* **24**(11), 1049-1053.
- Banner J. L., Musgrove M., and Capo R. C. (1994) Tracing ground-water evolution in a limestone aquifer using Sr isotopes; effects of multiple sources of dissolved ions and mineral-solution reactions; with Suppl. Data 9435. *Geol.* **22**(8), 687-690.
- Bard E., Delaygue G., Rostek F., Antonioli F., Silenzi S., and Schrag D. P. (2002) Hydrological conditions over the western Mediterranean basin during the deposition of the cold sapropel 6 (ca. 175 kyr BP). *Earth Planet. Sci. Lett.* **202**(2), 481-494.
- Bar-Matthews M., Ayalon A., Gilmour M., Matthews A., and Hawkesworth C. J. (2003a) Sea-land oxygen isotopic relationships from planktonic foraminifera and speleothems in the Eastern Mediterranean region and their implication for paleorainfall during interglacial intervals. *Geochim. Cosmochim. Acta* **67**(17), 3181-3199.
- Bar-Matthews M., Ayalon A., Gilmour M., Matthews A., and Hawkesworth C. J. (2003b) Sea-land oxygen isotopic relationships from planktonic foraminifera and speleothems in the Eastern Mediterranean region and their implication for paleorainfall during interglacial intervals. *Geochim. Cosmochim. Acta* **67**(17), 3181-3199.
- Bar-Matthews M., Ayalon A., and Kaufman A. (2000) Timing and hydrological conditions of Sapropel events in the Eastern Mediterranean, as evident from speleothems, Soreq cave, Israel. *Chem. Geol.* **169**(1-2), 145-156.
- Bar-Matthews M., Ayalon A., Kaufman A., and Wasserburg G. J. (1999) The Eastern Mediterranean paleoclimate as a reflection of regional events: Soreq cave, Israel. *Earth Planet. Sci. Lett.* **166**(1-2), 85-95.
- Baskaran M. and Krishnamurthy R. V. (1993) Speleothems as proxy for the carbon isotope composition of atmospheric CO<sub>2</sub>. *Geophys. Res. Lett.* **20**(24), 2905-2908.

- Beck J. W., Edwards R. L., Ito E., Taylor F. W., Recy J., Rougerie F., Joannot P., and Henin C. (1992) Sea-surface temperature from coral skeletal strontium/calcium ratios. *Science* **257**(5070), 644-647.
- Berstad I. M., Lundberg J., Lauritzen S.-E., and Linge H. C. (2002) Comparison of the climate during marine isotope stage 9 and 11 inferred from a speleothem isotope record from Northern Norway. *Quat. Res.* **58**(3), 361-371.
- Bottinga Y. (1968) Calculation of fractionation factors for carbon and oxygen isotopic exchange in the system calcite-carbon dioxide-water. *J. Phys. Chem.* **72**, 800-808.
- Burns S. J., Fleitmann D., Mudelsee M., Neff U., Matter A., and Mangini A. (2002) A 780-year annually resolved record of Indian Ocean monsoon precipitation from a speleothem from South Oman. *J. Geophys. Res.-Atmos.* **107**(D20 4434), doi10.1029/2001JD001281, 2002.
- Clark I. D. and Lauriol B. (1992) Kinetic enrichment of stable isotopes in cryogenic calcites. *Chem. Geol.* **102**(1-4), 217-228.
- Curtis J. H. (1997) Climatic variability in the Circum-Caribbean during the Holocene. Dissertation, University of Florida.
- Dansgaard W. (1964) Stable isotopes in precipitation. *Tellus* **16**, 436-468.
- Deines P., Langmuir D. and Harmon, R.S. (1974) Stable Carbon isotope ratios and the existence of a gas phase in the evolution of carbonate ground waters. *Geochim. Cosmochim. Acta* **38**, 1147-1164.
- Dennis P. F., Rowe P. J., and Atkinson T. C. (2001) The recovery and isotopic measurement of water from fluid inclusions in speleothems. *Geochim. Cosmochim. Acta* **65**(6), 871-884.
- Denniston R. F., Gonzalez L. A., Asmerom Y., Polyak V., Reagan M. K., and Saltzman M. R. (2001) A high-resolution speleothem record of climatic variability at the Allerod-Younger Dryas transition in Missouri, central United States. *Palaeogeogr. Palaeoclimat. Palaeoecol.* **176**, 147-155.
- Denniston R. F., Gonzalez L. A., Baker R. G., Asmerom Y., Reagan M. K., Edwards R. L., and Alexander E. C. (1999) Speleothem evidence for Holocene fluctuation of the prairie-forest ecotone, north-central USA. *Holocene* **9**(6), 671-676.
- Desmarchelier J. M., Goede A., Ayliffe L. K., McCulloch M. T., and Moriarty K. (2000) Stable isotope record and its palaeoenvironmental interpretation for a late middle Pleistocene speleothem from Victoria Fossil Cave, Naracoorte, South Australia. *Quat. Sci. Rev.* **19**(8), 763-774.
- Dorale J. A., Edwards R. L., Ito E., and González L. A. (1998) Climate and vegetation history of the midcontinent from 75 to 25 ka: a speleothem record from Crevice Cave, Missouri, USA. *Science* **282**, 1871-1874.
- Dorale J. A., Gonzalez L. A., Reagan M. K., Pickett D. A., Murrell M. T., and Baker R. G. (1992) A high-resolution record of Holocene climate change

- in speleothem calcite from Cold Water Cave, Northeast Iowa. *Science* **258**(5088), 1626-1630.
- Dulinski M. and Rozanski K. (1990) Formation of  $^{13}\text{C}/^{12}\text{C}$  isotope ratios in speleothems; a semi-dynamic model. *Radiocarbon* **32**(1), 7-16.
- Duplessy J. C., Labeyrie J., Lalou C. L., and Nuygen H. V. (1971) La mesure des variations climatiques continentales-application à la période comprise entre 130,000 et 90,000 ans BP. *Quat. Res.* **1**, 162-174.
- Duplessy J. C., Lalou C., de Azevedo G., and Expedito A. (1969) Etude des conditions de concretionnement dans les grottes au moyen des isotopes stables de l'oxygene et du carbone. *Comptes Rendus Hebdomadaires des Seances de l'Academie des Sciences, Serie D: Sciences Naturelles* **268**(19), 2327-2330.
- Edwards R. L., Chen J. H., and Wasserburg G. J. (1987)  $^{238}\text{U}$ - $^{234}\text{U}$ - $^{230}\text{Th}$ - $^{232}\text{Th}$  systematics and the precise measurement of time over the past 500,000 years. *Earth Planet. Sci. Lett.* **81**(2-3), 175-192.
- Fairbanks R. G. (1989) A 17,000-year glacio-eustatic sea level record: influence of glacial melting rates on the Younger Dryas event and deep-ocean circulation. *Nature* **342**, 637-642.
- Fantidis J. and Ehhalt D. H. (1970) Variations of the carbon and oxygen isotopic composition in stalagmites and stalactites; evidence of non-equilibrium isotopic fractionation. *Earth Planet. Sci. Lett.* **10**(1), 136-144.
- Finch A. A., Shaw P. A., Weedon G. P., and Holmgren K. (2001) Trace element variation in speleothem aragonite; potential for palaeoenvironmental reconstruction. *Earth Planet. Sci. Lett.* **186**(2), 255-267.
- Fischer M. J., Gale S. J., Heijnis H., and Drysdale R. N. (1996) Low latitude speleothems and palaeoclimatic reconstruction. *Karst Waters Inst. Spec. Pub.* **2**, 26-29.
- Fornaca-Rinaldi G. (1968)  $^{230}\text{Th}/^{234}\text{Th}$  dating of cave concretions. *Earth and Planetary Sci. Letters* **5**(2), 120-122.
- Fornaca-Rinaldi G., Panichi C., and Tongiorgi E. (1968) Some causes of the variation in the isotopic composition of carbon and oxygen in cave concretions. *Earth Planet, Sci, Lett.* **4**(4), 321-324.
- Frappier A., Sahagian D., Gonzalez L. A., and Carpenter S. J. (2002) El Nino events recorded by stalagmite carbon. *Science* **298**, 565.
- Friedman I. and O'Neil J. R. (1977) Compilation of isotopic fractionation factors of geochemical interest. *U.S.G.S. Professional Paper* **440-KK**.
- Frumkin A., Carmi I., Gopher A., Ford D. C., Schwarcz H. P., and Tsuk T. (1999) A Holocene millennial-scale climatic cycle from a speleothem in Nahal Qanah Cave, Israel. *Holocene* **9**(6), 677-682.
- Frumkin A., Ford D. C., and Schwarcz H. P. (2000) Paleoclimate and vegetation of the glacial cycles in Jerusalem from a speleothem record. *Glob. Biogeochem. Cyc.* **14**(3), 863-870.

- Gascoyne M. (1992) Palaeoclimate determination from cave calcite deposits. *Quat. Sci. Rev.* **11**(6), 609-632.
- Gascoyne M., Ford D. C., and Schwarcz H. P. (1981) Late Pleistocene chronology and paleoclimate of Vancouver Island determined from cave deposits. *Can. J. Earth Sci.* **18**(11), 1643-1652.
- Genty D., Blamart D., Ouahdi R., Gilmour M., Baker A., Jouzel J., and van Exter S. (2003) Precise dating of Dansgaard-Oeschger climate oscillations in Western Europe from stalagmite data. *Nature* **421**(6925), 833-837.
- Genty D., Plagnes V., Causse C., Cattani O., Stievenard M., Falourd S., Blamart D., Ouahdi R., and Van-Exter S. (2002) Fossil water in large stalagmite voids as a tool for paleoprecipitation stable isotope composition reconstitution and paleotemperature calculation. *Chem. Geol.* **184**(1-2), 83-95.
- Genty D., Vokal B., Obelic B., and Massault M. (1998) Bomb  $^{14}\text{C}$  time history recorded in two modern stalagmites; importance for soil organic matter dynamics and bomb  $^{14}\text{C}$  distribution over continents. *Earth Planet. Sci. Lett.* **160**(3-4), 795-809.
- Gewelt M. (1981) Les variations isotopiques du carbone et de l'oxygene dans une stalagmite de la grotte de Remouchamps (Belgique); Methodes et premiers resultats/Carbon and oxygen isotope variations in a stalagmite from Remouchamps Cave, Belgium; methods. *Annales de la Societe Geologique de Belgique* **104**(2), 269-279.
- Goede A. (1994) Continuous early last glacial palaeoenvironmental record from a Tasmanian speleothem based on stable isotope and minor element variations. *Quat. Sci. Rev.* **13**(3), 283-291.
- Goede A., Green D. C., and Harmon R. S. (1986) Late Pleistocene palaeotemperature record from a Tasmanian speleothem. *Austral. J. Earth Sci.* **33**(3), 333-342.
- Goede A., McDermott F., Hawkesworth C., Webb J., and Finlayson B. (1996) Evidence of Younger Dryas and Neoglacial cooling in a late Quaternary palaeotemperature record from a speleothem in eastern Victoria, Australia. *J. Quat. Sci.* **11**(1), 1-7.
- Goede A., Veeh H. H., and Ayliffe L. K. (1990) Late Quaternary palaeotemperature records for two Tasmanian speleothems. *Austral. J. Earth Sci.* **37**(3), 267-278.
- Goede A. and Vogel J. C. (1991) Trace element variations and dating of a late Pleistocene Tasmanian speleothem. *Palaeogeogr. Palaeoclimat. Palaeoecol.* **88**(1-2), 121-131.
- Gonzalez L. A. and Gomez R. (2002) High-resolution speleothem paleoclimatology of northern Venezuela: a progress report. *Boletín Sociedad Venezolana de Espeleología* **36**, 27-29.



- Gonzalez L. A. and Lohmann K. C. (1988) *Controls on mineralogy and composition of spelean carbonates; Carlsbad Caverns, New Mexico*. Springer-Verlag.
- Guilderson T. P., Fairbanks R. G., and Rubenstone J. L. (1994) Tropical temperature variations since 20,000 years ago: Modulating interhemispheric climate change. *Science* **263**, 663-665.
- Harmon R. S., Schwarcz H. P., and Ford D. C. (1978a) Stable isotope geochemistry of speleothems and cave waters from the Flint Ridge-Mammoth Cave system, Kentucky; implications for terrestrial climate change during the period 230,000 to 100,000 years B.P. *J. Geol.* **86**(3), 373-384.
- Harmon R. S., Thompson P., Schwartz H. P., and Ford D. C. (1978b) Late Pleistocene paleoclimates of North America as inferred from stable isotope studies of speleothems. *Quaternary Res.* **9**, 54-70.
- Hellstrom J., McCulloch M. T., and Stone J. (1998) A detailed 31,000-year record of climate and vegetation change, from the isotope geochemistry of two New Zealand Speleothems. *Quaternary Res.* **50**, 167-178.
- Hendy C. H. (1969) Isotopic studies of speleothems. *New Zeal. Speleo. Bull.* **4**(71), 306-319.
- Hendy C. H. (1971) The isotopic geochemistry of speleothems; 1, The calculation of the effects of different modes of formation on the isotopic composition of speleothems and their applicability as paleoclimatic indicators. *Geochim. Cosmochim. Acta* **35**(8), 801-824.
- Hendy C. H. and Wilson A. T. (1968) Palaeoclimatic data from speleothems. *Nature* **219**(5149), 48-51.
- Hobbs H. H. (1994) A study of environmental factors in Harrison's Cave, Barbados, West Indies., pp. 106. National Speleological Society.
- Holmgren K., Karlen W., and Shaw P. A. (1995) Paleoclimatic significance of the stable isotopic composition and petrology of a late Pleistocene stalagmite from Botswana. *Quat. Res.* **43**(3), 320-328.
- Holmgren K., Lee-Thorp J. A., Cooper G. R. J., Lundblad K., Partridge T. C., Scott L., Sithaldeen R., Talma A. S., and Tyson P. D. (2003) Persistent millennial-scale climatic variability over the past 25,000 years in Southern Africa. *Quat. Sci. Rev.* **22**(21-22), 2311-2326.
- Horvatincic N., Krajcar Bronic I., and Obelic B. (2003) Differences in the  $^{14}\text{C}$  age,  $\delta^{13}\text{C}$  and  $\delta^{18}\text{O}$  of Holocene tufa and speleothem in the Dinaric Karst. *Palaeogeogr. Palaeoclimat. Palaeoecol.* **193**(1), 139-157.
- Hou J. Z., Tan M., Cheng H., and Liu T. S. (2003) Stable isotope records of plant cover change and monsoon variation in the past 2200 years: evidence from laminated stalagmites in Beijing, China. *Boreas* **32**, 304-313.

- Huang J. (1992) The isotopic characteristics of carbon and oxygen of the Quaternary stalagmite in Shiquan Cave, Hubei, and paleoclimatic study. *Carsologia Sinica* **11**(3), 245-249.
- Huang J., Hu C., Zhou Q., and Lin X. (2001) Stable isotope and trace element record of a stalagmite in Heshang Cave, Hubei and its palaeoclimatic significance. *Sci. China Ser. E* **44 Supp.**, 123-128.
- IAEA/WMO. (2001) Global Network for Isotopes in Precipitation. The GNIP Database. Accessible at: <http://isohis.iaea.org>.
- Jimenez de Cisneros C., Caballero E., Vera J. A., Duran J. J., and Julia R. (2003) A record of Pleistocene climate from a stalactite, Nerja Cave, southern Spain. *Palaeogeogr. Palaeoclimat. Palaeoecol.* **189**(1-2), 1-10.
- Jones I. C. and Banner J. L. (2003) Estimating recharge thresholds in tropical karst island aquifers: Barbados, Puerto Rico and Guam. *Jour. Hydro.* **278**(1-4), 131-143.
- Jones I. C., Banner J. L., and Humphrey J. D. (2000) Estimating recharge in a tropical karst aquifer. *Water Resour. Res.* **36**(5), 1289-1299.
- Jones I. C., Banner J. L., and Mwansa B. J. (1998) Geochemical constraints on recharge and groundwater evolution; the Pleistocene aquifer of Barbados. In *Proceedings of the 3rd international symposium on Water resources and 5th Caribbean Islands water resources congress 3rd international symposium on Water resources and 5th Caribbean Islands water resources congress*, Vol. TPS-98-2 (ed. R. I. Segarra-Garcia), pp. 9-14. AWRA Tech. Publ. Ser.
- Kacanski A., Carmi I., Shemesh A., Kronfeld J., Yam R., and Flexer A. (2001) Late Holocene climatic change in the Balkans; speleothem isotopic data from Serbia. *Radiocarbon* **43**(2B), 647-658.
- Kadlec J., Hladikova J., and Zak K. (1996) Isotopic study of cave carbonates from Moravian Karst, Czech Republic. *Karst Waters Inst. Spec. Pub.* **2**, 67-71.
- KDL. <http://www.karst.edu.cn/paleo/paleo.htm>.
- Ketcham R. A. and Carlson W. D. (2001) Acquisition, optimization and interpretation of X-ray computed tomographic imagery; applications to the geosciences. *Computers & Geosciences* **27**(4), 381-400.
- Kim S.-T. and O'Neil J. R. (1997) Equilibrium and nonequilibrium oxygen isotope effects in synthetic carbonates. *Geochim. Cosmochim. Acta* **61**, 3461-3475.
- Labonne M., Hillaire-Marcel C., Ghaleb B., and Goy J.-L. (2002) Multi-isotopic age assessment of dirty speleothem calcite; an example from Altamira Cave, Spain. *Quat. Sci. Rev.* **21**, 1099-1110.
- Lauriol B., Ford D. C., Cinq-Mars J., and Morris W. A. (1997) The chronology of speleothem deposition in northern Yukon and its relationships to permafrost. *Can. J. Earth Sci.* **34**(7), 902-911.

- Lauritzen S.-E. (1995) High-resolution paleotemperature proxy record for the last interglaciation based on Norwegian speleothems. *Quat. Res.* **43**(2), 133-146.
- Lauritzen S.-E. and Lundberg J. (2004) Isotope Stage 11, the "Super-Interglacial", from a North Norwegian Speleothem. In *Studies of Cave Sediments* (ed. J. Mylroie), pp. 257-272. Kluwer Academic.
- Lauritzen S.-E. and Onac B. P. (1999) Isotopic stratigraphy of last interglacial stalagmite from northwestern Romania; correlation with the deep-sea record and northern-latitude speleothem. *J. Cave Karst Stud.* **61**(1), 22-30.
- Li B., Yuan D., Qin J., and Lin Y. (1996) A high resolution record of climate change in a stalagmite from Panlong Cave of Guilin since 36000 years B.P. *Karst Waters Inst. Spec. Pub.* **2**, 93-96.
- Li H., Gu D., Stott L. D., and Chen W. (1998) Applications of interannual-resolution stable isotope records of speleothem; climatic changes in Beijing and Tianjin, China during the past 500 years; the  $\delta^{18}\text{O}$  record. *Sci. China Ser. D* **41**(4), 362-368.
- Linge H., Lauritzen S.-E., and Lundberg J. (2001) Stable isotope stratigraphy of a late last interglacial speleothem from Rana, northern Norway. *Quat. Res.* **56**(2), 155-164.
- Ma Z., Li H., Xia M., Ku T., Peng Z., Chen Y., and Zhang Z. (2003) Paleotemperature changes over the past 3000 years in eastern Beijing, China: A reconstruction based on Mg/Sr records in a stalagmite. *Chinese Science Bulletin* **48**(4), 395-400.
- Masson V., Vimeux F., Jouzel J., Morgan V., Delmotte M., Ciais P., Hammer C., Johnsen S., Lipenkov V. Y., Mosley-Thompson E., Petit J.-R., Steig E. J., Stievenard M., and Vaikmae R. (2000) Holocene climate variability in Antarctic based on 11 ice-core isotopic records. *Quaternary Res.* **54**(3), 348-358.
- Matthews A., Ayalon A., and Bar-Matthews M. (2000) D/H ratios of fluid inclusions of Soreq cave (Israel) speleothems as a guide to the Eastern Mediterranean Meteoric Line relationships in the last 120 ky. *Chem. Geol.* **166**(3-4), 183-191.
- McCrea J. M. (1950) On the isotopic chemistry of carbonates and a paleotemperature scale. *J Chem Phys* **18**, 849-857.
- McDermott F., Frisia S., Huang Y., Longinelli A., Spiro B., Heaton T. H. E., Hawkesworth C. J., Borsato A., Keppens E., Fairchild I. J., van der Borg K., Verheyden S., and Selmo E. (1999) Holocene climate variability in Europe; evidence from  $\delta^{18}\text{O}$ , textural and extension-rate variations in three speleothems. *Quat. Sci. Rev.* **18**, 1021-1038.
- Michaelis J., Usdowski E., and Menschel G. (1985) Partitioning of  $^{13}\text{C}$  and  $^{12}\text{C}$  on the degassing of  $\text{CO}_2$  and the precipitation of calcite- Rayleigh type fractionation and a kinetic model. *Am. J. Sci.* **285**, 318-327.

- Mickler P. J. (2004) Controls on the O isotopic composition of speleothems, Barbados, West Indies. *unpublished data*.
- Mickler P. J., Banner J. L., Asmerom Y., Edwards R. L., Ito E., and Stern L. (2003) Stable isotope variations in modern tropical speleothems: Evaluating applications to paleoenvironmental reconstructions. *In Prep*.
- Mickler P. J., Ketcham R. A., Colbert M. W., and Banner J. L. (2004) Application of high-resolution X-Ray computed tomography in determining the suitability of speleothems for use in paleoclimatic, paleohydrologic reconstructions. *J. Cave Karst Stud.* **66**(1), 4-8.
- Mills G. A. and Urey H. C. (1940) The kinetics of isotopic exchange between carbon dioxide, bicarbonate ion, carbonate ion, and water. *J. Am. Chem. Soc.* **62**, 1019-1026.
- Mook W. G., Bommerson J. C., and Staverman W. H. (1974) Carbon isotope fractionation between dissolved bicarbonate and gaseous carbon dioxide. *Earth Planet. Sci. Lett.* **22**, 169-176.
- Musgrove M. (2000) Temporal links between climate and hydrology: Insights from central Texas caves and groundwater, The University of Texas at Austin.
- Musgrove M., Banner J. L., Mack L. E., Combs D., M., James E. W., Cheng H., and Edwards R. L. (2001) Geochronology of late Pleistocene to Holocene speleothems from central Texas: Implications for regional paleoclimate. *Geol. Soc. Am. Bull.* **113**(12), 1532-1543.
- Niggemann S., Mangini A., Mudelsee M., Richter D. K., and Wurth G. (2003a) Sub-Milankovitch climatic cycles in Holocene stalagmites from Sauerland, Germany. *Earth Planet. Sci. Lett.* **216**(4), 539-547.
- Niggemann S., Mangini A., Richter D. K., and Wurth G. (2003b) A paleoclimate record of the last 17,600 years in stalagmites from the B7 Cave, Sauerland, Germany. *Quat. Sci. Rev.* **22**, 555-567.
- Onac B. P., Constantin S., Lundberg J., and Lauritzen S.-E. (2002) Isotopic climate record in a Holocene stalagmite from Ursilor Cave (Romania). *J. Quat. Sci.* **17**(4), 319-327.
- O'Neil J. R., Clayton R. N., and Mayeda T. K. (1969) Oxygen isotope fractionation in divalent metal carbonates. *J. Chem. Phys.* **51**, 5547-5558.
- Parkhurst D. L. and Appelo C. A. J. (1999) PHREEQC (Version 2) A computer program for speciation, batch-reaction, one-dimensional transport, and inverse geochemical calculations. *U.S. Geological Survey Water-Resources Investigations Report* **99-4259**, 1-310.
- Paulsen D. E., Li H.-C., and Ku T.-L. (2003) Climate variability in central China over the last 1270 years revealed by high-resolution stalagmite records. *Quat. Sci. Rev.* **22**, 691-701.

- Pazdur A., Pazdur M. F., Pawlyta J., Górny A., and Olszewski M. (1995) Paleoclimatic implications of radiocarbon dating of speleothems from the Cracow-Wielun Upland, Southern Poland. *Radiocarbon* **37**(2), 103-110.
- Plagnes V., Causse C., Genty D., Paterne M., and Blamart D. (2002) A discontinuous climatic record from 187 to 74 ka from a speleothem of the Clamouse Cave (south of France). *Earth Planet. Sci. Lett.* **201**(1), 87-103.
- Plummer L. N. and Busenberg E. (1982) The solubilities of calcite, aragonite and vaterite in CO<sub>2</sub>-H<sub>2</sub>O solutions between 0 and 90C, and an evaluation of the aqueous model for the system CaCO<sub>3</sub>-CO<sub>2</sub>-H<sub>2</sub>O. *Geochim. Cosmochim. Acta* **46**, 1011-1040.
- Polyak V. J. and Asmerom Y. (2001) Late Holocene Climate and Cultural Changes in the Southwestern United States. *Science* **294**(5540), 148-151.
- Proctor C. J., Baker A., Barnes W. L., and Gilmour M. A. (2000) A thousand year speleothem proxy record of North Atlantic climate from Scotland. *Climate Dynamics* **16**(10/11), 815-820.
- Repinski P., Holmgren K., Lauritzen S. E., and Lee-Thorp J. A. (1999) A late Holocene climate record from a stalagmite, Cold Air Cave, Northern Province, South Africa. *Palaeogeogr. Palaeoclimat. Palaeoecol.* **150**(3-4), 269-277.
- Roberts M. S., Smart P. L., and Baker A. (1998) Annual trace element variations in a Holocene speleothem. *Earth Planet. Sci. Lett.* **154**(1-4), 237-246.
- Schwarcz H. P. (1986) Geochronology and isotopic geochemistry of speleothems. In *Handbook of environmental isotope geochemistry*, Vol. 2 (ed. J. C. Fontes), pp. 272-303. Elsevier.
- Serefiddin F., Schwarcz H. P., Ford D. C., and Baldwin S. (2004) Late Pleistocene paleoclimate in the Black Hills of South Dakota from isotope records in speleothems. *Palaeogeogr. Palaeoclimat. Palaeoecol.* **203**(1-2), 1-17.
- Shopov Y. Y., Ford D. C., and Schwarcz H. P. (1994) Luminescent microbanding in speleothems; high-resolution chronology and paleoclimate. *Geol.* **22**(5), 407-410.
- Spero H. J. (1992) Do planktic foraminifera accurately record shifts in the carbon isotopic composition of seawater Epsilon CO<sub>2</sub>? *Mar. Micropaleontol.* **19**(4), 275-285.
- Spero H. J. and Williams D. F. (1988) Extracting environmental information from planktonic foraminiferal delta <sup>13</sup>C data. *Nature* **335**(6192), 717-719.
- Spötl C., Burns S. J., and Mangini A. (2001) Stable isotopes in speleothems as proxies of past environmental changes in the Alps. *International Conference on the Study of Environmental Change Using Isotope Techniques*.

- Talma A. S. and Vogel J. C. (1992) Late Quaternary paleotemperatures derived from a speleothem from Congo Caves, Cape Province, South Africa. *Quat. Res.* **37**(2), 203-213.
- Talma A. S., Vogel J. C., and Partridge T. C. (1974) Isotopic contents of some transvaal speleothems and their palaeoclimatic significance. *S. African Jour. Sci* **70**, 135-140.
- Tan M., Liu D., Zhong H., Qin X., Li H., Zhao S., Li T., Lu J., and Lu X. (1998) Preliminary study on climatic signals of stable isotopes from Holocene speleothems under monsoon condition. *Chinese Science Bulletin* **43**(6), 506-509.
- Tan M., Liu T. S., Hou J., Qin X., Zhang H., and Li T. (2003) Cyclic rapid warming on centennial-scale revealed by a 2650-year stalagmite record of warm season temperature. *Geophys. Res. Lett.* **30**(12), 1617.
- Thompson P., Schwarcz H. P., and Ford D. C. (1976) Stable isotope geochemistry, geothermometry, and geochronology of speleothems from West Virginia. *Geol. Soc. Amer. Bull.* **87**(12), 1730-1738.
- Udowski E. and Hoefs J. (1993) Oxygen isotope exchange between carbonic acid, bicarbonate, carbonate, and water: A re-examination of the data of McCrea (1950) and an expression for the overall partitioning of oxygen isotopes between the carbonate species and water. *Geochim. Cosmochim. Acta* **57**, 3815-3818.
- Vaks A., Bar-Matthews M., Ayalon A., Schilman B., Gilmour M., Hawkesworth C. J., Frumkin A., Kaufman A., and Matthews A. (2003) Paleoclimate reconstruction based on the timing of speleothem growth and oxygen and carbon isotope composition in a cave located in the rain shadow in Israel. *Quat. Res.* **59**(2), 182-193.
- van Beynen P., Schwarcz H. P., and Ford D. C. (2004) Holocene climatic variation recorded in a speleothem from McFail's Cave, New York. *J. Cave Karst Stud.* **66**(1), 20-27.
- Verheyden S., Keppens E., Fairchild I. J., McDermott F., and Weis D. (2000) Mg, Sr and Sr isotope geochemistry of a Belgian Holocene speleothem; implications for paleoclimate reconstructions. *Chem. Geol.* **169**(1-2).
- Vogel J. C., Grootes P. M., and Mook W. G. (1970) Isotopic fractionation between gaseous and dissolved carbon dioxide. *Physik* **230**, 225-238.
- Wang X. (1986) U-dating and  $\delta^{18}\text{O}$ ,  $\delta^{13}\text{C}$  features of speleothems in Maomaotou Big Cave, Guilin. *Kexue Tonbao* **31**(12), 835-838.
- Wang Y., Chen Q., Liu Z., Chen Y., Zhou C., and Lu C. (1998) A continuous 200-ka palaeoclimate record from a stalagmite in Tangshan Cave, Nanjing. *Chinese Science Bulletin* **43**(3), 233-237.
- Wang Y., Wu J., Wu J., Mu X., Xu H., and Chen J. (2001) Correlation between high-resolution climate records from a Nanjing stalagmite and GRIP ice core during the last glaciation. *Sci. China Ser. D* **44**(1), 14-23.

- Wang Z., Huang P., Peng Z., Yang H., Jin S., Liang R., Zhang H., and Quan Y. (1995) ESR and U series dating of stalagmites and isotope paleoclimatology. *Earth Science - Journal of China University of Geosciences* **20**(6), 677-681.
- Wefer F. L. (1994) The meteorology of Harrison's Cave, Barbados, West Indies in Hobbs, H. H., A study of environmental factors in Harrison's Cave, Barbados, West Indies. *Nat. Speleo. Soc.*
- Williams P. W., Marshall A., Ford D. C., and Jenkinson A. V. (1999) Palaeoclimatic interpretation of stable isotope data from Holocene speleothems of the Waitomo District, North Island, New Zealand. *Holocene* **9**(6), 649-657.
- Winograd I. J., Coplen T. B., Landwehr J. M., Riggs A. C., Ludwig K. R., Szabo B. J., Kolesar P., and Revesz K. M. (1992) Continuous 500,000-year climate record from vein calcite in Devils Hole, Nevada. *Science* **258**, 255-258.
- Xia Q., Zhao J.-x., and Collerson K. D. (2001) Early–Mid Holocene climatic variations in Tasmania, Australia: multi-proxy records in a stalagmite from Lynds Cave. *Earth Planet. Sci. Let.* **194**(1-2), 177-187.
- Zhang M., Yuan D., Lin Y., Cheng H., Qin J., and Zhang H. (2004) The record of paleoclimatic change from stalagmites and the determination of termination II in the south of Guizhou Province, China. *Sci. China Ser. D* **47**(1), 1-12.
- Zhao J.-X., Wang Y.-J., Collerson K. D., and Gagan M. K. (2003) Speleothem U-series dating of semi-synchronous climate oscillations during the last deglaciation. *Earth Planet. Sci. Let.* **216**(1-2), 155-161.

## VITA

Patrick J. Mickler was born in Red Hook, NY on December 19<sup>th</sup>, 1967, the son of Dorothy Mickler and Robert Mickler. After graduating from Red Hook High School in 1986 he enrolled in Dutchess Community College before transferring to The State University of New York at Buffalo in 1988. He graduated with a B. A. in Geology from SUNY Buffalo in 1992. He worked in the private industry as a Geologist until 1994 when he enrolled in The University of Cincinnati. He graduated with a M.S. in Geology from the University of Cincinnati in 1988. Prior to graduation from Cincinnati he enrolled at the University of Texas at Austin in 1996.

Permanent address: 20 Eldridge Lane, Red Hook, NY 12571

This dissertation was typed by the author.